Universidade de Aveiro Departamento de Electrónica, Telecomunicações e Informática,
2013

João Ricardo Duarte Miranda

Desenvolvimento de um robô quadrotor autónomo
Development of an autonomous quadrotor robot

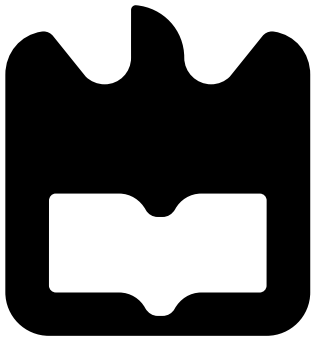

João Ricardo
Duarte Miranda

Desenvolvimento de um robô quadrotor autónomo
Development of an autonomous quadrotor robot

Dissertação apresentada à Universidade de Aveiro para cumprimento dos requisitos necessários à obtenção do grau de Mestre em Engenharia Electrónica e Telecomunicações, realizada sob a orientação científica de Manuel Bernardo Salvador Cunha e José Luís Costa Pinto de Azevedo, Professores Auxiliares do Departamento de Electrónica, Telecomunicações e Informática da Universidade de Aveiro.

o júri / the jury

presidente / president	**Professor Doutor Alexandre Manuel Moutela Nunes da Mota** Professor Associado da Universidade de Aveiro
vogais / examiners committee	**Professor Doutor António Paulo Gomes Mendes Moreira** Professor Associado da Faculdade de Engenharia da Universidade do Porto
	Professor Doutor Manuel Bernardo Salvador Cunha Professor Auxiliar da Universidade de Aveiro (orientador)
	Professor Doutor José Luís Costa Pinto de Azevedo Professor Auxiliar da Universidade de Aveiro (co-orientador)

agradecimentos / acknowledgements

Um especial agradecimento aos meus orientadores, Prof. Bernardo Cunha e Prof. José Luís Azevedo, pela proposta de dissertação, pela total disponibilidade e pelos conhecimentos que me transmitiram ao longo da realização deste projecto.

Agradeço aos meus pais pela dedicação, carinho e educação que me proporcionaram e ainda mais pelo esforço que fizeram para que esta caminhada fosse possível. Ao meu irmão pelos bons momentos e companheirismo. Agradeço à Sofia, por todo o apoio e motivação dedicados ao longo destes anos.

Aos meus colegas da sala 303, pelo bom ambiente criado, essencial para este trabalho.

Aos meus amigos, pela entreajuda e pelos momentos fantásticos que me proporcionaram ao longo destes anos.

Resumo

Existe actualmente um interesse visível por parte de grupos de investigação e entusiastas em veículos aéreos não tripulados de descolagem e aterragem vertical, especialmente numa aeronave denominada de quadrotor. Este interesse surge, em grande parte, devido à capacidade destes veículos desempenharem funções em ambientes de difícil acesso ao homem.

O Grupo de Actividade Transversal em Robótica Inteligente (ATRI) do Instituto de Engenharia Electrónica e Telemática de Aveiro (IEETA) com experiência em diversos tipos de plataformas robóticas terrestres, pretende iniciar o estudo neste tipo de aeronaves com o objectivo de, a prazo, as tornar totalmente autónomas. Esta dissertação consiste, consequentemente, no estudo da dinâmica neste tipo de veículos, assim como na construção de um primeiro protótipo de testes.

São descritas as várias etapas de construção, desde a escolha dos componentes, desenvolvimento de uma placa de controlo e estabilização à assemblagem final da aeronave. São explicados quais os sensores necessários para efectuar a estimativa da orientação do veículo, assim como a implementação de filtros de fusão sensorial para uma estimativa mais precisa. Além disso, é descrito do algoritmo de controlo PID aplicado para controlo e estabilização do quadrotor.

No final são expostos os testes realizados e os resultados experimentais, retirando conclusões para trabalhos futuros.

Abstract

Nowadays, many research groups and enthusiasts developed an interest in Vertical Take Of and Landing (VTOL) vehicles due to the ability to perform tasks in hazardous environments for human beings.

The Transverse Activity on Intelligent Robotics (ATRI) research group, part of the Institute of Electronics and Telematics Engineering of Aveiro (IEETA), which has a lot of experience in terrestrial robots, wants to start the research in these kind of aircrafts, setting the future goal of developing a fully autonomous quadrotor. Therefore, this dissertation overviews the study of the quadrotor dynamics and the developing of a first version of a VTOL prototype.

Several stages of research are discussed, since the components selection, the required sensors to estimate the quadrotor attitude and the implemented fusion filters to improve that estimation. The implemented control algorithms(PID) necessary to perform control and stabilization are also discussed.

Finally, the experimental results are presented, followed by the conclusions and future work.

Contents

List of Figures

List of Tables

Acronyms

ADC Analog to Digital Converter.

AHRS Attitude and Heading Reference Systems.

ATRI Transverse Activity on Intelligent Robotics.

BEC Battery Eliminator Circuit.

BLDC BrushLess Direct Current Motor.

CCW Counter Clockwise.

CW Clockwise.

DC Direct Current.

DOF Degrees of Freedom.

EKF Extended Kalman Filter.

EMF Electromotive force.

ESC Electronic Speed Controller.

FPV First Person View.

GUI Graphical User Interface.

I^2C Inter-Integrated Circuit.

IMU Inertial Measurement Unit.

MARG Magnetic, Angular Rate, and Gravity.

MEMS Microelectromechanical systems.

PC Personal Computer.

PID Proportional Integral Derivative.

PWM Pulse Width Modulation.

RC Radio-Controlled.

RP Roll-Pitch.

RPM Rotations Per Minute.

RPY Roll-Pitch-Yaw.

SF Slow-Fly.

SFD Start of Frame Delimiter.

SPI Serial Peripheral Interface.

UAV Unmmaned Aerial Vehicle.

VTOL Vertical Take-Off and Landing.

Chapter 1

Introduction

This chapter provides a brief introduction to this dissertation and how it is structured. The motivation, proposed objectives and some application areas are presented.

1.1 Context

The multirotor aircrafts characteristics bring many advantages comparing with other solutions of Unmmaned Aerial Vehicles (UAVs) like airplanes or even helicopters. The fact that they belong to the Vertical Take-Off and Landing (VTOL) type, give them advantages over other systems, such as the ability of hover still in a specific region, take off and landing in small places and fly at small velocities. These kind of aircrafts are perfect to perform tasks that are difficult to humans, decreasing operational costs and life risks.

A quadrotor is a type of multirotor which has normally a structure of four arms with four rotors disposed on the tip of each arm performing a 90°angle between them. Attached to each rotor is the propulsive system which is generally a two blade propeller. At the center of the structure, which is also the center of mass of the aircraft, are disposed the sensors, control unit and power system. This kind of aircrafts can fly in a fully autonomous way, requiring no human intervention, semi-autonomous way, where a pilot controls the vehicle with a remote control but the system is self-stabilizing or can be fully tele-operated giving the pilot the total control over the aircraft.

The quadrotor offers some advantages over other VTOL vehicles like helicopters, because it has an extremely simple mechanical structure where all the rotors are fixed to the structure. Also, the fact that it has more propulsive systems than a helicopter makes possible to them to be smaller which helps to fly in small places.

1.2 Objectives and Motivation

This dissertation is part of the research made in Transverse Activity on Intelligent Robotics (ATRI). During the last years, the multi-rotors have been a field of study for many research groups, but they also had an enormous growth in the Radio-Controlled (RC) community. Generally this kind of applications have a remote control and it needs a pilot to operate it. Huge efforts are being made to turn them on autonomous robots able to perform tasks efficiently without human intervention. The objective of this dissertation is to start, within the ATRI group, the research in this kind of aerial vehicles thinking at long-term of building a

fully autonomous aircraft. ATRI has defined a R&D timeline where the following milestones need to be covered:

- Familiarization with the multirotor specifications and needs.
- Identification of requirements in terms of mechanical and electrical design.
- Architectural modeling of a prototype infrastructure.
- Development of a first version of a remote operated quadrotor according to the previous definitions and capable of lift 800g of extra payload.
- Development of a dedicated control and stabilization board with associated sensors for partially tele-operated flying as well as autonomous flying.
- Develop autonomous flying behaviours.

The high comprehensiveness of this project was a big motivational factor for this work development. The fact that is the first project of this kind within the ATRI group, still with very ambitious objectives, turn it to be much desired.

1.3 Applications

Many applications emerged recently in this area, filling more and more different fields. Generally, and within all fields, a video camera is used and attached to the aircraft allowing, among others, the following kind of applications:

- Research platform to test and evaluate new ideas in different fields, such as flight control theory, real time systems, localization and mapping and other robotics research fields.
- Civil protection applications like preventing and helping coordination when fighting fires and inspecting contaminated areas.
- Aerial video recording for social events, news coverage, professional photography and shooting movies.
- Security, performing surveillance sites[1].
- Inspecting farms for noxious weeds and help eliminating them[2].
- Structures inspections, like defective roofs, bridge inspection and places of difficult access.
- Military use for search and rescue missions in urban environments[3].
- Hobby for RC enthusiasts and First Person View (FPV) piloting.

1.4 Document Structure

The document outline is as follows:

- **Chapter 2:** Shows the evolution of the multirotor systems focusing essentially on the recent years developments, comparing custom built research solutions against commercial solutions. It is also presented the multirotor system modelling, overviewing some of the possible configurations and their advantages.
- **Chapter 3:** Presents the mechanical and electrical design solution for the project, overviewing all the required components individually. The implemented architecture is described, explaining in detail the purpose of each block of that architecture. The control board implementation will be explained as well as all the communication protocols associated with it. A software implementation is exposed, as well as the graphical user interface developed for the system.
- **Chapter 4:** Presents the algorithms used to perform the sensor fusion in order to acquire precise attitude angles measurements and estimations. The algorithms used to perform closed loop control are also explained in detail.
- **Chapter 5:** Describes the test-bed conditions and presents and analyses the results obtained during this project.
- **Chapter 6:** Presents conclusions regarding the implementation of the system and future work to be considered in the improvement of the system.
- **Appendices:** Present complementary information about the development of the system.

Chapter 2

State of the Art

This chapter provides a brief description of the first quadrotor experiments as well as the recent years development. Several multirotor configurations are presented and compared.

2.1 Quadrotor history

The first multirotor experiments were made at the beginning of the 20th century by Professor Richet and the Bréguet brothers. In 1907 they manage to build the first quadrotor named *Bréguet-richet Gyroplane No.1* (Figure 2.1) that weighted 578Kg and had propellers of 8.1 meters of diameter. Although it managed to lift, the maximum height achieved was 1.5m due lack of stability[4][5].

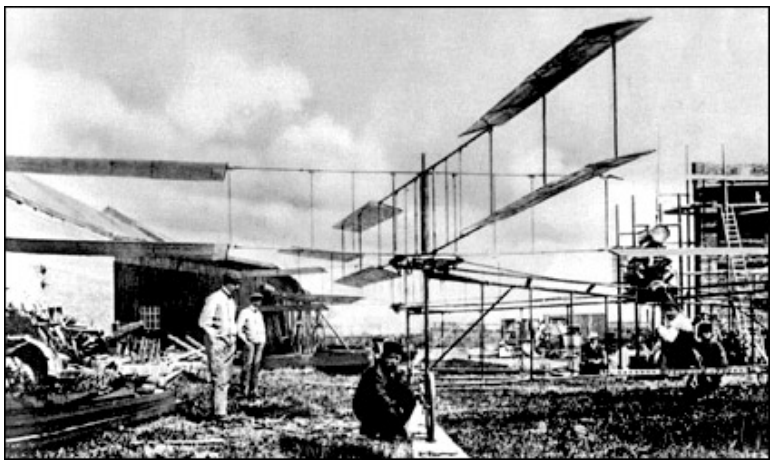

Figure 2.1: Bréguet-Richet Gyroplane No.1.[5]

Later, in 1920, Etienne Hemichen started his experiments with VTOL aircrafts. After some difficulties, in 1922, he managed to build the *Hemichen No.2 Quadrotor*. The aircraft weighted 800Kg, had four rotors and eight propellers. He made more than 1000 tests and established a record of flying distance of 1 km in 7m40s. The maximum flying autonomy he achieved was 14min.[6]

After these successful but unimpressive attempts, scientists and engineers efforts were focused on the helicopter development, creating a several years gap in quadrotor developments.

2.2 Recent Years

During more recent years, the interest in quadrotors has increased significantly due to the progress in some of the technologies used, like sensors, actuators, processors and mainly the batteries. Universities, students and researchers have been working hard developing better control and modelling methods to turn quadrotors more reliable and robust. There are several studies with the purpose of build fully autonomous multirotors.

Nowadays, multirotor aircrafts have small dimensions, a reasonable battery life and are able to perform group tasks. There are several multirotor implementations, including commercial, research and custom built versions.

2.2.1 University Research Projects

STARMAC I and II

STARMAC project started during 2003 and results of research done by Stanford and Berkeley Universities. The goal was to build autonomous multirotors capable of follow a path designated by the ground station.

STARMAC I[7] is based on the commercial platform DraganFlyer X4, but with electronic changes that provide more control over the aircraft. It has two PIC microcontrollers, responsible to control the motors and communicate with ground station over bluetooth. Additionally it has a GPS sensor to know absolute position. The sensor fusion and position estimation are achieved using an Extended Kalman Filter (EKF). Several control techniques such as Proportional Integral Derivative (PID), Sliding Mode and Reinforcement Mode were implemented.[8]

STARMAC II[9] is based on its predecessor with some evolutions. It has two microcontrollers, an Atmega to low level control and a Crossbow Stargate 1.0 with Linux to estimate position and implement planning techniques. The communication was changed from bluetooth to Wi-Fi improving the reliability of the communications.

OS4

OS4 is an indoor micro quadrotor platform developed by S. Bouabdallah in EPFL (École Polytechnique Fédérale de Lausanne). In his PhD Thesis[10] he described the mechanical design, dynamic modelling, sensing, control of orientation angles and he implemented several control techniques, like PID, LQ (Linear Quadratic), Lyapunov, Slidding mode, Backstepping and Integral Backstepping. The last one, proved to be the most reliable one for autonomous flight applications[11].

A simulation tool based in Matlab Simulink was also developed in order to simulate the OS4 dynamics with different types of sensors and control techniques.

ETH Flying Machine Arena

The Flying Machine Arena[1] is a controlled environment that allows the test and validation of mobile robots and is part of the Swiss Federal Institute of Tecnology Zurich (ETH). This project began during the Summer of 2008 and is ongoing. The Arena has several multirotors,

[1] `http://www.flyingmachinearena.org/`

based on Hummingbird[2] from Ascending Technologies, a motion capture system composed of eight cameras on the ceiling, that provide milimeter-accuracy localization and a charging platform, that is capable of recharge lithium batteries without human intervention.

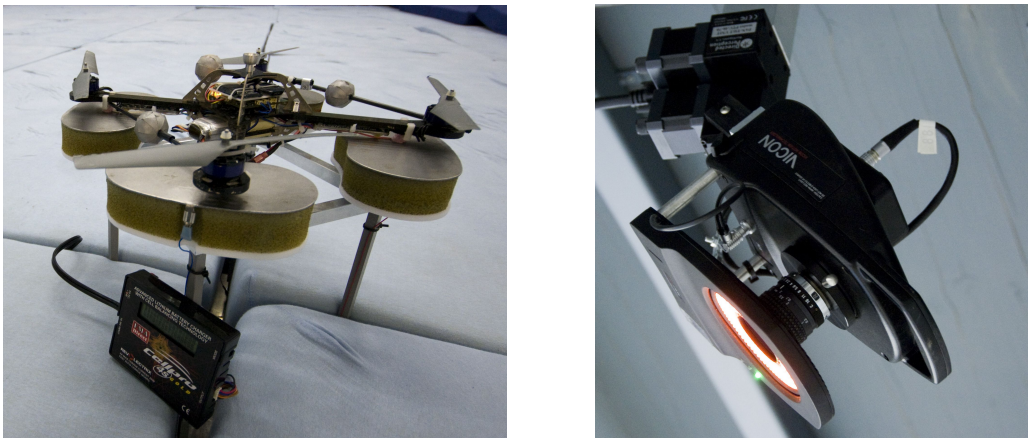

(a) (b)

Figure 2.2: a) ETH charging platform. b) ETH motion cameras.

Their most popular project was Mark Müller's Master Thesis titled "Ball juggling experiments with Quadrotors in the ETH Flying Machine Arena"[12] where a quadrotor equipped with a badminton racket can make several operations with a ping-pong ball, autonomously.

Figure 2.3: ETH quadrotor with attached badminton racket head.

Very recently, Raffaello D'Andrea showed the latest quadrotor experiments progress during a TED Talk[13]. In a series of demos, he exhibited progressions of cooperative quadrotors and demonstrated some physical experiments, such as balancing a glass of water while performing aggressive maneuvers, or cause a virtual change of the room gravity.

[2] http://www.asctec.de/uav-applications/research/products/asctec-hummingbird/

GRASP LAB

The General Robotics, Automation, Sensing and Perception Laboratory (GRASP Lab)[3] integrates the University of Pennsylvania and researches in computer science, electrical engineering and mechanical engineering. Like ETH, the GRASP Lab also have a flying arena with motion cameras. Several articles within the field have been presented, such as Aggressive Maneuvers for Autonomous Quadrotor Flight, Swarm of Nano Quadrotors and Construction with Quadrotor Teams.

Aggressive Maneuvers for Autonomous Quadrotor Flight Quadrotor flies precisely along aggressive trajectories[14]. Flips, flight through windows and perch on surfaces. Using the motion cameras to locate the important points in the path, they calculate the trajectory segments and associated controllers, each of which is redefined in simulation and experimentation. With a limited number of trials (about four) they are able to generate controllers that show repeatability and precision. The quadrotors used are the hummingbirds by Ascending Technologies.

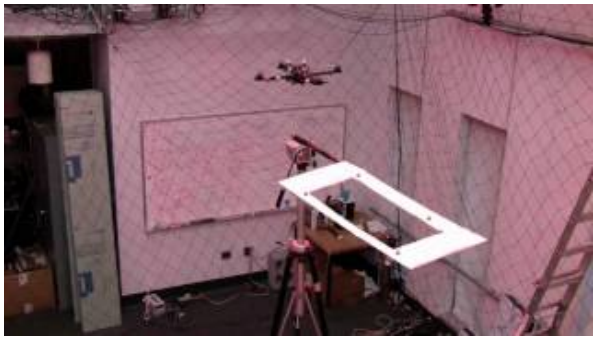

Figure 2.4: Quadrotor preparing to flight through a window.

Swarm of Nano Quadrotors Teams of twenty agile flight capable quadrotors that can flight in various complex formations[4]. They can fly autonomously avoiding obstacles, while maintaining an organized formation[15].

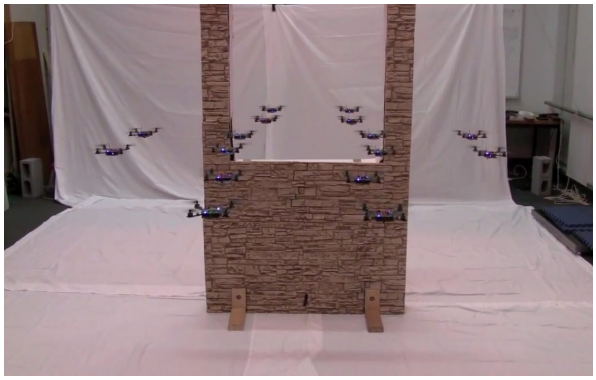

Figure 2.5: Swarm of nano quadrotors flying through a window.

[3] https://www.grasp.upenn.edu/

[4] https://www.grasp.upenn.edu/success_story/swarm_nano_quadrotors

2.2.2 Commercial Projects

Usually, multirotor manufactures have the RC community as their selling target. The devices used for that kind of application are very limited, closed and with lack of information. However, there are some companies that produce devices designed for research institutes as described below.

Ascending Technologies Ascending Technologies[5] produces ready-to-fly custom products to research institutes such as the GRASP Labs and the ETH University. The Hummingbird, used by both institutes, is a small and light quadrotor capable of lifting extra 200g of payload.

Ascending Technologies has other available options such as the AscTec Firefly[6] and the AscTec Pelican[7] which can handle more extra payload and already comes with additional sensors and a Software Development Kit.

ARDrone Parrot The ARDrone Parrot[8] is one of the most successful quadrotor implementations used for both RC community and research institutes. It is a very light platform with propeller protection that provides a SDK environment for research or entertainment applications, that uses the built-in hardware.

2.3 System Modelling

To better understand the quadrotor movements and manoeuvring, it is important to introduce a reference frame that describes the coordinate system and the environment where the aircraft moves. This reference frame will also be used in following sections.

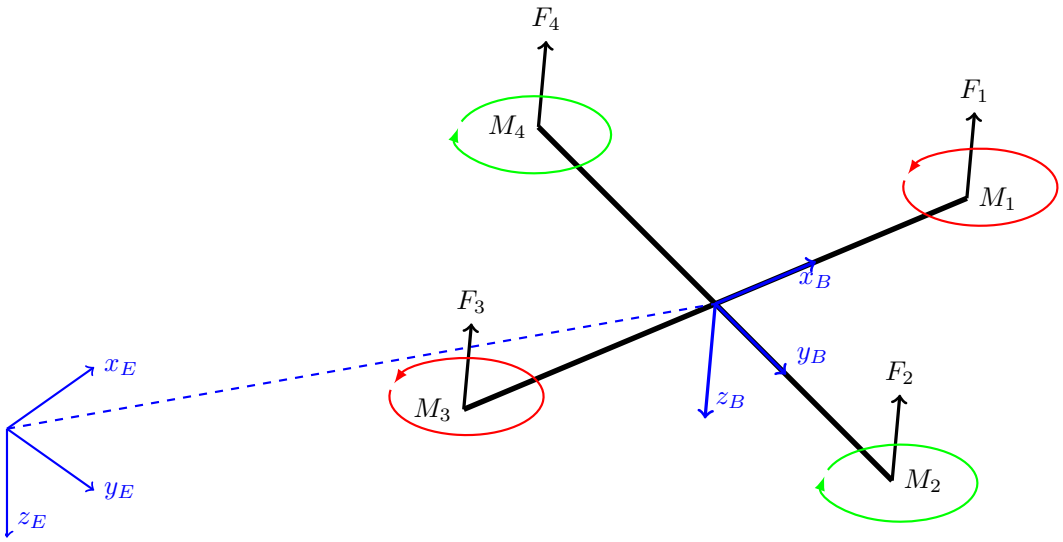

Figure 2.6: Earth(E) and Body(B) reference frames

[5] http://www.asctec.de/
[6] http://www.asctec.de/uav-applications/research/products/asctec-firefly/
[7] http://www.asctec.de/uav-applications/research/products/asctec-pelican/
[8] http://ardrone2.parrot.com/

Figure 2.6 represent both Earth(E) and body(B) frames. The frame E is the reference frame and frame B is related to the quadrotor where x_B is aligned with the front of the aircraft.

2.3.1 System Analysis

A quadrotor aircraft is composed of four arms with a 90°angle between each other and four propulsive pairs fixed on the tip of each arm. The propulsive pair (motor + propeller) is responsible to generate vertical and horizontal forces. Unlike helicopters, the blade angle of attack does not change. Maneuvers are possible by applying different angular velocities to each rotor. Quadrotors don't have a tail rotor to cancel the induced moment generated by the main motors. However the moment is cancelled by applying different types of propellers to opposite pairs of motors. As shown in figure 2.6, motor 2 and 4 have clockwise propellers and motors 1 and 3 have counter clockwise propellers.

Given the Newton's second law of motion (eq. 2.1) and the rotational analogue of the law(eq. 2.2):

$$\sum F = ma \tag{2.1}$$

$$\sum \tau = I\alpha \tag{2.2}$$

where F is the total force applied to the body, m is the mass of the body, a the linear acceleration, τ is the total torque exerted at the body, I the moment of inertia and α the angular acceleration. If all rotors are applying the same angular velocity to the propellers, the forces generated by each of them will be equal. The total torque exerted to the frame body(x_B,y_B,z_B) and angular acceleration will be zero, which means that the vehicle will be stabilized (ϕ,θ,ψ).

$$U = \sum_{i=1}^{4} F_i \tag{2.3}$$

In order to hover, the total force U, produced by the motors, must be equal to the force in opposite direction due to gravity P. From this, we can state some conditions:

- if $U > P$, the aircraft will ascend.
- if $U < P$, the aircraft will descend.

We can also change the ascend and descend velocity, by increasing or decreasing the difference between U and P.

Roll (ϕ)

Roll occurs when the aircraft performs a rotation around the x-axis. This maneuver is achieved by changing the angular velocity at motor 2 and motor 4, while maintaining the same velocity at motor 1 and 3. To produce a positive rotation of ϕ angle, motor 4 should increase the angular velocity and motor 2 should decrease the angular velocity. This maneuver is illustrated in figure 2.7.

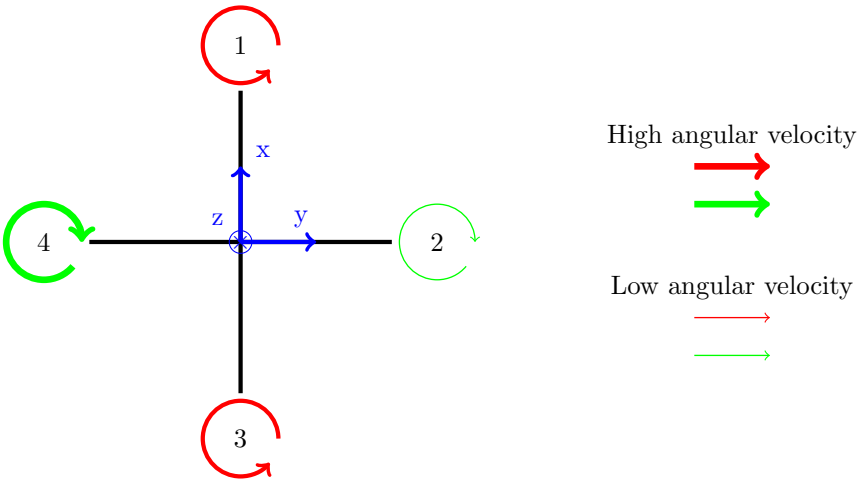

Figure 2.7: Aircraft performing a positive rotation of ϕ angle

Pitch (θ)

Pitch occurs when the aircraft performs a rotation around the y-axis. This maneuver is achieved by changing the angular velocity at motor 1 and motor 3, while maintaining the same velocity at motor 2 and 4. To produce a positive rotation of θ angle, motor 3 should increase the angular velocity and motor 1 should decrease the angular velocity. This maneuver is illustrated in figure 2.8.

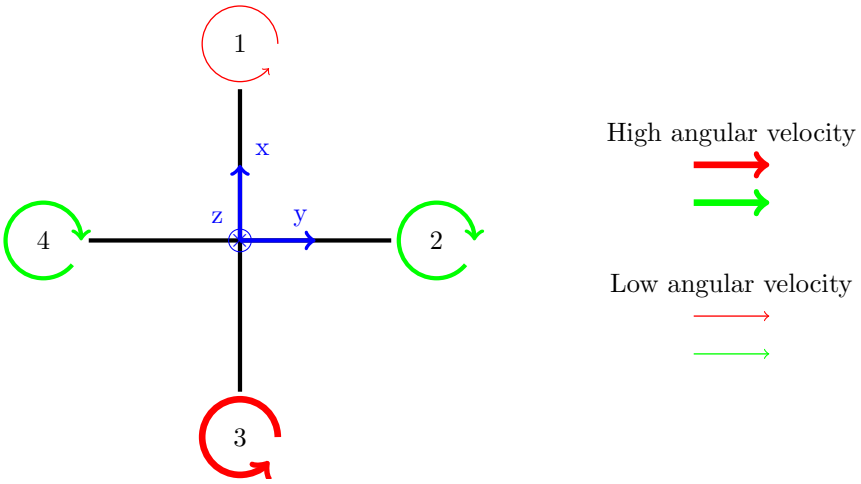

Figure 2.8: Aircraft performing a positive rotation of θ angle

Yaw (ψ)

Yaw occurs when the aircraft performs a rotation around the z-axis. This maneuver is achieved by increasing the angular velocity of a pair of two opposite motors, while decreasing the angular velocity of the other pair of motors.

Increasing the angular velocity of the odd motors while decreasing the angular velocity of even motors performs a positive rotation of ψ angle. This maneuver is illustrated in figure 2.9.

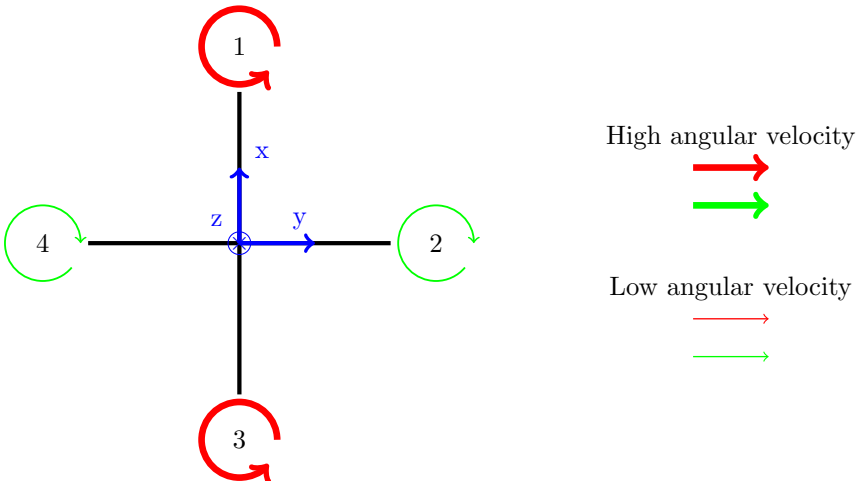

Figure 2.9: Aircraft performing a positive rotation of ψ angle

2.3.2 Multirotor configurations

There are several multirotor configurations that must be studied before decide which one provides the best fit to the intended application. The configurations varies from the number of rotors to the disposition of them. In this section we'll compare the most used configurations, stating the advantages and disadvantages of each of them.

Configuration types

Quadrotor The quadrotor is the most used configuration worldwide. It can be used in '+' or 'x' configurations as shown in figure 2.10

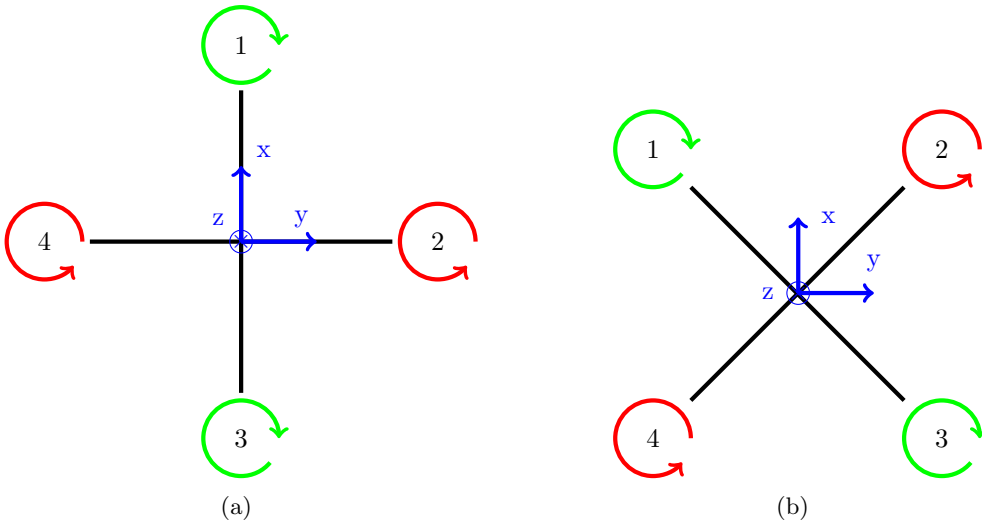

Figure 2.10: a) Quadrotor '+' configuration. b) Quadrotor 'x' configuration.

Some reasons to be widely used are:

- Mechanically simple.

- Easy to control.
- Inexpensive.

However, there are some disadvantages to take into account:

- It can't handle to much weight.
- Not fault tolerant (It loses yaw controllability).

In '+' configuration, the pitch and roll movements are done by increasing the speed of only one rotor, while in 'x' configuration the movement is accomplished through the change of speed in two rotors.

Hexarotor Although less used, the hexarotor has several advantages over the quadrotor:

- It can produce more thrust, therefore it can lift more weight.
- Motors may spin at lower Rotations Per Minute (RPM), working in a more efficient way.
- Fault tolerant.

However, there are obvious disadvantages:

- It needs to be large and heavier.
- More expensive than quadrotor (more arms, motors, Electronic Speed Controller (ESC) and batteries).

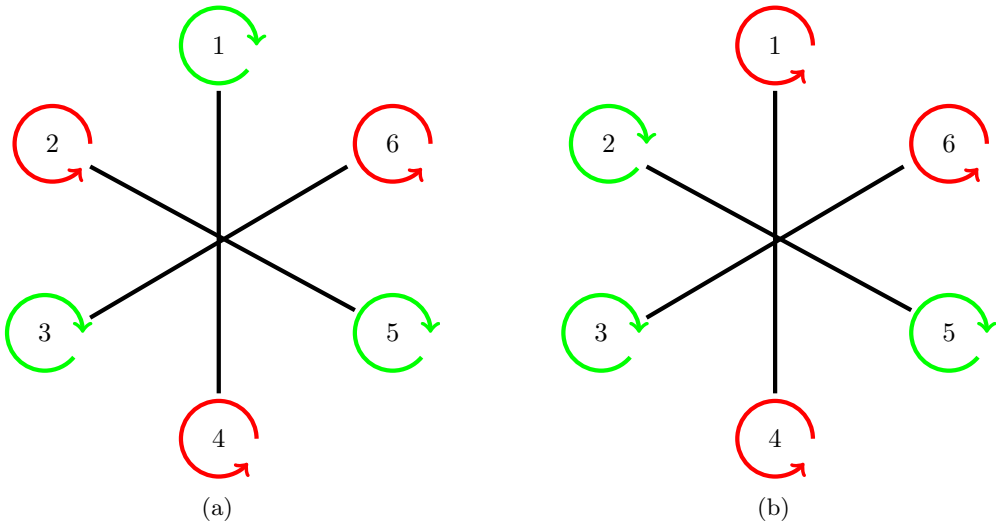

Figure 2.11: a) Hexarotor configuration 1 b) Hexarotor configuration 2

Octorotor The octorotor has the same advantages/disadvantages that the hexarotor has over the quadrotor. It is larger, heavier, more expensive and consumes more power than the hexarotor, although it is the easiest to control (from the pilot point of view). It has less vibrations, smooth movements and can lift more weight. Hence, it is extremely used by aerial photographers.

There are two different, but often used configurations with eight motors. Figure 2.12 illustrates radial configurations, while figure 2.13 shows coaxial configuration

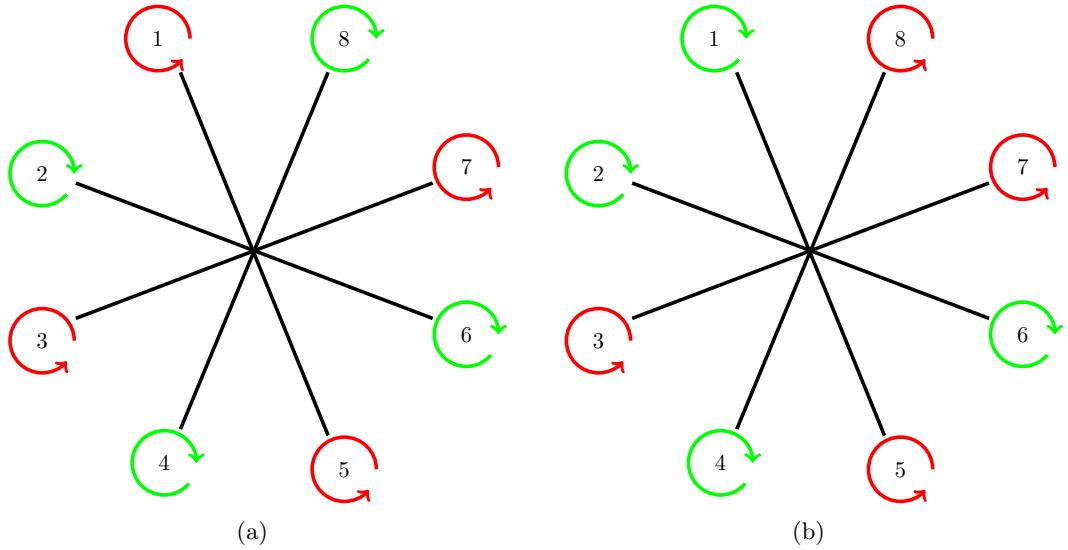

Figure 2.12: a) Octorotor configuration 1 b) Octorotor configuration 2

Coaxial configuration (X8) has the same structure of a normal quadrotor, but with an additional rotor at the bottom of each arm. Since it doesn't need 8 arms, the total weight of the aircraft is reduced. However, coaxial configuration is less efficient than radial one. Both of them are fault tolerant as stated in the next section (Fault Tolerance).

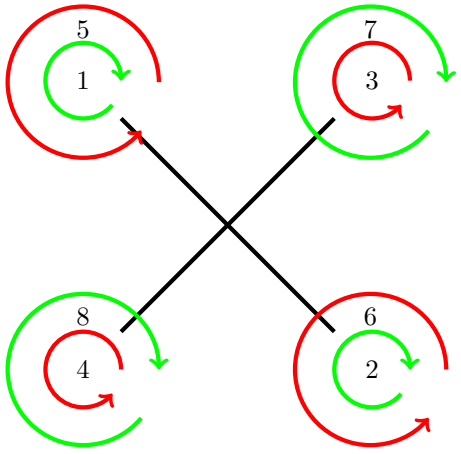

Figure 2.13: Octorotor coaxial configuration.

Fault Tolerance

The number of rotors and their arrangements have an important influence on the fault tolerance of the system. As discussed above, quadrotors aren't fault tolerant unlike the other aircrafts with a higher number of rotors. However, even hexarotors and octorotors can lose performance and capabilities when they lose a motor.

When a quadrotor motor fails, the controller board needs to shutdown the motor of the opposite arm, losing Clockwise (CW) or Counter Clockwise (CCW) propulsive system turning it into a bicopter without yaw controllability.

When reliability is a key factor, the best option is to use an hexarotor or an octorotor. The arrangements illustrated in figure 2.11 and 2.12 have been studied[16] quantifying the fault-tolerance capability, comparing how many fault tolerant configurations are Roll-Pitch-Yaw (RPY) or Roll-Pitch (RP) controllable compared to the total number of possible fault configurations.

Table 2.1 shows the probability of keeping the ability to perform certain maneuvers when the aircraft loses one or two motors, randomly. The configurations studied are the ones illustrated in Figures 2.11 and 2.12.

Configuration	**RPY**	**RP**
Hexarotor Radial a)	0%	57%
Hexarotor Radial b)	33%	71%
Octorotor Radial a)	78%	100%
Octorotor Radial b)	89%	100%

Table 2.1: Fault tolerant comparison between different multirotor configurations. [16]

As expected, as the number of rotors increases, the system becomes more reliable to rotor failures. However, it is curious to see that the hexarotor a) configuration loses RPY feature with any of rotor failure, but it is still the most used one. This factor can be explained by the performance losses when using the type b) configuration. [16]

2.4 Summary

In this chapter it was shown what are the state of the art projects developed in research institutes as well as some of existing commercial solutions. It is clear that buying a commercial solution reduces the development time. However, the knowledge that can be acquired developing a system from scratch is much more attractive. Moreover, that approach results in a system that certainly fits the user needs.

The system modelling was also shown during this chapter, comparing the existing multirotor configurations and explaining what is their work principle. This lead to the decision of building a quadrotor, acquiring the components individually and assembling them all together.

The next chapter will present the architecture of the system as well as the chosen components for the project.

Chapter 3

Architecture and Implementation

This chapter provides a brief discussion of the system architecture, overviewing all the important components of the system, their function and why they were chosen. It explains how the system is implemented, describing all the steps from the control and stabilization board to the software implementation.

3.1 Architecture Overview

The developed system can be seen as a group of blocks that interact with each other. These blocks are represented in figure 3.1 and will be described in this section.

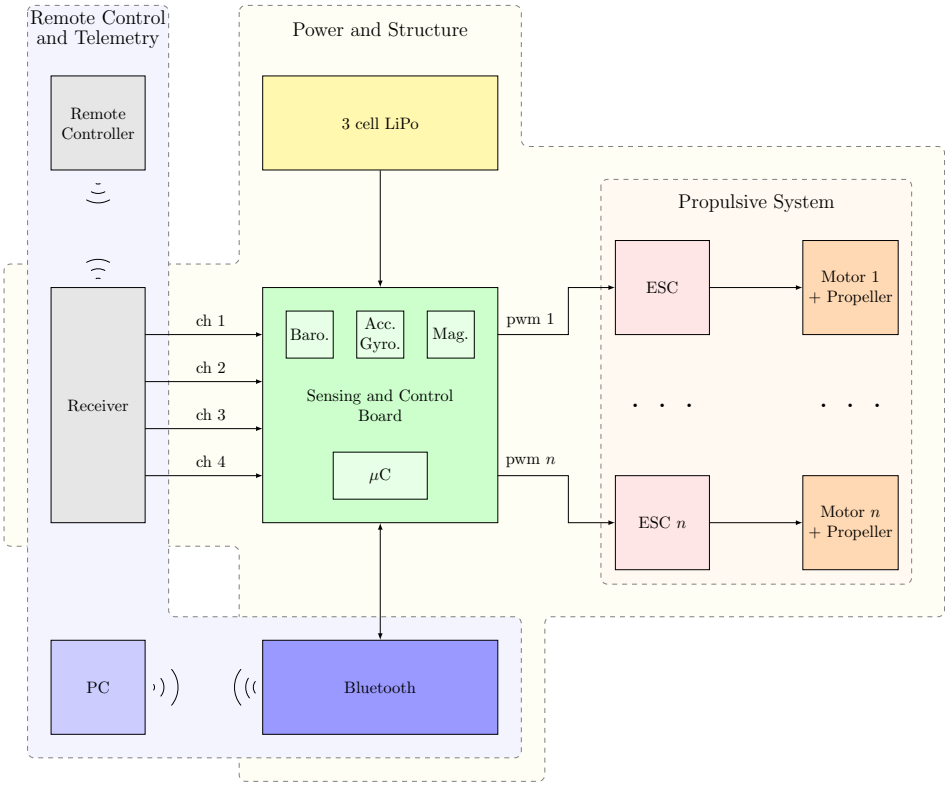

Figure 3.1: Overview of the system architecture

3.1.1 Structure and Power System

This block is composed of two major systems, that although share the same space in the block diagram, have completely different tasks. These systems are the structure and the power system, which will be explained in the paragraphs below.

Structure Multi-rotor aircrafts have a frame that supports all the components that the system needs to operate. The structure is mechanically simple, although it must fit some requirements:

- It must be symmetrical, with the center of mass at the center of the structure.
- Needs to be rigid while lighter enough to take flight.
- The vibrations provoked by the motors shouldn't affect the inertial motion sensors located at the center of the structure.

Many commercial frames are made of glass fiber, aluminium or even wood. However, one of the most effective materials is carbon fiber, due to the low density and high strength ratio. For this reason, the chosen frame was the Turnigy Talon V2.0. The structure is crafted from genuine carbon fiber offering great performance, body strength and lightweight. The motor plates have different bolt sizes, offering the possibility of using several different motors. In some cases it is also possible to mount the motor on both sides of the plate (top and bottom).

Since this frame is to be used in a development environment, accidents are more likely to happen, so the disadvantage of this structure is the lack of protection for the electronics and propellers.

The frame specifications are $280g$ of weight and $550mm$ width (from motor to motor).

Power System This block is composed of the battery and it is responsible to power all the electronic components in the other blocks. Although figure 3.1 shows that the block feeds all the blocks directly, in fact only the Electronic Speed Controller (ESC) are powered directly by the battery. The ESC have a functionality called Battery Eliminator Circuit (BEC) that provides a regulated 5V line power used to source other electronic components. In this project, the BEC powers the control board, which in turn powers all the other blocks such as bluetooth and radio receiver.

The battery selection for this type of application must follow a certain criteria:

- Should be rechargeable.
- Must be as light and small as possible (High energy density).
- Must have high discharge rate to supply high amounts of current to the motors.
- Low maintenance requirements.
- Low price.

Within the secondary category of batteries there are several cell chemistries. Analyzing figure 3.2, we notice that the technology with better relation weight-dimension / energy density is Lithium Polymer(LiPo). This kind of battery started appearing in consumer electronics

around 1995, and had been highly used by the RC community where the advantages of both lower weight and high power deliver justify their price.

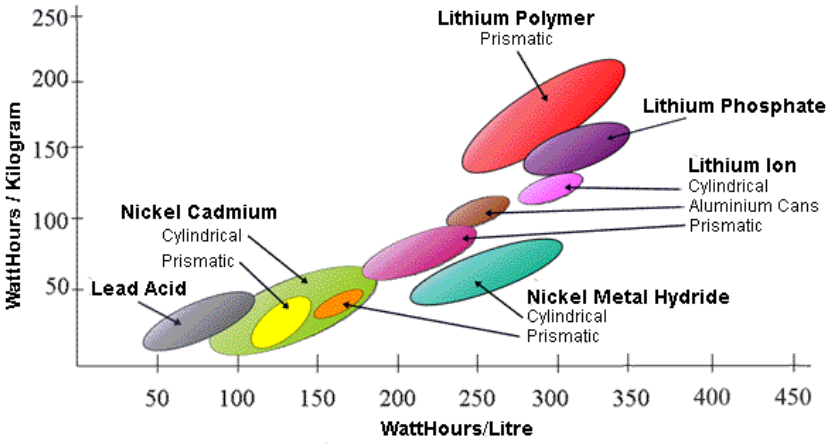

Figure 3.2: Relative Energy density of some secondary cell chemistries. [17]

For more information regarding LiPo batteries, check appendix A.

Two different batteries were chosen for this project to check which of them fits better to the aircraft needs. Table 3.1 shows the specifications of both chosen batteries.

Product Specifications		
	Turnigy 3300mAh	Zippy 5000mAh
Capacity	3300mAh	5000mAh
Configuration	3SP1 11.1V	4SP1 14.8V
Peak discharge	40C	20C
Weight	297g	469g

Table 3.1: LiPo characteristics.

3.1.2 Propulsive System

The propulsive system in this kind of applications is usually composed of a pair motor/propeller. In this case, and since the motors used need special control, it was also included in this block the ESC which will be explained in more detail during this section.

Propeller Multirotor aircrafts use propellers as part of their propulsive system. A propeller is a mechanical device formed by two or more blades that spins around a shaft. It provides propulsive force by converting the torque of its power source into thrust, and rotational speed into linear speed.

There are several characteristics to define a propeller such as diameter, pitch, number of blades, bore, etc. Although it is important to design the propeller according to the specific needs, the most important parameters are diameter (D) and pitch (P).

Diameter is the distance between tip to tip, while pitch measures the displacement a propeller makes in a complete revolution (360^{o}). The concept of pitch is the same of other mechanical devices, like screws. In fact, sometimes a propeller is referred as an airscrew. The

size is usually expressed in the form `Diameter x Pitch`, measured in inches. For example, a 10x4 propeller, has a 10 inches diameter and a pitch of 4 inches.

Pitch depends on the angle the blade makes from the center to the tip. Since the speed is highest at the tip and lower near the hub, the blade angle also changes in order to produce the same amount of thrust at different points.

If the propeller has a fixed blade angle it is known as fixed-pitch propeller. Since the fixed-pitch propeller achieves the maximum performance at a given combination of RPM and airspeed, it is not excellent for both high speed and low speed aircrafts. Nevertheless, this type of propeller is far more used in this type of application due to its simplicity, low weight and low cost.

The other type of propeller is called variable-pitch or constant speed propeller, and allows changes on the angle of attack of the blade. Although not widely used, there are some cases of success using this type of propeller.[18]

For this project the propellers were chosen according to the motor specifications (current drawn) and to match the total thrust goal that we want to reach. Two types of propeller have been ordered allowing to perform some tests to find the best diameter x pitch relation to the motors, while fulfilling the minimum thrust specification for this project. The propellers ordered were 10x45 and 9x47 Slow-Fly (SF). Also, the chosen propellers have different colors in order to easily provide visual feedback of which ones are rotating clockwise and counter-clockwise.

Motor The motors normally used in this kind of application are electric Direct Current (DC) motors. They can be brushed or brushless motor. BrushLess Direct Current Motor (BLDC) motors offer several advantages over the traditional brushed motors, including longer lifetime, reduced maintenance, higher torque per weight, higher torque per watt ratio, reduced noise and more efficiency. Brushed motors are cheaper, don't require additional electronics to control them, but need regular maintenance to change the brushes and are less efficient due to friction. For these reasons, and since this kind of equipment must be reliable, BLDC are far more used. For more information regarding brushless motors, please refer to appendix A.

Unlike brushed motors, the commutation in brushless motors is controlled electronically. This control is managed by an ESC module, that uses information about the rotor position and energizes the stator windings in sequence, thus producing rotation. The rotor position is estimated using Hall effect sensors or measuring the Electromotive force (EMF) voltage. The EMF is generated by each winding, is opposite to the main voltage supply and depends on the angular velocity of the rotor. For more information please refer to appendix A.

Most motors available at RC hobby stores have some information about their parameters, including kV (RPM per volt), maximum input voltage, maximum current, maximum power and some physical properties such as weight, shaft and motor case dimensions.

The motor used in this project was the Turnigy D2830/11 with the characteristics described in table 3.2. The motor is an outrunner BLDC that can handle high currents, excellent for producing high thrust.

Product Specifications	
K_v (rpm/V)	1000
Voltage	2S $\sim$ 4S (7.4V to 14.8V)
Max Power	210W
Weight	52g
Dimensions	30x28mm

Table 3.2: Motor characteristics.

Electronic Speed Controller As it was referred above, brushless motors need to be controlled externally in order to energize the windings in sequence. The electronic device responsible to do that job is called Electronic Speed Controller (ESC). The ESC module drive the 3-phase brushless motor by sending a sequence of signals causing rotation. It is required to know the position of the rotor to switch the control signals in the correct order.

Most of commercial ESC have information about their characteristics and features. The most important parameter is the maximum current that it handles. Usually, manufacturers give information about constant current and burst current. The first one is the current that the ESC can handle indefinitely, while the other is the value that it can handle for short periods of time, typically less than 20 seconds. Other given specification is the battery supported (range of input voltage) and physical dimensions. Some ESC have extra features:

- **Brake:** It forces the motor to stop spinning since the speed controller stops delivering power. To do so, the ESC puts a load between the motor terminals forcing it to stop.

- **Soft Start:** The control will go from off to full throttle slowly, instead of instantly. This is important for aircrafts that use gear system, avoiding the damage of such component.

- **BEC:** BEC it is typically a $5V1A$ regulator integrated in the ESC that provides power to the electronic circuits, such as the receiver and servos. This feature is important because removes the need to have extra batteries to power the electronics. It leads to a costless and weightless aircraft.

- **Low Cut-Off:** This feature measures when a battery is almost depleted, reserving some power for the radio, reducing the power delivered to the motors gradually or even instantaneously.

- **Optical Isolation:** Isolates the ESC from the receptor.

The ESC uses a microcontroller to manage the signals to send to the motor and read input signals from the controller board. The controller board controls the motors through the ESC using pulse width modulation Pulse Width Modulation (PWM).

Like other types of RC equipment, the ESC data sheets usually don't provide some important information. For instance, some manufacturers don't reveal the refresh rate of the signals applied to the motor, which can be a problem when we want to perform close loop control.

For this project the chosen ESC was the Turnigy Plush 30A, with the specifications described at table 3.3.

Product Specifications	
Const. Current	30A
Burst Current	40A
BEC	5V/2A
LiPo Cells	$2 \sim 4$
Weight	25g
Dimensions	45x24x11mm

Table 3.3: Electronic Speed Controller characteristics.

This ESC can handle high current (30A) which is enough for the motors ordered and with a good margin to upgrade to new powerful ones if necessary.

3.1.3 Remote Control and Telemetry

This block is responsible for transmitting to a Personal Computer (PC) the actual state of the vehicle and gives the user the possibility of controlling it.

Remote Controller In this first phase of development, before turning the vehicle fully autonomous, it is very important to give the user the possibility of piloting the vehicle. On one hand, it is required to perform flight tests to realize how the control board stabilizes the vehicle. On the other hand, on more advanced tests where the vehicle is able to perform some autonomous tasks, it is very important to have a remote control for safety reasons if something goes wrong. For these reasons it was mandatory to purchase a commercial solution to pilot the vehicle. The chosen solution was the Turnigy 9x Transmitter with 8 channel receiver, because is highly configurable, being able of using it on different multirotor configurations, helicopter and airplanes. It uses 2.4GHz as transmitter frequency, providing fast reaction times and interference free control. The fact that has 8 channels is also very important for future versions of the vehicle because adds the possibility of controlling other components in the aircraft like servo motors for video cameras operation, since only 4 channels are required to ensure basic flight control. Figure 3.3 represents how the control inputs are related with the quadrotor movements. Note that it was used Mode 2 for control inputs, which means that throttle and rudder are on the left stick while aileron and elevator on the right stick.

Bluetooth interface with PC Another important feature for this kind of applications, specially the academic ones, is the possibility to have visual feedback of the actual state of the vehicle and their sensors. This is possible by sending periodical data frames to a ground station to display the data. This section will only refer to the components needed to perform telemetry, while the communication protocol and graphical user interface to display the data will be explained in sections 3.2.3 and 3.3.4, respectively.

The solution used to transmit data to the PC was a bluetooth module connected to the UART port of the control board. This enables communication to the ground station without any physical connection attached to the vehicle. The chosen module was the RN-42 from Roving Networks which is highly configurable in terms of baudrate speeds and provides a distance range of 20m.

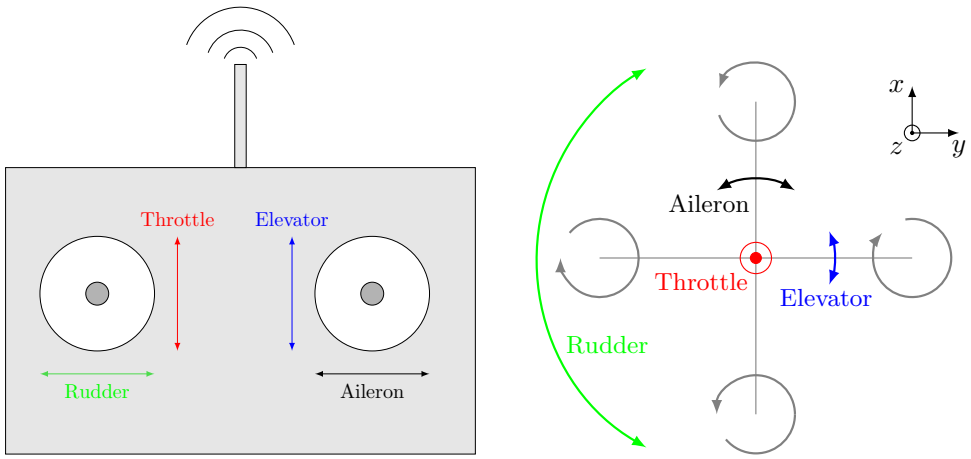

(a) Remote controller inputs. (b) .

Figure 3.3: Remote controller actions applied at the quadrotor.

3.1.4 Sensing and Control Board

The sensing and control board is responsible to read, process and act on the other blocks of the system. It is composed of a processor unit, a set of sensors and communication routes to other blocks.

Motion Sensor For this kind of application it is required the use of an Inertial Measurement Unit (IMU) composed of an accelerometer, a gyroscope and a magnetometer. The output of one of these devices, or the combination of multiple outputs give us the aircraft orientation and attitude estimation. This information is crucial to have a precise and stable flight. For detailed information regarding accelerometer, gyroscope and magnetometer characteristics and operation please refer to appendix A.

The basic circuit chosen for the IMU implementation was the Invensense MPU-6050[1] which combines a 3-axis Microelectromechanical systems (MEMS) gyroscope and a 3-axis MEMS accelerometer. This device has the obvious advantage of combining 6 Degrees of Freedom (DOF) in a single package avoiding misalignments on the axis of the devices and waste of space on the PCB. Although the chosen product was the MPU-6050, the first choice was the MPU-9150 from Invensense which also provides magnetometer readings supplying a single package with 9 DOF. Unfortunately current financial control prevented the arrival of the device in time for this project.

Since the MPU-6050 doesn't provide magnetic heading measures, the use of a magnetometer urged. The chosen component was the 3-axis magnetometer HMC5883L from Honeywell[2] which provides offset cancellation and a 12-bit Analog to Digital Converter (ADC) enabling a 1^{o} to 2^{o} compass heading accuracy.

Barometer It is a device with applications in meteorology that can measure atmospheric pressure. A barometer can be used to implement an altimeter. As altitude increases, at-

[1] `http://www.invensense.com/`
[2] `http://honeywell.com/`

mospheric pressure decreases because there are fewer air molecules[19]. A good resolution barometer can provide a good estimate of the altitude of the quadrotor, which is useful to control the aircraft. The chosen device for this application was the BMP085 from Bosch Sensortec[3]. This sensor is an excellent high-resolution sensor for measuring absolute atmospheric pressure, very flexible, with several modes of resolution and update rates, fast response and low power. It uses I^2C as communication protocol, making it easy to use in the controller board. However, it also presents some disadvantages, like the very complex calibration routine that needs to run for each sample and no possibility for changing its I^2C address.

For best results, specially outdoors, it is important that the barometer is in a sealed, insulated chamber. Otherwise, a smooth output should not be expected.

Processing Unit To process all the data received from the sensors, perform closed loop control and act on the motors, a processing unit is needed. The experience the author have acquired during the student years was based on Microchip PIC microcontrollers[4], which are also widely used in the ATRI group. Therefore, the manufacturer choice naturally fell on the Microchip. Nevertheless there were some requirements that constrained the choice of the model:

- At least 8 PWM outputs in order to be capable of controlling an octorotor.
- Inter-Integrated Circuit (I^2C) protocol to communicate to the other sensors.
- High number of I/O and Analog ports.
- High program memory capacity.
- At least 4K of RAM due to the complexity of some of the implemented fusion sensor filters, that require the buffering of several registers.

The choice fell on the dsPIC33EP512GP806 mainly because it has more than 8 PWM outputs, which is not very common in much of the PIC microcontrollers. Other advantage of the dsPIC33EP512GP806 is the remappable pins which turn the PCB layout design more simple and flexible.

Commercial Control Board One of the objectives of this dissertation is to design and build a custom control and stabilization board. However, it is important to have a commercial board to do some performance test comparisons and perform the first flight tests to validate the rest of the components of the system. Since the board is intended to only serve as an experiment product to be replaced in a near future, it was decided to order a cheap but versatile board. The choice was the HobbyKing KK 2.0[5] control board that offers the possibility to control quadrotor, hexarotor or even octorotor with a really easy way to configure. It has a dual chip 3 axis gyroscope and a single chip 3 axis accelerometer.

The use of a commercial board as the main controller for this dissertation was not an option. Usually they are closed-source and do not allow hardware changes. There are some cases of open-source devices developed by the RC community, however most of them use

[3] http://www.bosch-sensortec.com/

[4] http://www.microchip.com/pagehandler/en-us/products/picmicrocontrollers

[5] http://www.hobbyking.com/hobbyking/store/__24723__hobbyking_kk2_0_multi_rotor_lcd_flight_control_board.html

Atmega microcontrollers (which the author has no experience), are expensive and difficult to find in Europe.

3.2 Hardware Implementation

Section 3.1 shows the implemented architecture of the system, and describes the materials used for this project and their characteristics. This section will explain in detail how everything was implemented using the architecture and materials described before.

3.2.1 Power System

The LiPo battery is responsible to power all the electrical components in the vehicle, despite the fact that only some of them are directly connected to the battery. The motors are powered through the ESC with the nominal voltage of the battery, while the control board is powered through the ESC BEC system with 5V. The sensing and control board has a voltage regulator to 3.3V to power most of the sensors. The remote controller and bluetooth are powered with 5V from the sensing and control board.

Since all the ESC modules need to be supplied by the battery, it is necessary to find a practical way to do the connections to the LiPo without creating a mess of wires. It is also important to have the possibility of disconnect the ESC, which means that soldering it all is not a viable solution. The implemented solution was a power distribution board, that splits the power through all the controllers leading to a simple and easy to disassembly system. Figure 3.4 shows the power distribution board.

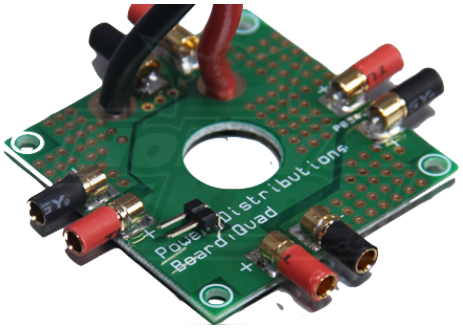

Figure 3.4: Power distribution board.

3.2.2 Sensing and Control Board

The sensing and control board is responsible for almost all the processing in the aircraft. Figure 3.5 presents the architecture of the board describing the sensors used, how they interact with the processing unit and how signals from/to the PC are interfaced. The design of this module should take into account a set of requirements, including:

- It should be small and lightweight
- It should be designed to support other aircraft configurations (hexarotor / octorotor).

- It should have additional ports to be capable of adding more hardware/sensors in the future (scalability capacity).

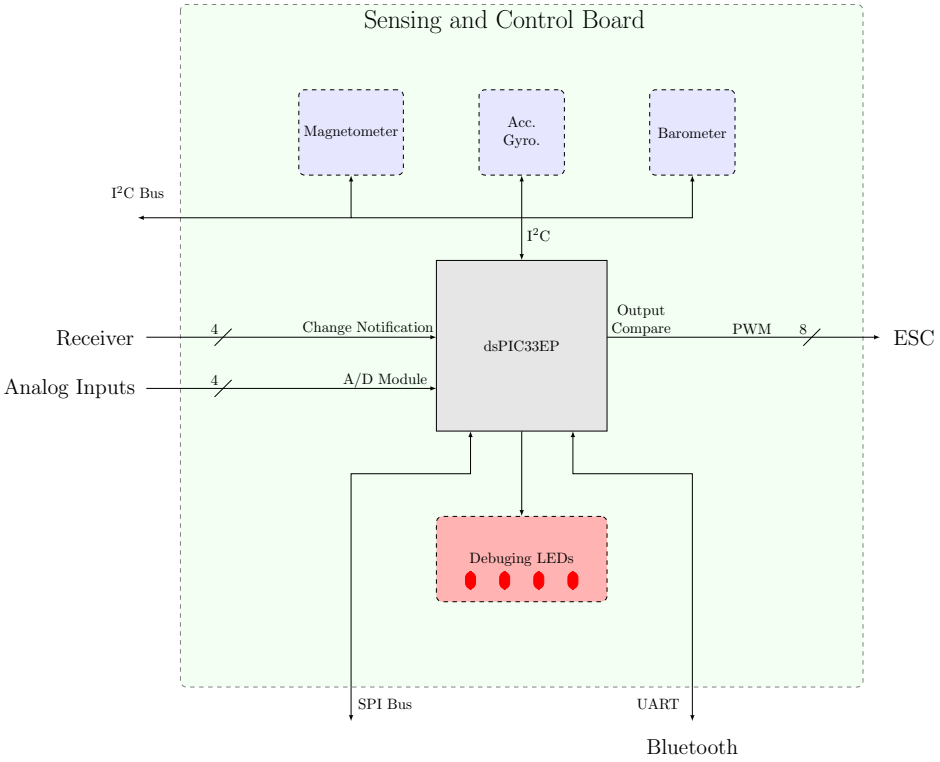

Figure 3.5: Overview of the sensing and control board architecture

Pulse Width Modulation to Electronic Speed Controller The ESC which is responsible to act on the motor, requires a PWM input that specifies how much the motor should rotate. The PWM should be similar to the ones generally used in servo motors, where the active state change from $1ms$ to $2ms$ meaning that the motor is stopped or rotating at it maximum force, respectively. These time values lead to a maximum PWM frequency of 500Hz. In this project the PWM frequency used was $400Hz$. The PWM is generated using the Output Compare module of the microcontroller which provides 8 PWM signals, giving the possibility of controlling an Octorotor.

Receiving Data from Radio Receiver The Turnigy 9x comes with a 8-channel receiver that once again, came with very few information about how it works, and none information about the output signals of the receiver. After some experiments using the oscilloscope to measure the signals, it was uncovered that they are similar to the ones applied in servo motors. Every command (throttle, rudder, elevator and rudder) outputs in a different channel with a PWM signal of $50Hz$ of frequency and active state from $1ms$ to $2ms$ where $1,5ms$ is the neutral position.

Note that the signals outputted from the receiver are not burst at the same time. Instead they are sequential occupying the $20ms$ time slot were the first channel has a signal of $1ms$ to

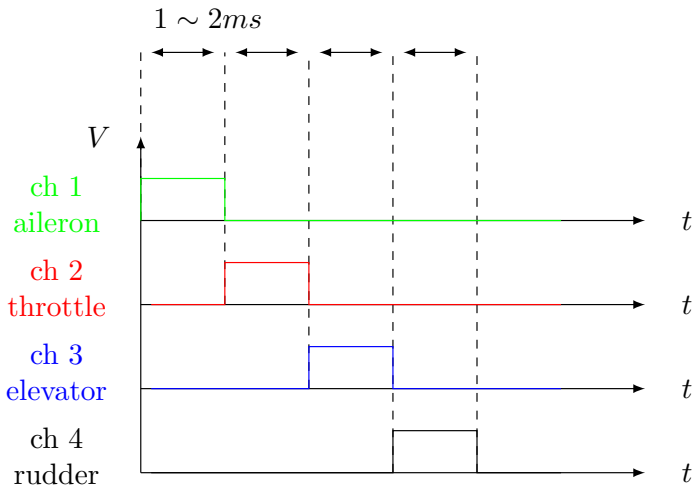

Figure 3.6: Distribution of the control signals by the different channels.

$2ms$, while the second one starts right after first one stops, and so on for the other channels (TDM). Figure 3.6 describes how the channels are related with different manoeuvres and it respective order. In order to detect and process all these signals, it was used the Change Notification module of the microcontroller.

Extra I/O and Analog Inputs As represented in figure 3.5 some pins are reserved for extra components connection that can be attached in the near future. In that set of pins are 4 digital or analog pins, a Serial Peripheral Interface (SPI) port and the I^2C bus. Also an extra UART is reserved to a future GPS module connection. A set of four LEDs were also added to the board for debugging purposes.

Control Board Printed Circuit Board Design The board was designed using the free PCB software design CadSoft Eagle [6].

The layout has the following design requirements:

- It must be square of 5cm for 5cm to match with the power distribution board and structure bolts.
- The connectors must be compatible with the ones used by the commercial components.
- Other special cares in design layout advised by the components manufactures in their datasheets.

The circuit schematics and PCB layout are shown in appendix B. Before sending the board to production, it was designed a 3D model using EagleUP[7] to check if any big fault was detected. Figure 3.7 compares the final version of the control board with the designed using the 3D CAD software.

[6] `http://www.cadsoftusa.com/`
[7] `http://eagleup.wordpress.com/`

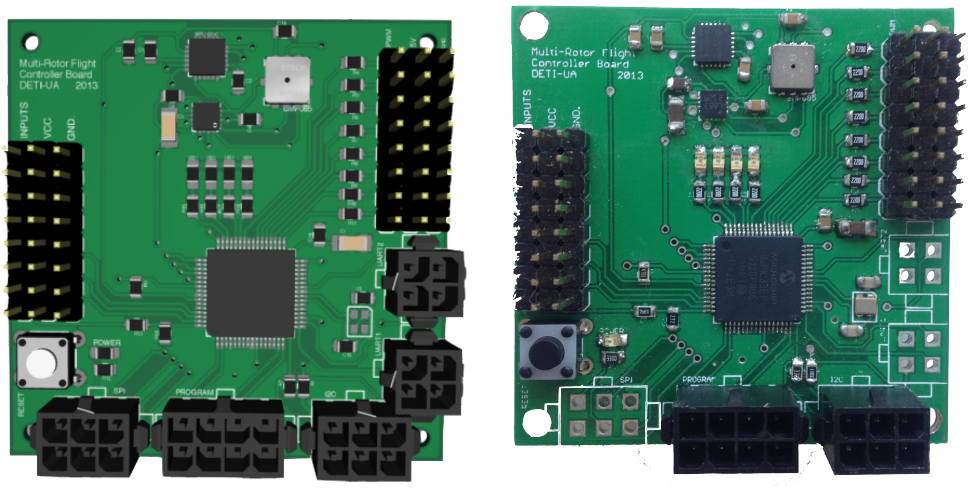

(a) 3D CAD Model of the control board. (b) Control board after being manufactured.

Figure 3.7: 3D CAD model and real board comparison.

3.2.3 Telemetry and Communication Protocol

When dealing with this kind of applications where the number of components to read and to act upon is high, it is difficult to perform tests and debug only based on simple actuators like LED or through text-based serial port interfaces. With the aim of simplifying these tasks and thinking of developing a Graphical User Interface (GUI) it was implemented a communication protocol between the sensing and control board and the PC through the UART interface and the bluetooth module.

Communication Model The solution adopted is based on the use of small serial commands that contain information only about a single sensor or actuator, allowing the external device to sense or act on a single component if desired. Therefore the frames used to send information from the control board to external devices follow the structure described in figure 3.8.

Figure 3.8: Communication frame example.

The number of bytes per frame depends on what kind of data transfer is occurring, since the number of data bytes varies from sensor to sensor. The frame fields are composed of ASCII characters. The first byte of the frame is the Start of Frame Delimiter (SFD), denoted by the % character, and it notifies that a new message is starting. The message is then identified by fetching the ID field followed by the NDB that has the Number of Data Bytes of that message. The message is terminated with a checksum byte that enables verification of the integrity of the received message.

The checksum is the two's complement of the sum of the values of all fields of the communication frame. It is calculated by adding together all the frame field values (two hexadecimal ASCII digits converted to their equivalent 8-bit binary value), then leaving only the least significant byte of the result, and making the two's complement.

Types of Messages The communication is bi-directional, so messages flow from the control board to the PC and vice-versa. The messages that flow from the control board to the PC are all about the system actual state, like sensor values, system information, battery voltage, motor PWM values and remote control sticks current values. The list below, has a complete description of all the messages used:

- **Accelerometer:** Raw values of the three axes (A_x, A_y and A_z).
- **Gyroscope:** Raw values of the three axes (G_x, G_y and G_z).
- **Magnetometer:** Raw values of the three axes (H_x, H_y and H_z).
- **Barometer:** Altitude value in meters calculated from barometer readings.
- **Angle estimation:** Current attitude estimation of the vehicle (Roll, Pitch and Yaw angles).
- **Motors:** Current applied PWM values for all four motors.
- **Remote Control:** Current stick values of the remote control (Throttle, Rudder, Elevator and Aileron).
- **Info:** Info values of the current state of the vehicle, like battery voltage, if it is armed or not and if remote control and control algorithm are turned on or off.

On the other hand, the messages that flow from PC to the control board are the following:

- **Motors:** Change the PWM applied to the four motors.
- **Arm / Disarm:** Arm or Disarm the vehicle.

For detailed information about the message frames, containing number of data bytes, identifiers and the order of the bytes, please refer to appendix C.

3.2.4 Hardware Summary and First Prototype Assembly

As this project targets the development of an autonomous version, more and more sensors will be attached to the system, and these kind of modifications have to be carefully studied and analyzed before being implemented in order to avoid compatibility issues. For this reason, all the parts were designed in a 3D CAD Software, giving the possibility of studying future modifications to the current model. This gave the opportunity to find if all the parts matched together before moving on to the final assembly. Figure 3.9 shows the CAD model, while figure 3.10 shows the aircraft assembled.

The total weight of the prototype is 1115g.

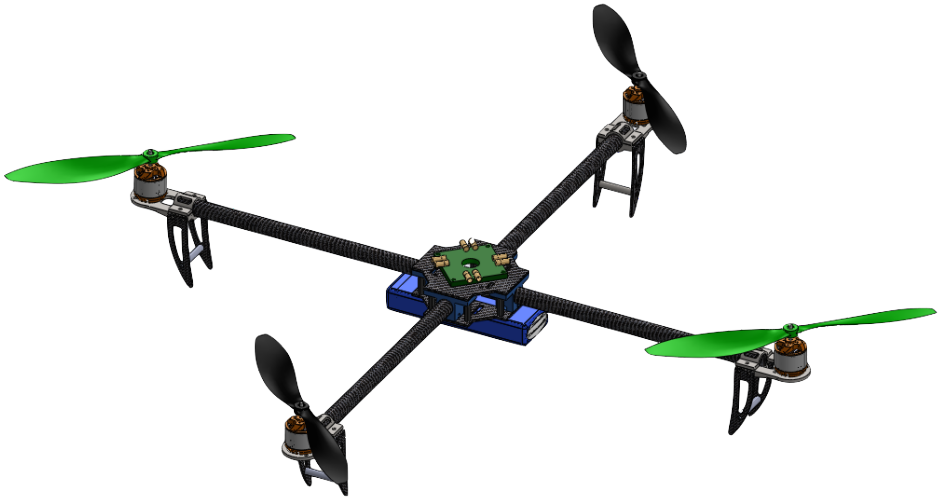

Figure 3.9: CAD representation of the prototype assembled.

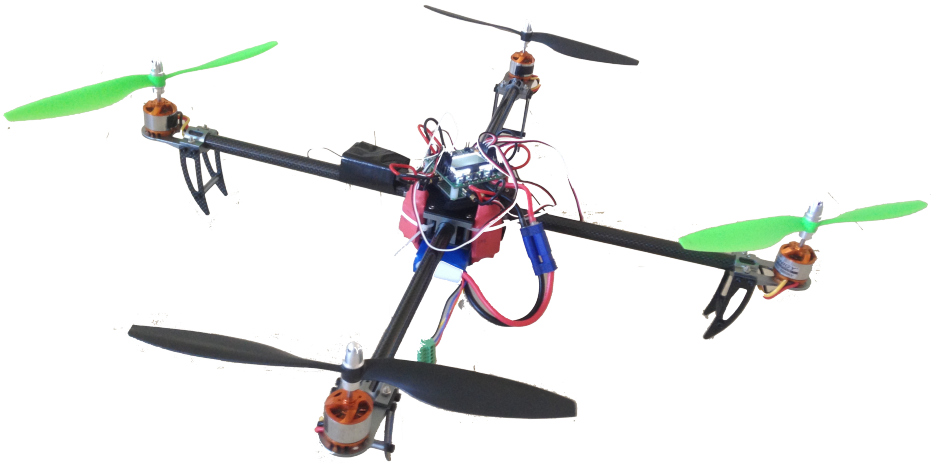

Figure 3.10: Photo of the quadrotor after assembled.

3.3 Software Implementation

In this section, an overview of the software basic structure and the way it was implemented will be given. The adopted implementation can be divided in two blocks as described in figure 3.11: Initialization/calibration and main loop. The first one occurs only one time during lifetime cycle and is responsible to initialize and calibrate all the sensors and actuators. The second one is the main loop and is always processing new data values and acting on the system. These two blocks can be divided in smaller ones that will be explained in detail in this section. The Sensor Fusion and Control blocks, due to their complexity, will be explained in detail in chapter 4.

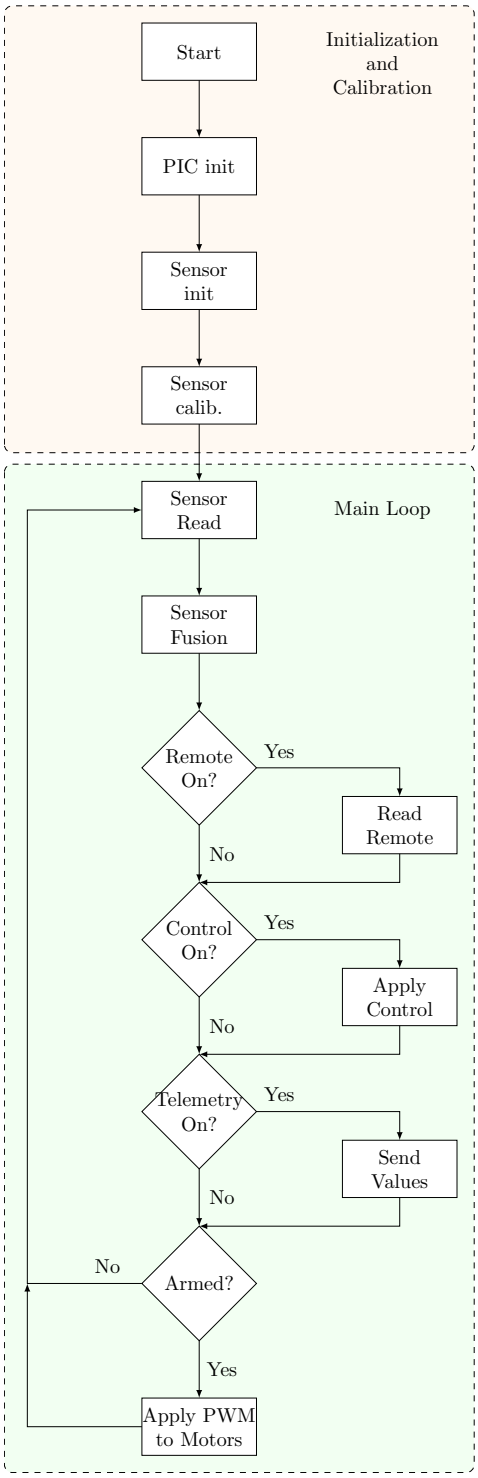

Figure 3.11: Flowchart of the main actions of the developed software.

3.3.1 Microprocessor Initialization

As any other application that involves a microcontroller as a processing unit, it is necessary to perform some basic configurations as I/O and specific modules initialization. In this project the configurations are as follows:

- Configure digital ports as inputs or outputs.
- Configure analog ports.
- Configure timers to notify the system to perform some action or just add a delay.
- Configure communication protocols, such as UART and I^2C.
- Configure Output Compare module to the ports where the ESC is connected.
- Configure the Change Notification module to the ports where the receiver is connected.

3.3.2 Sensors initialization and reading routines

In order to initialize, calibrate and read sensors there were developed the necessary libraries. They are developed in C language and contain methods to perform the necessary steps for initializing, calibrating and reading from all registers.

MPU-6050 The MPU-6050 initialization is composed of some basic configurations of the accelerometer and gyroscope. The full scale range of both accelerometer and gyroscope were programed to the minimum allowed($\pm 2g$ and $\pm 250^\circ/s$ respectively) in order to have better resolution of the measured signals.

If no problem occurred during configuration, it is possible to fetch the sampled data from the accelerometer and gyroscope data registers. This can be done reading sequentially the data registers obtaining the raw value for all the accelerometer and gyroscope axis. The values for each axis are in two 8-bits separate registers, which requires to merge the 8 MSB with the 8 LSB forming an 16 bits signed integer. For the configurations above, the accelerometer values are outputted as $16384 LSB/g$ and the gyroscope as $131 LSB/(^\circ/s)$, which means that to get the real value, the measured one needs to be divided by LSB, such as the example at equation 3.1. By default, the MPU-6050 works in a continuous mode, updating the registers always with the latest measured value.

$$\text{Acc}_g = \frac{\text{Acc}_{\text{register}}}{16384} \qquad \text{Gyro}_{^\circ/s} = \frac{\text{Gyro}_{\text{register}}}{131} \tag{3.1}$$

Magnetometer The magnetometer also needs some initialization procedures. The full scale range was set to $0.88Ga$ (the minimum value) to have a measured signal with better resolution. It is also configured to continuous measurement mode, where the readings are made in a continuous way replacing the values in the register with the new ones.

The method to perform readings is similar to the MPU-6050. The microcontroller accesses the registers where are stored the last readings, merging two 8 bits values into a single 16

bits integer. Then the value needs to be divided by the LSB to convert the value to gauss (equation 3.2.) This procedure needs to be performed for the 3-axis.

$$\text{Mag}_{\text{gauss}} = \frac{\text{Mag}_{\text{register}}}{1090} \tag{3.2}$$

Barometer The BMP085 has a non trivial calibrating and reading procedure which will not be explained here in detail. For further information please refer to the product user manual or appendix C. The reading process involves reading uncompensated temperatures and uncompensated pressure values to process the true pressure value which can be applied to equation 3.3 in order to obtain the absolute altitude in meters.[20]

$$altitude = 44330 \times \left(1 - \left(\frac{p}{p_0}\right)^{\frac{1}{5.255}}\right) \tag{3.3}$$

where p is the measured pressure and p_0 the sea level pressure.

Sensor Calibration Routines Some sensors need to be calibrated to provide useful readings to the processor. To calibrate the sensors the following tasks need to be accomplished:

- Put the control board in a stable and horizontal place.
- Perform a high number of readings and apply a mean to those values.
- Subtract the averaged values to the expected values to get the offsets.

After the offset values are found, every time the processor gets a new reading from the sensors it needs to subtract the offsets to get the real values. Since the accelerometer offsets seem to be consisting over the time, they can be stored in the flash memory removing the need to calibrate the sensor every time the vehicle is used. This is very important because sometimes it can be difficult to find a leveled place to park the vehicle before flying.

3.3.3 Safety procedures

Since this kind of applications can be very dangerous for human interaction, due to the propellers rotation speed and sharp material, some safety procedures are required. It is mandatory to have ways to enable or disable the propulsive system via software. In this project it was adopted the armed/disarmed flag that enables or disables the system on top of any other orders. There are two ways to enable/disable the system:

- **Remote Controller:** If a user turns on the vehicle with the throttle stick not in the rest position, the system must not start immediately, since that would put in risk the user safety. In order to arm the vehicle, the user must push the throttle stick to the minimum and the rudder stick to the maximum right position during 1 second. This will avoid the vehicle from start working by mistake, and will guarantee that after it is armed it will not starts rotating because the throttle is at rest position.
- **Graphical User Application:** As can be seen in section 3.3.4 the GUI has a toggle button that can arm/disarm the vehicle. This button will not work if the remote controller is active and does not have the throttle stick at minimum position.

Other safety procedures were introduced in the software to avoid some unexpected behaviors of the quadrotor. If the control board senses that the vehicle is tilted more than 45 degree on the x-axis or y-axis the propulsive system will be turned off, because most likely the vehicle is uncontrolled and it will probably cause more damage if it continues working. Also, the propellers will only spin if the throttle stick is more than 10% active to avoid situations where the user wants to stop the vehicle, but the stick cannot reach an exact zero-throttle position.

3.3.4 Graphical User Interface (Quadrotor Ground Station)

The GUI is designed to provide the user with visual feedback of all the important data of the system and store logs of some of the values for future analysis. The GUI is connected to the system and provides the following information and features:

- Real-time attitude of the vehicle (Roll, Pitch and Yaw angles).
- Current PWM values applied to motors, with option to change them.
- Current position of the remote controller sticks.
- Current battery voltage.
- Toggle button to Arm/Disarm the aircraft.
- Graphs of the data of all sensors (accelerometer, gyroscope, magnetometer and barometer).
- Console mode where all the commands received in the serial port are printed.

For better organization, the GUI was divided in 3 tabs. At the top of the screen, and transversal to all the tabs, is placed the connection box where the user can choose the serial port, baudrate and connect to the quadrotor. At the bottom of the screen there is some important information that should be also transversal to all tabs, like battery voltage and if the quadrotor is armed or disarmed.

Quadrotor State This tab has all the information about the actual state of the vehicle and the necessary interaction to let the user connect to the aircraft as represented in figure 3.12. At the left of the screen information about the current position of the sticks of the remote control is represented, where 50% is the neutral position. At the center of the screen, information about the 4 motors is shown being possible to change the actual PWM applied to the ESC. At the right of the screen is placed the toggle button for arming / disarming the device. Finally, at the bottom of the tab is provided visual feedback about the current attitude of the aircraft by plotting an aircraft with the exact tilt position of the quadrotor.

Graphs The graphs tab displays in real-time a plot of all the sensors of the quadrotor including all axis of the accelerometer, gyroscope and magnetometer, and current altitude taken from the barometer. The graphs update their axis automatically to adjust to the signal. It was also included plots of Roll, Pitch and Yaw angles of the current quadrotor attitude.

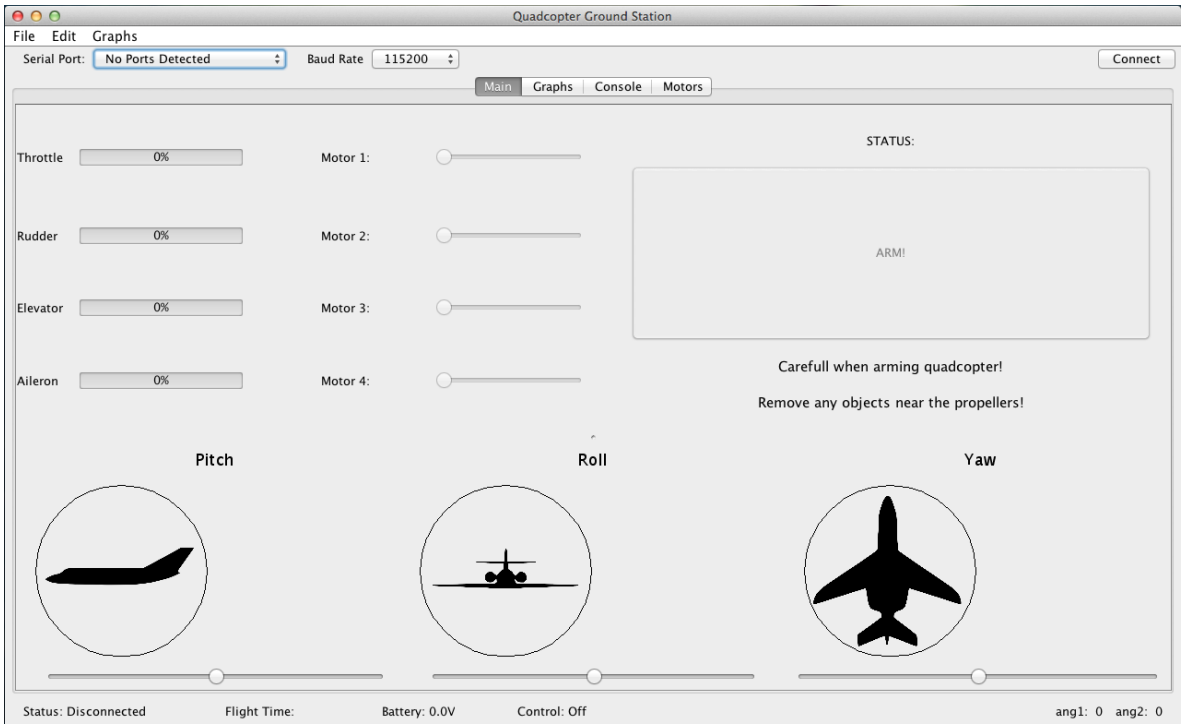

Figure 3.12: Quadrotor State tab of the GUI.

Console This tab was first used for debugging, and let the user view all the frames that were received from the quadrotor. It includes history, so when the transfer of information stops it is possible to roll back and view what happened before. It also lets the user to send frames to the quadrotor using the text box placed at the bottom of the tab.

3.4 Summary

In this chapter it was unveiled what were the components acquired to build this quadrotor, explaining in detail the function of each of them. The control board implementation was clarified, as well as the communication protocol.

It was also described the software organization and what are the relevant tasks for quadrotor control. It was also shown the Quadrotor Ground Station, that allow the user to have visual feedback from the device.

At this point, the materials were ordered and successfully assembled, creating the first quadrotor prototype. The sensing and control board is designed, tested and with basic operations implemented, such as controlling the actuators individually, or sending information to the Quadrotor Ground Station. The next step is to get estimations of the quadrotor attitude performing sensor fusion, and apply these values to a closed loop control algorithm.

Chapter 4

Sensor Fusion and Control

Two of the major blocks of this system are the sensor fusion and control algorithm. It is absolutely mandatory to have an excellent angle estimation and control algorithm in order to stabilize the quadrotor correctly. During this chapter, it will be explained how to measure the attitude angles of the quadrotor using different techniques from single sensor estimation to sensor fusion filters. Then, the applied control algorithm will be shown overviewing the implementation for different quadrotor layout configurations.

4.1 Tilt Measurement

4.1.1 Using Accelerometer

The accelerometer can measure inertial forces, but it can be also used to inclination sensing. This can be achieved by measuring the gravity and its projection on the accelerometer axis.

First let's see how to calculate the tilt in a single axis accelerometer like the one shown in figure 4.1. Referring to basic trigonometry, the output acceleration that x-axis produces is equal to the sine of the angle between the accelerometer x-axis and the plane orthogonal to the gravity vector. As figure 4.1 shows, for an ideal value of $1g$ for gravity the output will be:

$$A_x = 1g \times sin(\theta) \tag{4.1}$$

Since we are interested to get the angle using the accelerometer output value, we can use the following equation:

$$\theta = sin^{-1}\left(\frac{A_x}{1g}\right) \tag{4.2}$$

This approach uses only a single axis measurement and thus the calculated angle can only be accurate if the device is always orthogonal to the gravity vector. If we rotate the device about any other axis, it will reduce the magnitude of acceleration resulting in errors in the calculated tilt angle.[21]

Similarly it is possible to calculate the three angles if all the three axis are used. This makes it also possible to use the accelerometer in any position.

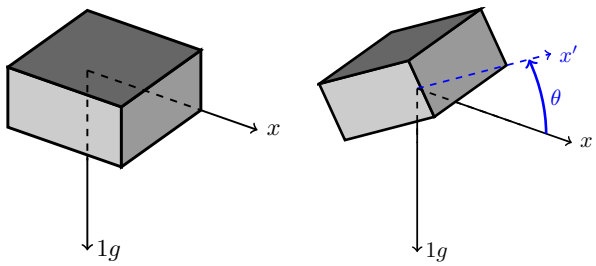

(a) No tilt (b) One axis tilt

Figure 4.1: Single axis tilting.

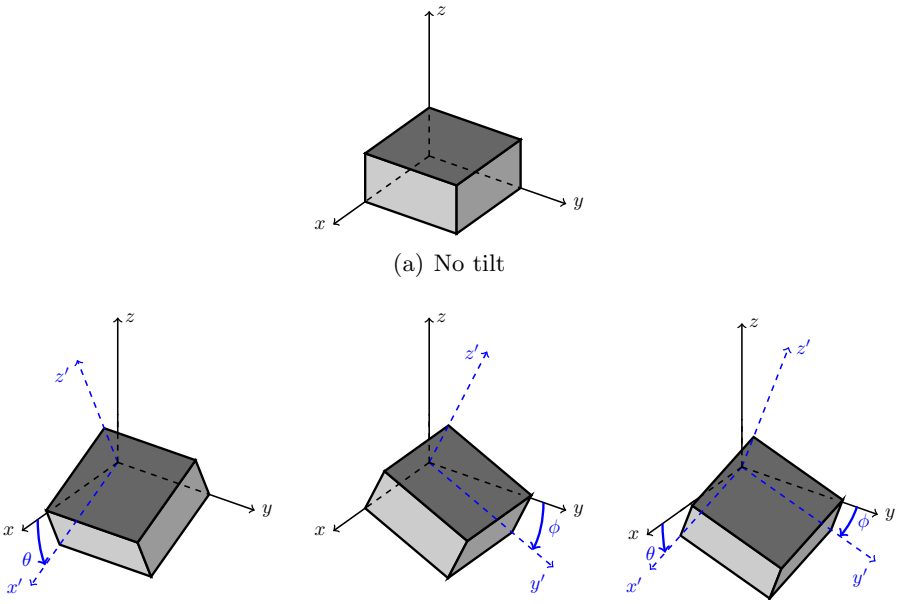

(a) No tilt

(b) Pitch tilting (c) Roll tilting (d) Pitch and Roll tilting

Figure 4.2: Angles for independent tilting sensing.

Figure 4.2 shows the angles for independent inclination sensing. These angles can be calculated as follows:

$$\phi = tan^{-1}\left(\frac{A_y}{\sqrt{A_x^2 + A_z^2}}\right) \tag{4.3}$$

$$\theta = tan^{-1}\left(\frac{A_x}{\sqrt{A_y^2 + A_z^2}}\right) \tag{4.4}$$

$$\psi = tan^{-1}\left(\frac{\sqrt{A_x^2 + A_y^2}}{A_z}\right) \tag{4.5}$$

It is important to know the sign of the X and Y accelerations in order to determine the quadrant of tilt because the outputs from the first and third quadrants will be the same, like

the outputs from the second and fourth quadrants. Knowing the quadrant of the outputs, it is possible to disambiguate equal outputs. Figure 4.3 shows the signs for all quadrants.

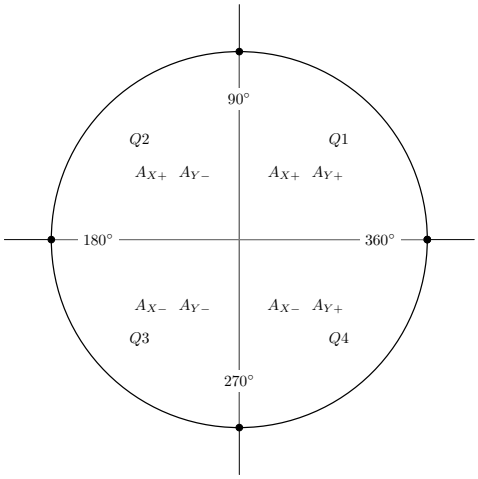

Figure 4.3: Signs of acceleration for quadrant detection.

Although it is possible to measure the tilt angles using the accelerometers, they are likely to be subject of high levels of noise. The accelerations due to motion will corrupt the measured direction of gravity.

4.1.2 Using Gyroscope

The gyroscope can measure angular velocity, which if initial conditions are known, can be integrated over the time to compute sensor orientation. Unlike accelerometers, gyroscopes are not affected by external accelerations which provide reliable output measures. However, when stationary, the gyroscope does not read perfectly zero. The integration of gyroscope measurement errors will lead to an accumulating error in the calculated orientation called drift error.

The Roll, Pitch and Yaw angles can be calculated using equations 4.6, 4.7 and 4.8, where g_x, g_y and g_z are the gyroscope readings of x-axis, y-axis and z-axis respectively.

$$\phi = \int g_x dt + \phi(0) \tag{4.6}$$

$$\theta = \int g_y dt + \theta(0) \tag{4.7}$$

$$\psi = \int g_z dt + \psi(0) \tag{4.8}$$

4.1.3 Tilt Compensation for Magnetometer

The magnetometer reads the Earth's magnetic fields in three axis, which allows to calculate the heading of the vehicle. If the aircraft is placed in an horizontal plane, where the roll and pitch angles are zero, then the heading can be calculated as follows:

$$\text{heading} = arctan\left(\frac{Y}{X}\right) \tag{4.9}$$

where the X and Y are the reading for the x and y axis respectively. As the aircraft rotates, the heading angle would change from 0°to 360°. Now as the aircraft is tilted, the roll and pitch angles change and the heading starts to take components in all of the 3 axis (x, y and z) and the heading needs now to be calculated in a different way. To use again the equation 4.9 to measure the heading, we need now to transform the X, Y and Z reading to an horizontal plane (X_h and Y_h) using equations 4.10 and 4.11[22].

$$X_h = X * cos(\phi) + Y * sin(\theta) * sin(\phi) - Z * cos(\theta) * sin(\phi) \tag{4.10}$$

$$Y_h = Y * cos(\theta) + Z * sin(\theta) \tag{4.11}$$

where ϕ and θ are the roll and pitch angles calculated from the accelerometer readings. Once calculated the horizontal heading values, equation 4.9 can be applied to find the vehicle heading.

4.2 Sensor Fusion

The accelerometer + gyroscope sensor fusion solves the problems mentioned above on single-sensor solution. Measuring the tilt angle only with accelerometer gives us noisy measurements, while only with gyroscope has drift errors. Working with both sensors helps fixing noise, drift and horizontal dependency. In order to fuse the data from the sensors a filter is needed. Next, it will be explained one of the most simple but accurate filters called Complementary Filter.

4.2.1 Complementary Filter

The Complementary filter[23] uses the accelerometer and gyroscope signals to estimate the quadrotor attitude angles.

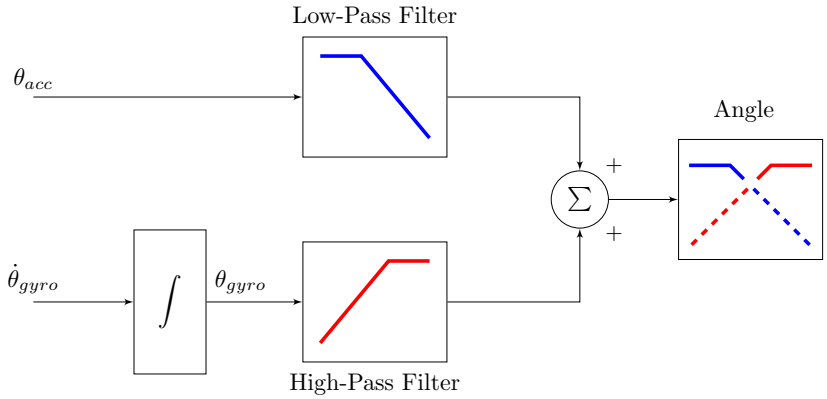

Figure 4.4: Complementary filter block diagram

Figure 4.4 shows us the block diagram of the complementary filter where the inputs are the accelerometer angle estimation and the gyro angular rate. The first one is low-pass filtered, reducing the influence of short term variations (noise) while maintaining the long term average. The second one is integrated in order to convert the angular rate to an attitude angle

estimation and then high-pass filtered to remove any long time drift. The two signals are then added together to create an estimate that combines the best part of both sensors.

$$\text{angle} = a \times (\text{angle} + \text{gyro} \times dt) + (a - 1) \times (\text{accelerometer}) \tag{4.12}$$

Equation 4.12 shows us the implementation of the complementary filter in discrete form. The first part of the sum corresponds to the gyro integration, while the second one match the accelerometer signal. The value a will determine the time scale of the high and low pass filters, and this value should be tweaked to give more weight to one of the sensors, depending on the quadrotor performance.

4.2.2 Sebastian Madgwick's IMU and MARG filter

This orientation filter[24] is applicable to IMUs consisting of 3-axis accelerometers and 3-axis gyroscopes, and a Magnetic, Angular Rate, and Gravity (MARG) implementation that incorporates magnetic distortion and gyroscope bias drift compensation. This filter uses quaternion representation, allowing accelerometer and magnetometer data to be used in an algorithm to compute the direction of the gyroscope measurement as a quaternion derivative. During this section we will overview some important aspects of the filter implementation, with information based in Madgwick's report.[24]

Quaternion representation To better understand how this filter works, let's take a look at quaternion representation, since it is widely used even on other aircrafts sensor fusion filters. A quaternion is a four-dimensional complex number that can be used to represent orientation of a body in a three-dimensional space. An orientation of frame B relative to frame A can be achieved through a rotation θ around ${}^{A}\hat{\boldsymbol{r}}$ defined in frame A. Figure 4.5 shows the rotation where $\hat{\boldsymbol{x}}_A$, $\hat{\boldsymbol{y}}_A$, $\hat{\boldsymbol{z}}_A$, $\hat{\boldsymbol{x}}_B$, $\hat{\boldsymbol{y}}_B$ and $\hat{\boldsymbol{z}}_B$ define the axis of frame A and B respectively. The quaternion that describes this orientation is shown in equation 4.13, where the following notation is used: a leading super-script denotes the reference frame while the leading sub-script denotes the frame being described. For example, ${}^{A}_{B}\hat{\boldsymbol{q}}$ describes the orientation of the frame B relative to frame A and ${}^{A}\hat{\boldsymbol{r}}$ is a vector described in frame A.

$${}^{A}_{B}\hat{\boldsymbol{q}} = \begin{bmatrix} q_1 & q_2 & q_3 & q_4 \end{bmatrix} = \begin{bmatrix} cos\frac{\theta}{2} & -r_x sin\frac{\theta}{2} & -r_y sin\frac{\theta}{2} & -r_z sin\frac{\theta}{2} \end{bmatrix} \tag{4.13}$$

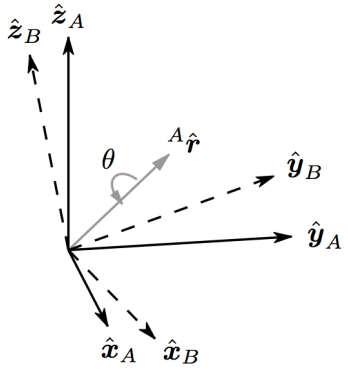

Figure 4.5: Rotation from A to B with respect to ${}^{A}\boldsymbol{r}$.

It is possible to perform some mathematical operations with quaternions. The quaternion conjugate, denoted by *, can be used to swap the relative frames described by an orientation defined as equation 4.14.

$$ {}^{A}_{B}\hat{\boldsymbol{q}}^{*} = {}^{B}_{A}\hat{\boldsymbol{q}} = \begin{bmatrix} q_1 & -q_2 & -q_3 & -q_4 \end{bmatrix} \tag{4.14} $$

The quaternion product can be used, using the Hamilton rule and defined as equation 4.15 that shows the product of two quaternions $\boldsymbol{a}$ and $\boldsymbol{b}$. A quaternion product is not commutative: $\boldsymbol{a} \otimes \boldsymbol{b} \neq \boldsymbol{b} \otimes \boldsymbol{a}$

$$ \boldsymbol{a} \otimes \boldsymbol{b} = \begin{bmatrix} a_1 & a_2 & a_3 & a_4 \end{bmatrix} \otimes \begin{bmatrix} b_1 & b_2 & b_3 & b_4 \end{bmatrix} = \begin{bmatrix} a_1 b_1 & -a_2 b_2 & -a_3 b_3 & -a_4 b_4 \\ a_1 b_2 & +a_2 b_1 & +a_3 b_4 & -a_4 b_3 \\ a_1 b_3 & -a_2 b_4 & +a_3 b_1 & a_4 b_2 \\ a_1 b_4 & +a_2 b_3 & -a_3 b_2 & a_4 b_1 \end{bmatrix}^{T} \tag{4.15} $$

A three-dimensional vector can be rotated by a quaternion using the equation 4.16, where ${}^{A}\boldsymbol{v}$ and ${}^{B}\boldsymbol{v}$ are the same vector but in different frames (A and B respectively), where each vector contains a 0 inserted as the first element to make them 4 element row vectors.

$$ {}^{B}\boldsymbol{v} = {}^{A}_{B}\hat{\boldsymbol{q}} \otimes {}^{A}\boldsymbol{v} \otimes {}^{A}_{B}\hat{\boldsymbol{q}}^{*} \tag{4.16} $$

The orientation can be defined by the rotational matrix described in equation 4.17.

$$ {}^{A}_{B}\boldsymbol{R} = \begin{bmatrix} 2q_1^2 - 1 + 2q_2^2 & 2(q_2 q_3 + q_1 q_4) & 2(q_2 q_4 + q_1 q_3) \\ 2(q_2 q_3 - q_1 q_4) & 2q_1^2 - 1 + 2q_3^2 & 2(q_3 q_4 + q_1 q_2) \\ 2(q_2 q_4 + q_1 q_3) & 2(q_3 q_4 - q_1 q_2) & 2q_1^2 - 1 + 2q_4^2 \end{bmatrix} \tag{4.17} $$

A more intuitive way for human perception to deal with this operations is the use of Euler Angles. A rotation of frame B can be described by sequential rotations, from alignment with frame A, ϕ (Roll) around $\hat{\boldsymbol{x}}_B$, θ (Pitch) around $\hat{\boldsymbol{y}}_B$ and ψ(Yaw) around $\hat{\boldsymbol{z}}_B$. The Euler angle representation of ${}^{A}_{B}\hat{\boldsymbol{q}}$ is defined by equations 4.18, 4.19 and 4.20.

$$ \phi = atan2(2q_3 q_4 - 2q_1 q_2, 2q_1^2 + 2q_4^2 - 1) \tag{4.18} $$

$$ \theta = -sin^{-1}(2q_2 q_4 + 2q_1 q_3) \tag{4.19} $$

$$ \psi = atan2(2q_2 q_3 - 2q_1 q_4, 2q_1^2 + 2q_2^2 - 1) \tag{4.20} $$

Orientation from angular rate A three-axis gyroscope will measure angular rate about the axes of the sensor. If the terms are arranged in vector form named ${}^{S}\boldsymbol{\omega}$, the quaternion derivative can be calculated as equation 4.22.

$$ {}^{S}\boldsymbol{\omega} = \begin{bmatrix} 0 & \omega_x & \omega_y & \omega_z \end{bmatrix} \tag{4.21} $$

$$ {}^{S}_{E}\dot{\boldsymbol{q}} = \frac{1}{2} {}^{S}_{E}\hat{\boldsymbol{q}} \otimes S\boldsymbol{\omega} \tag{4.22} $$

The orientation of the earth frame relative to the sensor frame can be computed integrating the quaternion derivative provided that the initial conditions are known like shown in equations 4.23 and 4.24 .

$$\overset{S}{E}\dot{\boldsymbol{q}}_{\omega,t} = \frac{1}{2}\overset{S}{E}\hat{\boldsymbol{q}}_{est,t-1} \otimes {}^{S}\boldsymbol{\omega} \tag{4.23}$$

$$\overset{S}{E}\boldsymbol{q}_{\omega,t} = \overset{S}{E}\hat{\boldsymbol{q}}_{est,t-1} + \overset{S}{E}\dot{\boldsymbol{q}}_{\omega,t}\Delta t \tag{4.24}$$

Orientation from vector observations A three-axis accelerometer measures magnitude and direction of gravity in sensor frame compounded with linear accelerations due to motion. A three-axis magnetometer measures magnitude and direction of earth magnetic field in the sensor frame compounded with local flux. In this filter context it will be assumed initially that accelerometer will only measure gravity and the magnetometer only the earth's magnetic field. A quaternion representation needs a unique sensor orientation solution. This can be achieved through the formulation of the optimisation problem where the orientation of the sensor $\overset{S}{E}\hat{\boldsymbol{q}}$, aligns with a predefined reference direction of the field ${}^{E}\hat{\boldsymbol{d}}$ with the measured direction of the field in sensor frame ${}^{S}\hat{\boldsymbol{s}}$. $\overset{S}{E}\hat{\boldsymbol{q}}$ may be found as the solution to equation 4.25.

$$\min \boldsymbol{f}(\overset{S}{E}\hat{\boldsymbol{q}}, {}^{E}\hat{\boldsymbol{d}}, {}^{S}\hat{\boldsymbol{s}}) \tag{4.25}$$

Where $\boldsymbol{f}$ is defined in equation 4.26 and $\overset{S}{E}\hat{\boldsymbol{q}}$, ${}^{E}\hat{\boldsymbol{d}}$ and ${}^{S}\hat{\boldsymbol{s}}$ are defined in equations 4.27, 4.28 and 4.29 respectively.

$$\boldsymbol{f}(\overset{S}{E}\hat{\boldsymbol{q}}, {}^{E}\hat{\boldsymbol{d}}, {}^{S}\hat{\boldsymbol{s}}) = \overset{S}{E}\hat{\boldsymbol{q}}^{*} \otimes {}^{E}\hat{\boldsymbol{d}} \otimes \overset{S}{E}\hat{\boldsymbol{q}} - {}^{S}\hat{\boldsymbol{s}} \tag{4.26}$$

$$\overset{S}{E}\hat{\boldsymbol{q}} = \begin{bmatrix} q_1 & q_2 & q_3 & q_4 \end{bmatrix} \tag{4.27}$$

$${}^{E}\hat{\boldsymbol{d}} = \begin{bmatrix} 0 & d_x & d_y & d_z \end{bmatrix} \tag{4.28}$$

$${}^{S}\hat{\boldsymbol{s}} = \begin{bmatrix} 0 & s_x & s_y & s_z \end{bmatrix} \tag{4.29}$$

If we assume that the direction of gravity defines the vertical z axis, and normalize the accelerometer measurement ${}^{S}\hat{\boldsymbol{a}}$ for ${}^{E}\hat{\boldsymbol{d}}$ and ${}^{S}\hat{\boldsymbol{s}}$ yields equation 4.32.

$${}^{E}\hat{\boldsymbol{g}} = \begin{bmatrix} 0 & 0 & 0 & 1 \end{bmatrix} \tag{4.30}$$

$${}^{S}\hat{\boldsymbol{a}} = \begin{bmatrix} 0 & a_x & a_y & a_z \end{bmatrix} \tag{4.31}$$

$$\boldsymbol{f}_g({}^{E}\hat{\boldsymbol{g}}, {}^{S}\hat{\boldsymbol{a}}) = \begin{bmatrix} 2(q_2q_4 - q_1q_3) - a_x \\ 2(q_1q_2 + q_3q_4) - a_y \\ 2(\frac{1}{2} - q_2^2 - q_3^2) - a_z \end{bmatrix} \tag{4.32}$$

The same way the earth's magnetic field can be considered to have components in only two of the three axis (one horizontal and the vertical one, due to the inclination of the field). Similarly to the accelerometer we have the following equation (4.35).

$${}^{E}\hat{\boldsymbol{b}} = \begin{bmatrix} 0 & b_x & 0 & b_z \end{bmatrix} \tag{4.33}$$

$$^{S}\hat{\boldsymbol{m}} = \begin{bmatrix} 0 & m_x & m_y & m_z \end{bmatrix} \tag{4.34}$$

$$\boldsymbol{f}_b(^{S}_{E}\hat{\boldsymbol{q}}, {}^{E}\hat{\boldsymbol{b}}, {}^{S}\hat{\boldsymbol{m}}) = \begin{bmatrix} 2b_x(\frac{1}{2} - q_3^2 - q_4^2) + 2b_z(q_2q_4 - q_1q_3) - m_x \\ 2b_x(q_2q_3 - q_1q_4) + 2b_z(q_1q_2 + q_3q_4) - m_y \\ 2b_x(q_1q_3 + q_2q_4) + 2b_z(\frac{1}{2} - q_2^2 - q_3^2) - m_z \end{bmatrix} \tag{4.35}$$

As discussed earlier, the measurements and directions of both accelerometer and magnetometer fields may be combined to provide a unique orientation of the sensor as described in equation 4.36.

$$\boldsymbol{f}_{g,b}(^{S}_{E}\hat{\boldsymbol{q}}, {}^{S}\hat{\boldsymbol{a}}, {}^{E}\hat{\boldsymbol{b}}, {}^{S}\hat{\boldsymbol{m}}) = \begin{bmatrix} \boldsymbol{f}_g(^{E}\hat{\boldsymbol{g}}, {}^{S}\hat{\boldsymbol{a}}) \\ \boldsymbol{f}_b(^{S}_{E}\hat{\boldsymbol{q}}, {}^{E}\hat{\boldsymbol{b}}, {}^{S}\hat{\boldsymbol{m}}) \end{bmatrix} \tag{4.36}$$

Filter fusion An estimated orientation of the sensor frame is obtained through the fusion of the gyroscope estimate ($^{S}_{E}\boldsymbol{q}_{\omega,t}$) and both accelerometer/magnetometer estimation ($^{S}_{E}\hat{\boldsymbol{q}}_{\nabla,t}$). The fusion is very similar to the complementary filter applying weights to each orientation calculation as in equation 4.37

$$^{S}_{E}\boldsymbol{q}_{est,t} = \gamma_t {}^{S}_{E}\boldsymbol{q}_{\nabla,t} + (1-\gamma_t){}^{S}_{E}\boldsymbol{q}_{w,t}, \;\; 0 \leq \gamma_t < 1 \tag{4.37}$$

The author also explains how to remove magnetic distortion and how to provide a gyroscope bias drift compensation. Since these sections are quite complex and extensive, we will leave these matters to the original authors paper [24] and show the final diagram block of the final Attitude and Heading Reference Systems (AHRS) filter.

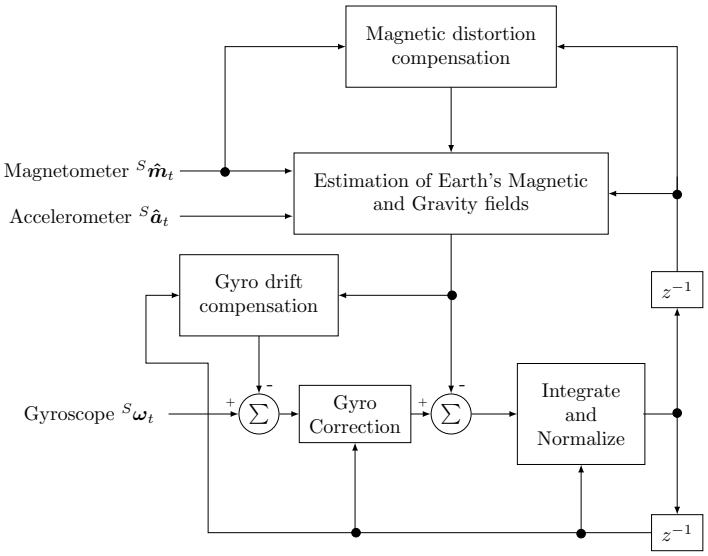

Figure 4.6: Block diagram of the complete orientation filter.

4.3 Control

The control theory is fundamental in this project allowing to control and stabilize the vehicle attitude. Since this is the first phase of developing of this project it was chosen to not

implement very complex control algorithms. A classical control theory approach was chosen implementing PID algorithms. The PID is a widely used algorithm with applications in many fields, including multirotor applications. Most of the commercial flight controller boards use PID as their algorithm for vehicle stabilization. Once again in this project the current goal is not to have a very complex algorithm but a simple and functional one.

4.3.1 PID for angle compensation

In order to stabilize the vehicle during flight, 3 PID were implemented, one for each Euler angle (Roll, Pitch and Yaw). Each PID algorithm follows the implementation described in figure 4.7. An error signal $e(t)$ is calculated subtracting the measured angle, obtained through sensor fusion, with the desired angle. The error signal is then used to calculate the proportional, derivative and integral parcels of the algorithm. The output signal $u(t)$ is the sum of those three components.

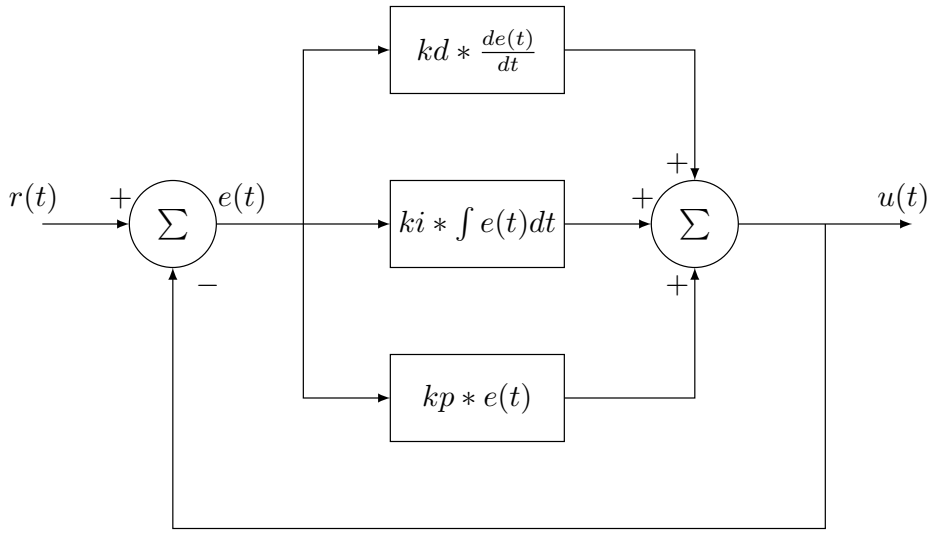

Figure 4.7: Generic PID algorithm.

The constants K_p, K_i and K_d are parameters of the controller and are designated as proportional gain, integral gain and derivative gain respectively.

- The K_p gain produces an output variation proportional to the error. It helps reducing the response time, but also producing some overshooting.

- The K_i gain produces an output variation integral to the error. It helps reducing the steady state error, although increasing the overshooting and response time.

- The K_d gain produces an output variation equal to the derivative of the error. It helps reducing the steady state time and reducing the overshooting.

Figure 4.7 shows the generic PID algorithm for continuous signals. However, since the system is discrete, the algorithm must be written in its digital form. Equation 4.38 describes mathematically the system.

$$u(n) = K_p e(n) + k_i x(n) + k_d \left(\frac{e(n) - e(n-1)}{T} \right), \quad x(n) = x(n-1) + e(n) \times T \tag{4.38}$$

PID Controller for Roll and Pitch Angles Two inputs are necessary to calculate the error signal. The measured values for the roll and pitch angles are given by the sensor fusion block, while the desired angle is given by the current position of the remote controller sticks. Figure 4.8 represents the applied algorithm.

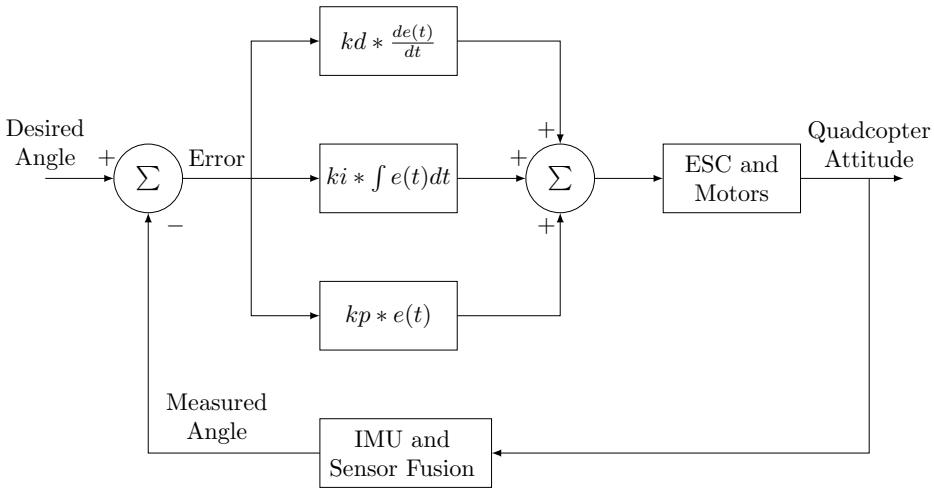

Figure 4.8: PID algorithm for Roll/Pitch compensation.

The following code example describes how to implement the PID algorithm in a microcontroller.

```
error = desired_angle - current_angle;
integral = integral + error*dt;
derivative = (error - previous_error)/dt;
output = error*kp + integral*ki + derivative*kd;
previous_error = error;
```

The derivative constant was set to zero, so in fact the applied algorithm was a Proportional Integral.

PID Controller for Yaw compensation For yaw compensation, there are two possible approaches:

- Perform closed loop control of the angular velocity around the z-axis. This is helpful for the remote controller integration. In this case, the inputs of the controller are the desired angular velocity and the measured angular velocity.

- Perform closed loop control of the yaw angle. In this case, the PID controller is similar to the roll/pitch one.

Remote Controller Integration One of the input parameters of the PID algorithm is the desired angle or desired angular velocity. Depending on the maneuver, the desired value can be given by the elevator, aileron or rudder values:

- Desired roll angle: It can change from -45°to 45°where the neutral position agrees with the aileron stick rest position.
- Desired pitch angle: It can change from -45°to 45°where the neutral position agrees with the elevator stick rest position.
- Desired yaw angular velocity: It can change from $-45°/s$ to $+45°/s$ where the neutral position agrees with the rudder stick rest position.
- The throttle controls the velocity applied to the motors. However, altitude control isn't performed.

The above values were chosen to ensure that the vehicle acts safely. Pitch/Roll values over 45°, or yaw rotations above $45°/s$ would lead to aggressive maneuvers that are not desired in this phase of development.

'+' and 'x' configurations In this phase it is mandatory to define what kind of configuration the aircraft will use, because the control algorithms are different from configuration to configuration. In the examples below it will be described how to implement the PID algorithms for both configurations.

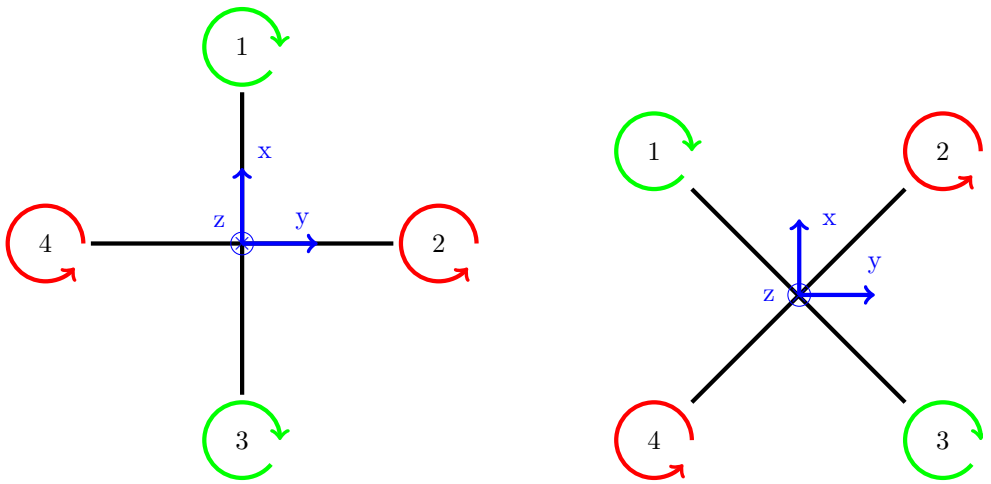

Figure 4.9: a) Quadrotor '+' configuration. b) Quadrotor 'x' configuration.

The following code example represents an implementation for the control and stabilization of the 'x' configuration, assuming the referential illustrated in figure 4.9(b). The `throttle` variable is the current throttle stick position that can change from $1ms$ to $2ms$. The `motor_x` variables are the PWM values applied to the ESC modules, while the `roll_output`, `pitch_output` and `yaw_output` are the output values of the PID algorithms, in the range 1ms to 2ms, as explained above.

```
// For x configuration
motor_1 = throttle + roll_output/2 - pitch_output/2 - yaw_output;
motor_2 = throttle - roll_output/2 - pitch_output/2 + yaw_output;
motor_3 = throttle + roll_output/2 + pitch_output/2 - yaw_output;
motor_4 = throttle - roll_output/2 + pitch_output/2 + yaw_output;
```

The following code example represents an implementation for the '+' configuration, assuming the referential illustrated in figure 4.9(a).

```
// For + configuration
motor_1 = throttle - pitch_output - yaw_output;
motor_2 = throttle - roll_output + yaw_output;
motor_3 = throttle + pitch_output - yaw_output;
motor_4 = throttle + roll_output + yaw_output;
```

4.4 Summary

Different techniques to estimate the Roll and Pitch angles were presented, such as the complementary filter and the Madgwick fusion filter.

The PID was chosen has the control algorithm for this project due to is simplicity and efficiency. It was shown how to apply the control and stabilization algorithm for both '+' and 'x' quadrotor configurations.

The fusion filters and control algorithms were implemented and tested in the sensing and control board. The results of these algorithms will be presented and discussed in the next chapter.

Chapter 5

Experimental Results

This chapter presents and analyses the results obtained during this project. This includes single motor tests, sensor fusion tests, autonomy tests and payload tests.

5.1 Single Motor Test

In order to perform some electrical and physical tests to the propulsive pair (motor and propeller) a test-bed was built as represented in figure 5.1 and 5.2. One of the axis of the motor is fixed at the tip of the platform, while the other end is placed on a digital scale plate. When the propulsive pair starts working a lifting force will be exerted creating an opposite force on the other end of the arm placed on top of the scale, measuring therefore the thrust produced by the propulsive pair. The distance from motor to center and from center to the scale is not the same, as represented in figure 5.1. This difference has to be taken into account when calculating the real thrust using equation 5.1.

$$\text{thrust}_{\text{real}} = \text{thrust}_{\text{measured}} * \left(\frac{14}{13.5}\right) + \text{motor}_{\text{weight}} \tag{5.1}$$

where $\text{thrust}_{\text{measured}}$ is the value measured by the scale, and $\text{motor}_{\text{weight}}$ is the weight on the motor side.

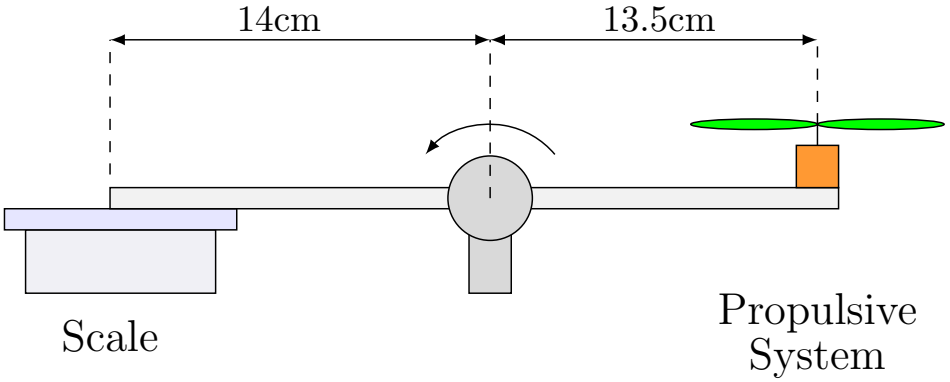

Figure 5.1: Single motor test with different configurations.

During the experiments, different configurations were used in order to find the perfect

match to the propulsive system. In all the configurations, the motor was the Turnigy D2830-11 and the ESC was the Turnigy Plush 30 Amp performing changes only in the propeller and the power system:

- 3 cell LiPo with 9x47 Propeller
- 3 cell LiPo with 10x45 Propeller
- 4 cell LiPo with 9x47 Propeller
- 4 cell LiPo with 10x45 Propeller

The 3 cell and 4 cell batteries were charged with 12.6V and 16.8V respectively.

These tests allowed us to find some important characteristics of the propulsive system as the total thrust force, current drained and power consumption.

In order to measure the total current consumed by the setup, a resistance of 0.02Ω was placed between the battery output and the ESC input. By measuring the voltage drop at the resistance it was possible to calculate a current estimation.

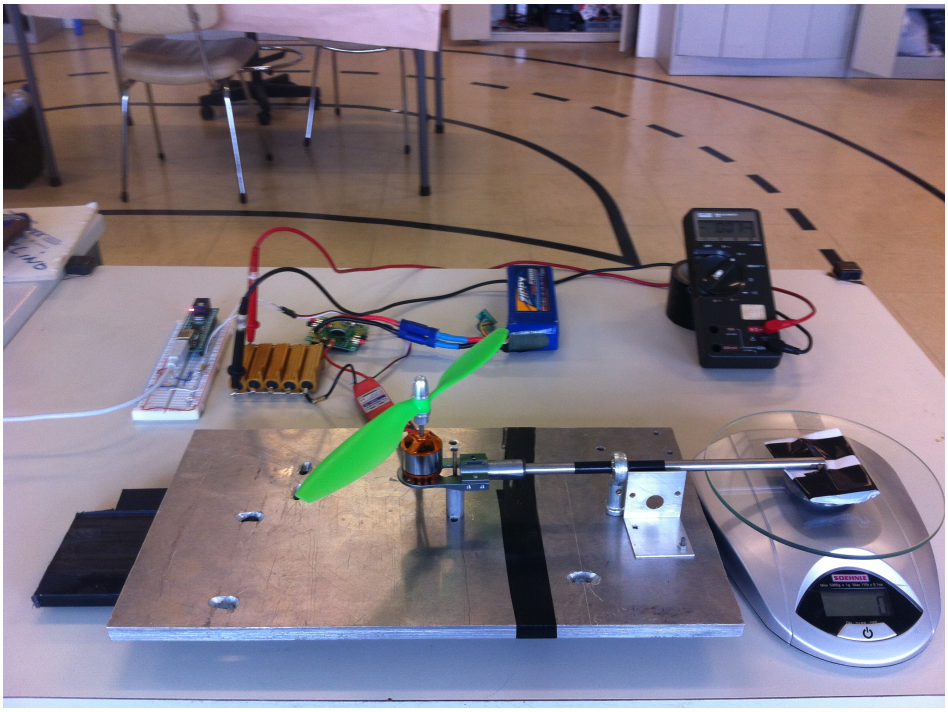

Figure 5.2: Photo of the test-bed setup.

In figure 5.3 it is possible to see how the thrust changes with different configurations. As it was expected, the thrust increases with the propeller diameter and with the battery voltage. The maximum thrust value of 1017g was achieved by the 4 cell LiPo with a 10x45 propeller. As it can be observed in figure 5.3 the 4 cell configurations were never pushed to the limit because they reached the maximum power supported by the motor (210W). To avoid permanent damage they were switched off before the limit.

Figure 5.4 describes the power consumption for all configurations, where it is possible to see that only the 3 cell 9x47 configuration doesn't reach the limit value of the motor. The

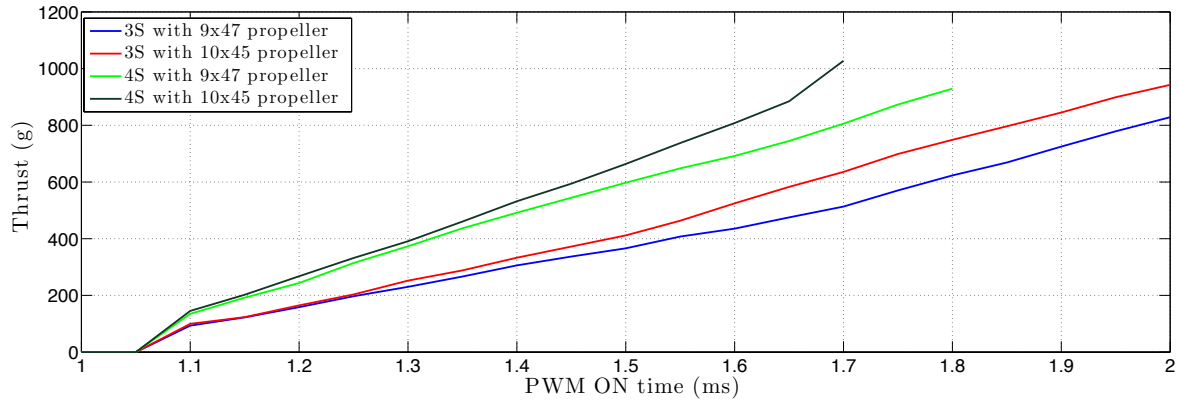

Figure 5.3: Measured Thrust for different configurations.

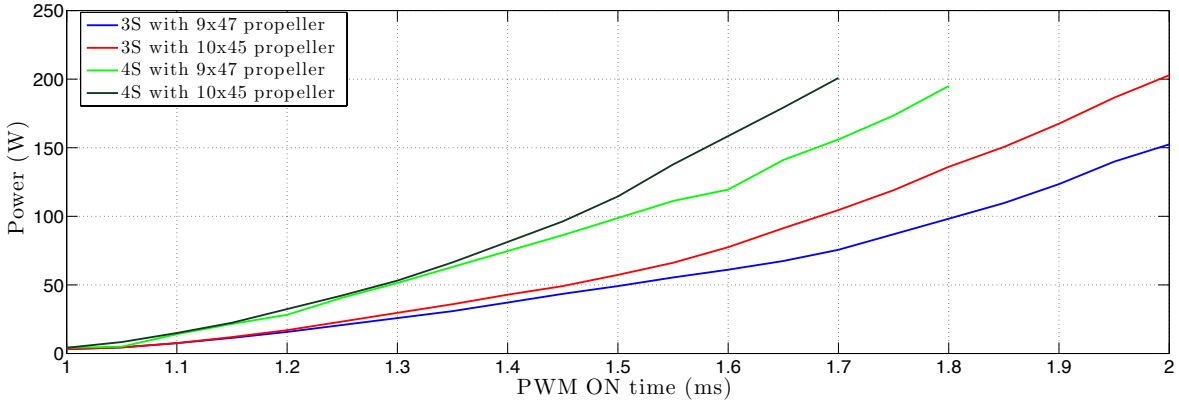

Figure 5.4: Estimated Power for different configurations.

---

configurations with 4 cell LiPo as said before, had to be turned off before their maximum values because they reach the motor power limit very early. The 3 cell 10x45 configuration although it also reaches values near the motor limit, it can go to the maximum speed values.

For the reasons above, the best match of all the configurations is the 3 cell LiPo with the 9x47 Propeller. The 10x45 propeller can lift more 106g, although consuming more 50W (more 4A) than the 9x47 propeller. These values increase when multiplied by the four rotors of the quadrotor where the maximum values of thrust and power are the following:

- 3316g and 608W for the 3 cell 9x47 configuration
- 3740g and 808W for the 3 cell 10x45 configuration

As can be observed the 3 cell 9x47 configuration have a better thrust/power ratio, however the 3 cell 10x45 configuration is more suitable for higher thrust requirements.

Detailed values of these experiments can be consulted in appendix D.

5.2 Sensor Fusion Filters Test

This section presents and discusses the results of the sensor fusion algorithms. The fusion algorithms are responsible to calculate the roll and pitch angles of the quadrotor attitude. The yaw angle it will not be discussed due to magnetometer functioning problems. [1] The system was tested in several working conditions described as follows:

- **Roll and Pitch Rotations:** The quadrotor was placed on top of a table. With human intervention, the table was rotated around the x-axis and y-axis from 0°to 90°and -90°. Two types of rotations were made, the first one was performing slow rotations, while on the second one, the rotations were fast and aggressive in order to stress the filters. In this phase, the motors were switched off so no vibrations were expected.

- **No rotations but motors active:** In this test-bed, the quadrotor was placed and attached on top of a table without any level of freedom. The motors were active creating mechanical vibrations. This allows to test the filter capacity to handle with noise.

- **Rotations with motors active:** With human intervention, the quadrotor performs several rotations while the motors are causing mechanical vibrations.

The sensor fusion algorithms applied in these set of tests were the complementary filter and Madgwick filter, both explained in detail in the previous chapter. The filters are also compared with single sensor estimations for both accelerometer and gyroscope. The sample rate used during the tests was 100Hz, in order to allow the transfer of data from the control board to the PC without losses. Regarding to the complementary filter constant (section 4.2.1) it was set to $a = 0.97$, giving more weight to the gyroscope than to the accelerometer.

Roll Movements Figure 5.5 shows the accelerometer values for the performed test. As expected the z-axis is measuring a $1g$ acceleration which corresponds to the gravitational acceleration. When the quadrotor starts rotating around the x-axis, the y-axis accelerometer values grow, unlike the z-axis that as expected is not anymore perpendicular to the Earth.

[1] The magnetometer was not fully working. Although it was possible to communicate with the device and receive the I^2C address, the measured values where always zero. This reason, along with other tests lead us to think that the device is damaged and needs to be replaced.

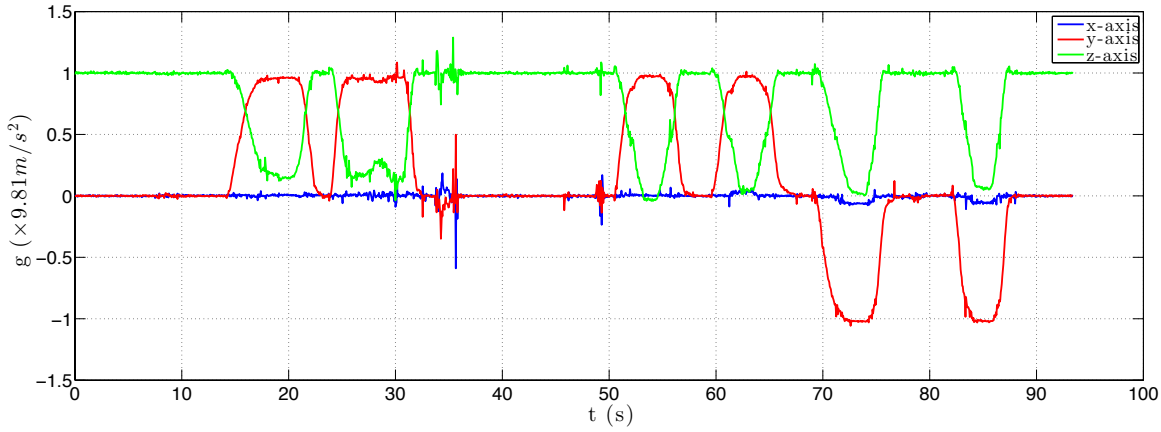

Figure 5.5: Accelerometer values for all axis during roll tilting.

Figure 5.6 shows the gyroscope values for the same rotation. As expected, it is noticeable that only the x-axis have significant angular velocity changes because the rotation is around that axis.

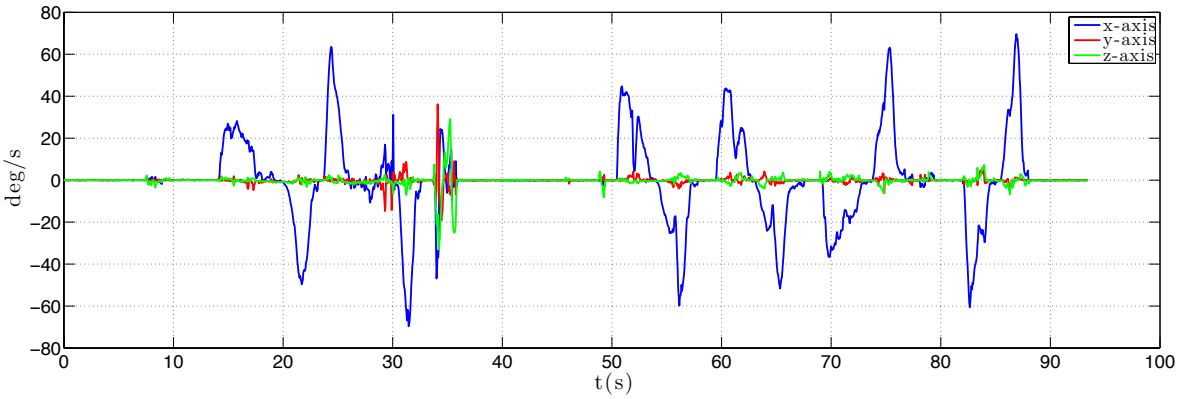

Figure 5.6: Gyroscope values for all axis during roll tilting.

Figure 5.7 shows the roll angle estimation using different techniques. The red signal is the angle estimation using only the accelerometer data, applying equation 4.4, while the cyan is based only in gyroscope data, integrating the readings over time. It is noticeable that the accelerometer estimation has a very sensible output, although with a quick response. The gyroscope estimation is more smoother and less sensible than the accelerometer.

Comparing the fusion filters, the Madgwick filter presents a more sensible and slower estimation than the complementary filter.

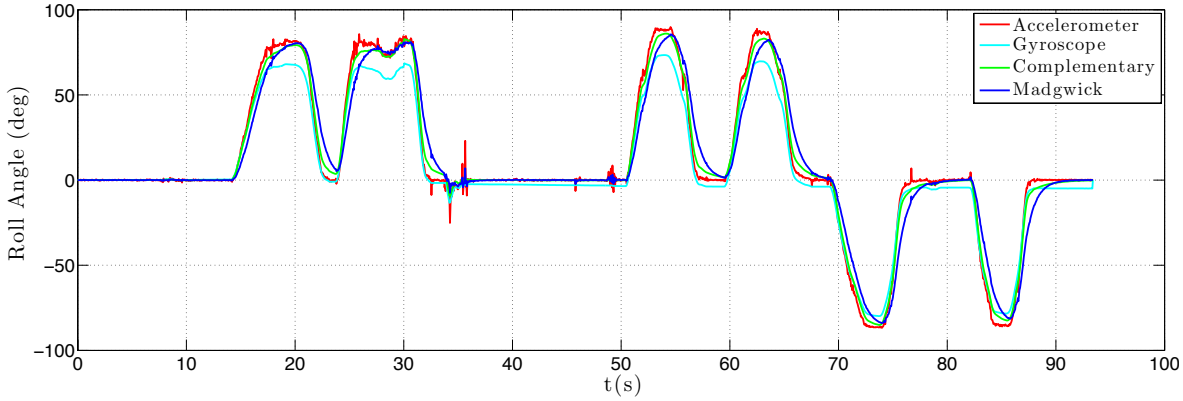

Figure 5.7: Roll angle calculated using different fusion filters.

Pitch Movements Figures 5.8 and 5.9 present the results for the accelerometer and gyroscope measures, while figure 5.10 shows the estimation of the pitch angle. Regarding to the fusion filters comparison, this time is more obvious to note that the Madgwick filter is slower than the complementary filter, sometimes not even achieving the desired estimation.

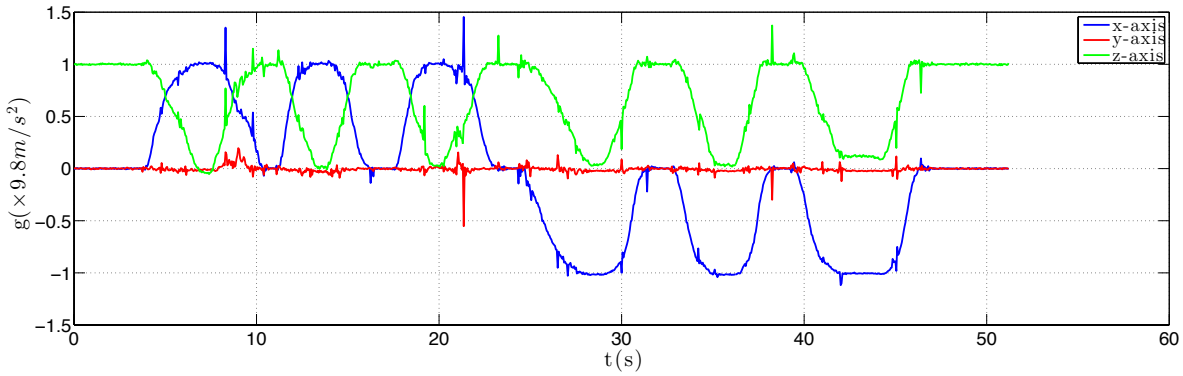

Figure 5.8: Accelerometer values for all axis during pitch tilting.

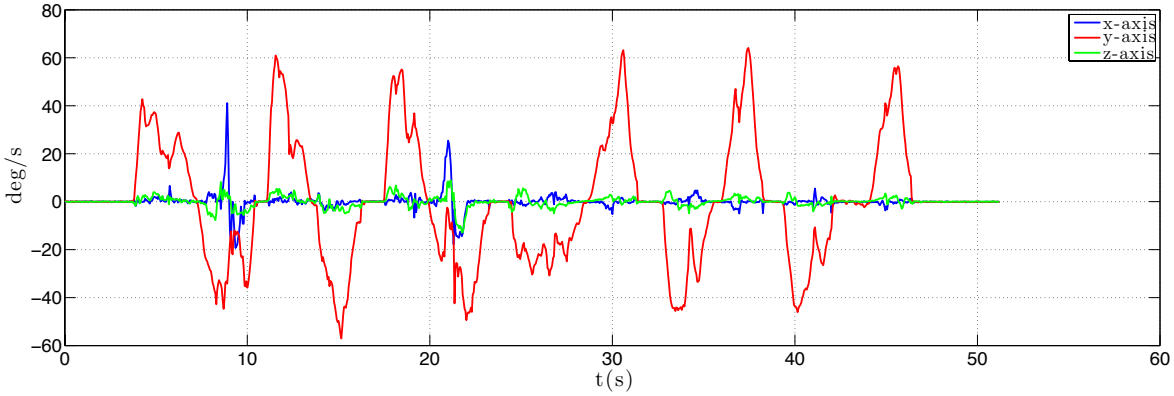

Figure 5.9: Gyroscope values for all axis during pitch tilting.

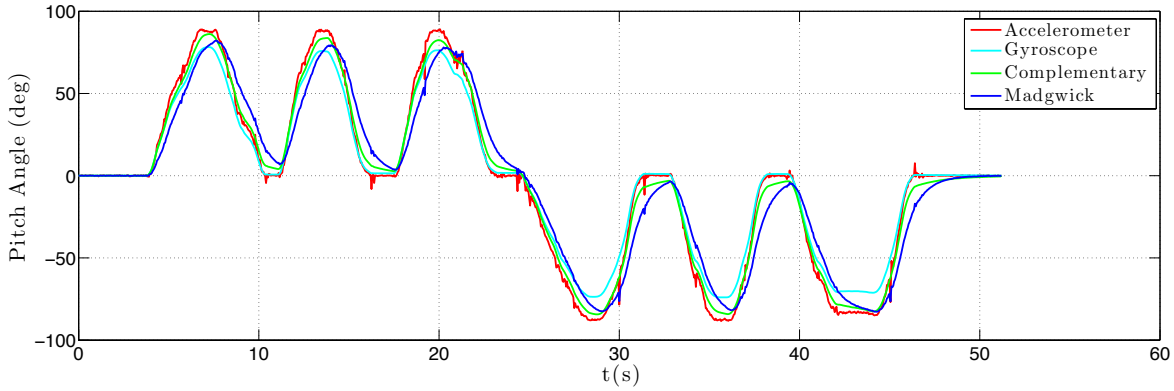

Figure 5.10: Pitch angle calculated using different fusion filters.

Fast Roll Movements Rotations were performed more rapidly in order to stress the system and see how the filters react.

Figure 5.11 and 5.12 present the accelerometer and gyroscope readings respectively. As expected, the accelerometer presents a very sensible output showing acceleration peaks at the end of each rotation. The gyroscope measures present a higher amplitude since this time the rotations were faster.

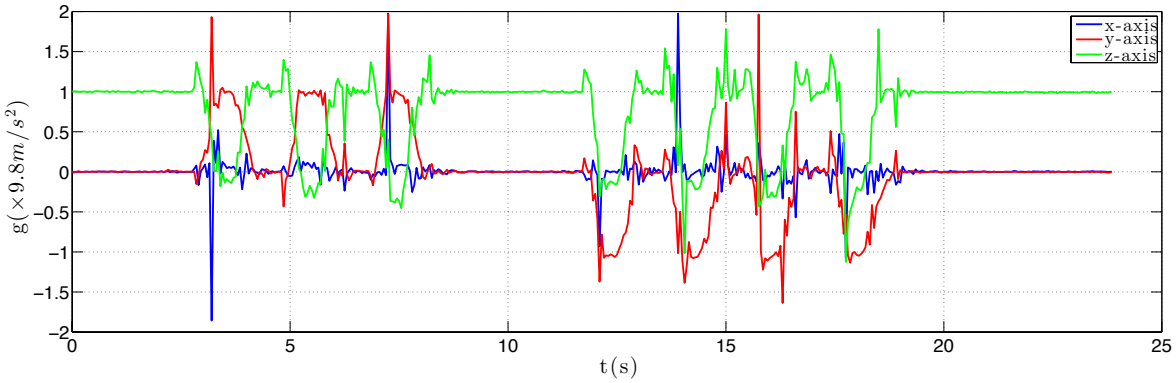

Figure 5.11: Accelerometer values for all axis during fast Roll tilting.

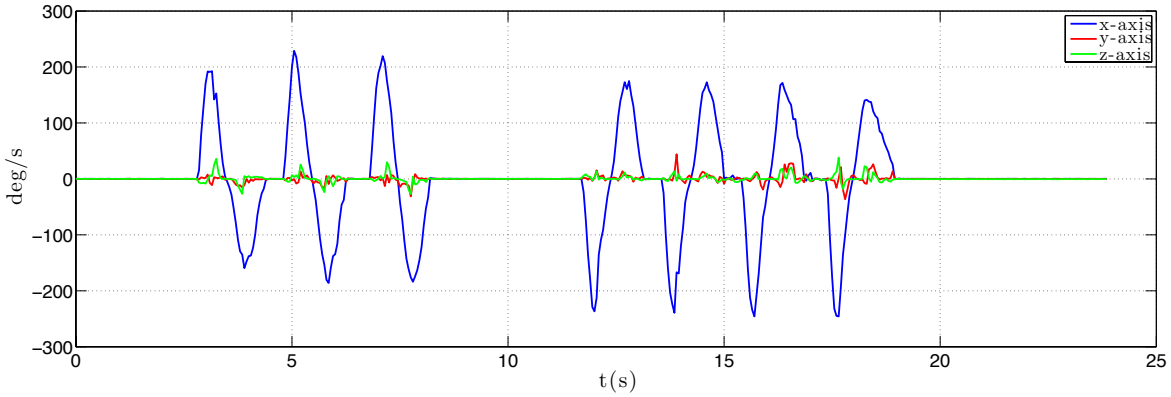

Figure 5.12: Gyroscope values for all axis during fast Roll tilting.

Regarding to figure 5.13, this test brings us new conclusions about the implemented fusion filters. The complementary reacts in a similar way compared with the other tests, while the Madgwick filter, due to the slow response doesn't reach in some cases, half of the expected amplitude.

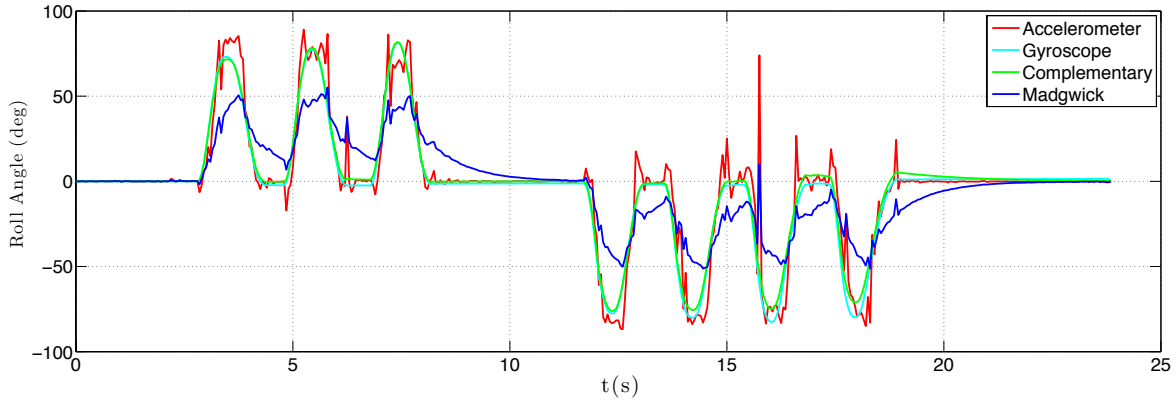

Figure 5.13: Roll angle calculated using different fusion filters.

Fast Pitch Movements Figures 5.14 and 5.15 demonstrate the accelerometer and gyroscope values respectively, which are similar to the roll rotation. However, figure 5.16 shows that, after a while, the gyroscope estimation diverged completely, which can be explained by the peaks represented in the gyroscope values from the 13th second to the 17th second. Although it also induced error in the complementary filter, it was still able to recover, unlike the gyro estimation that after accumulate that amount of error couldn't recover anymore.

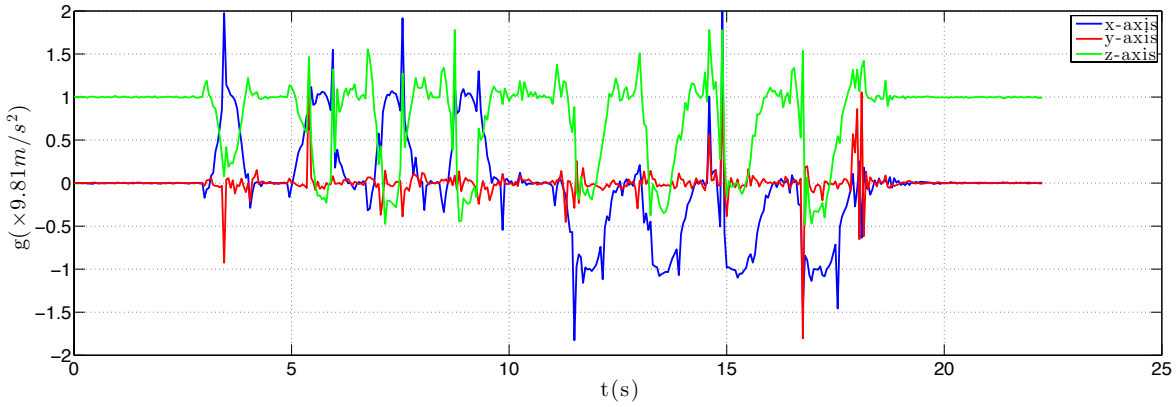

Figure 5.14: Accelerometer values for all axis during fast pitch tilting.

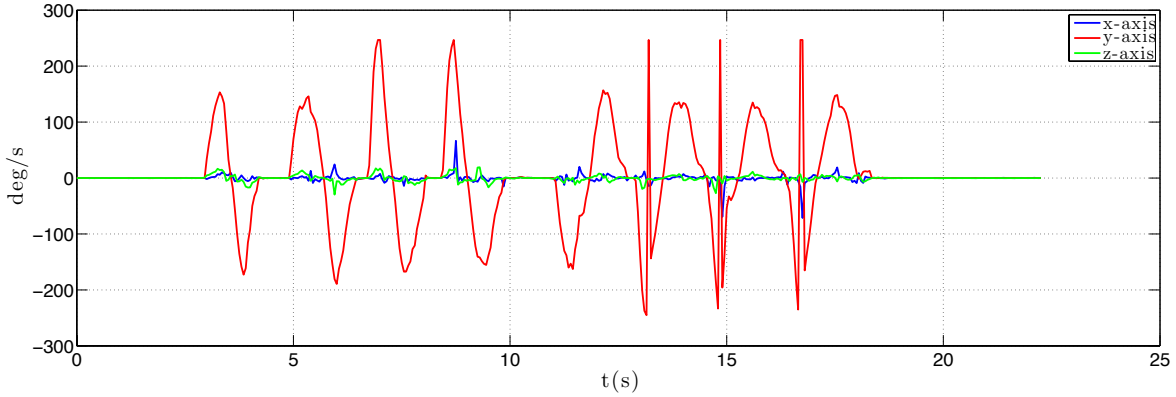

Figure 5.15: Gyroscope values for all axis during fast pitch tilting.

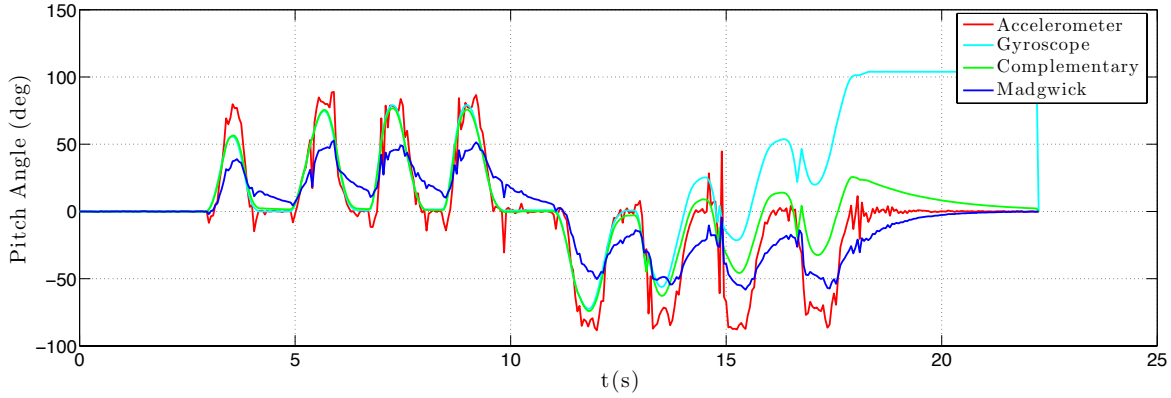

Figure 5.16: Pitch angle calculated using different fusion filters.

Gyroscope Drift As said in the previous chapter, usually gyroscopes have drift problems. This test intends to find out if the gyroscope angle estimation suffers from drift problems and if the fusion filters are able to remove it. The quadrotor was placed on top of a table during 4.5 minutes without performing any movement. Figure 5.17 presents the angle estimation, where it can be observed that the gyroscope estimation has 9°error. The fusion filters are able of cancelling that effect by presenting an error close to 0°.

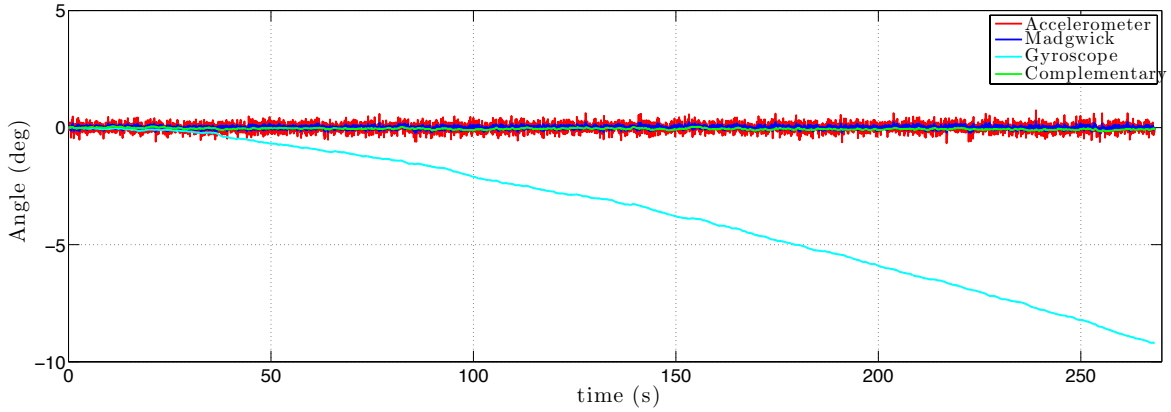

Figure 5.17: Drift test to angle estimation.

Introducing Motor Vibrations In this test, the motors were turned on using the remote controller. The quadrotor was attached to a table and did not have any level of freedom. The test started with motors turned off, activating them after a few seconds. The motors speed started very slow, and it was increased almost till the maximum, making few stops in the middle in order to stress the system. It is expected to see if the vibrations caused by the motors into the quadrotor structure affects the roll and pitch angle estimation.

As can be observed from figures 5.18, 5.19, 5.20 and 5.21, the noise due to vibrations increased with the activation of the motors. From the accelerometer values is noticeable when the motors are working or not. In some cases the accelerometer amplitude is almost $2g$, which will turn the correct angle estimation extremely difficult to calculate. The same happens for

the gyroscope measures where in some cases the noise amplitude reaches 100°/s. Regarding to the angle estimation, figures 5.20 and 5.21 show the pitch and roll angle estimation, where can be observed that the accelerometer estimation is full of noise and is completely impossible to use. The same occurs with the Madgwick filter, which seems to be also very sensible to vibrations. The best estimation for this case is the complementary filter, although in some cases reaches a 10°error.

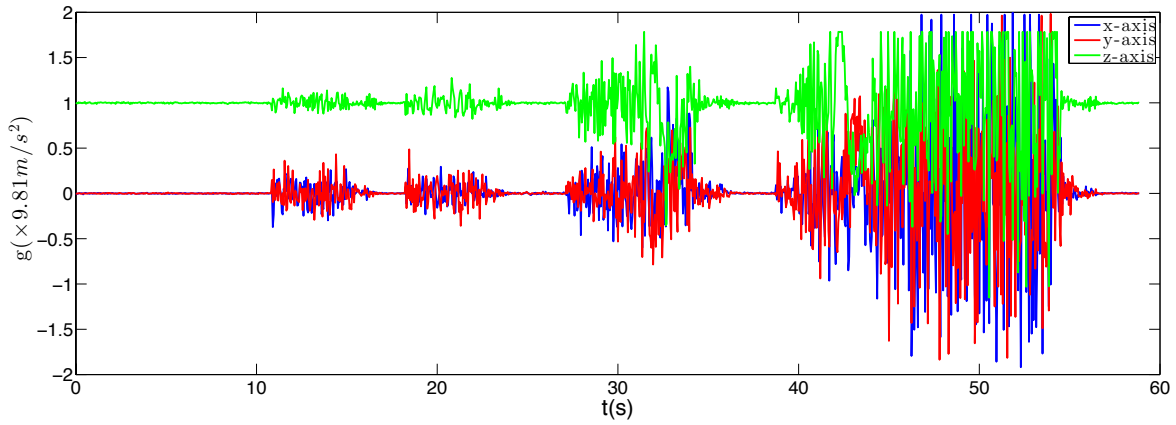

Figure 5.18: Accelerometer readings when exposed to motor vibrations.

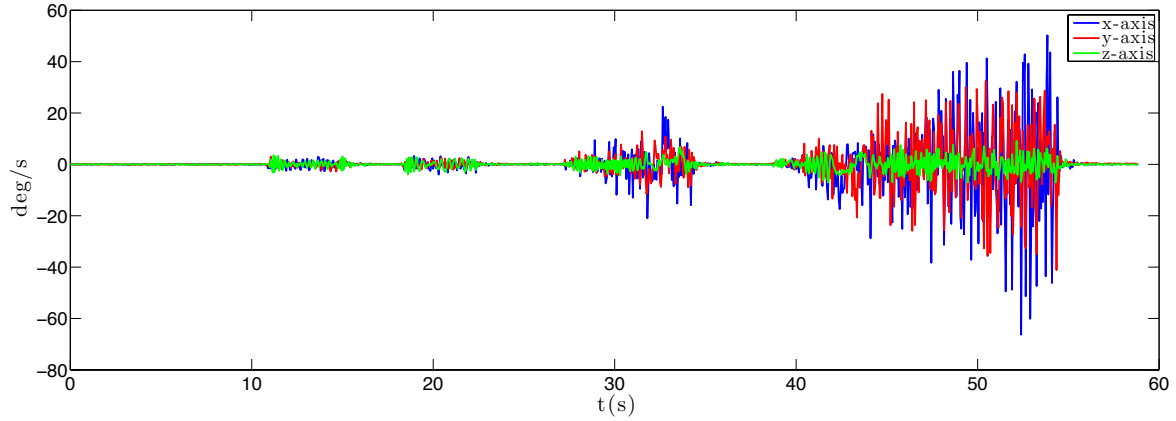

Figure 5.19: Gyroscope readings when exposed to motor vibrations.

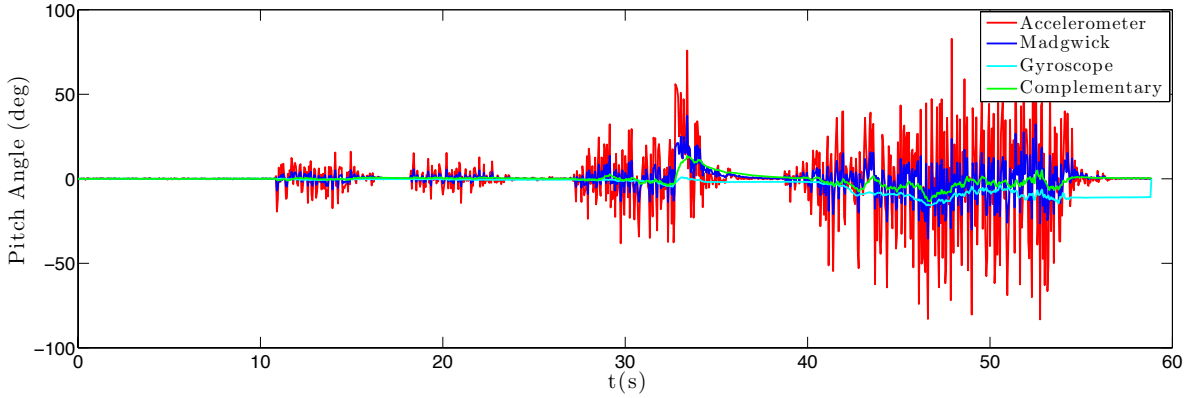

Figure 5.20: Pitch angle estimation using different fusion filters when exposed to motor vibrations.

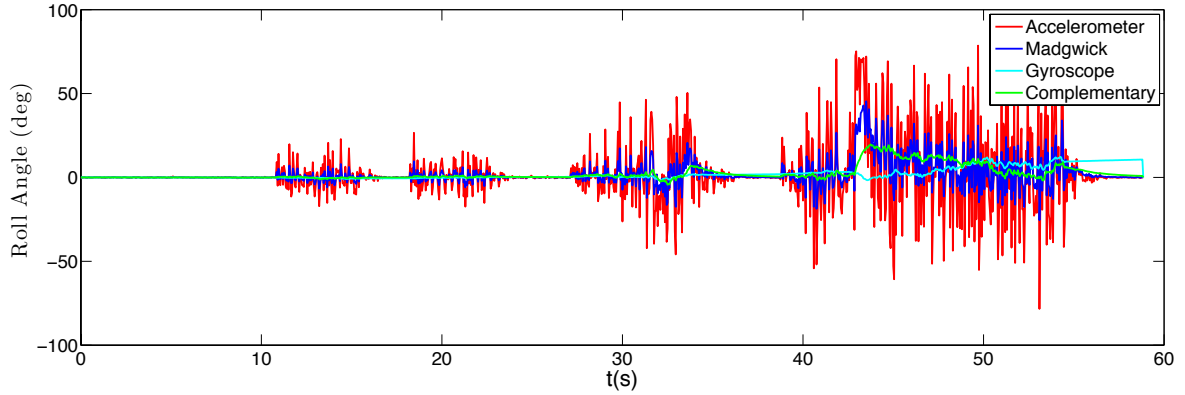

Figure 5.21: Roll angle estimation using different fusion filters when exposed to motor vibrations.

Performing rotations with motors active In this test, rotations are made in the quadrotor with the motors active producing vibrations in the aircraft structure. Figures 5.22 and 5.23 present accelerometer and gyroscope readings, while figures 5.24 and 5.25 show the angle estimation for both pitch and roll angles. As can be observed, the complementary filter presents better angle estimations. However, in some cases the error reaches 15°which is not acceptable in this kind of applications.

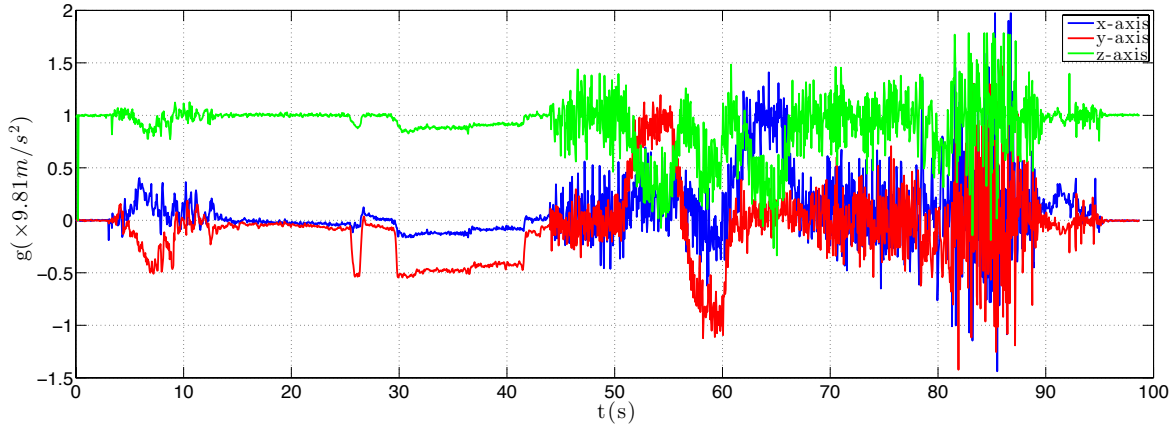

Figure 5.22: Accelerometer readings when exposed to motor vibrations.

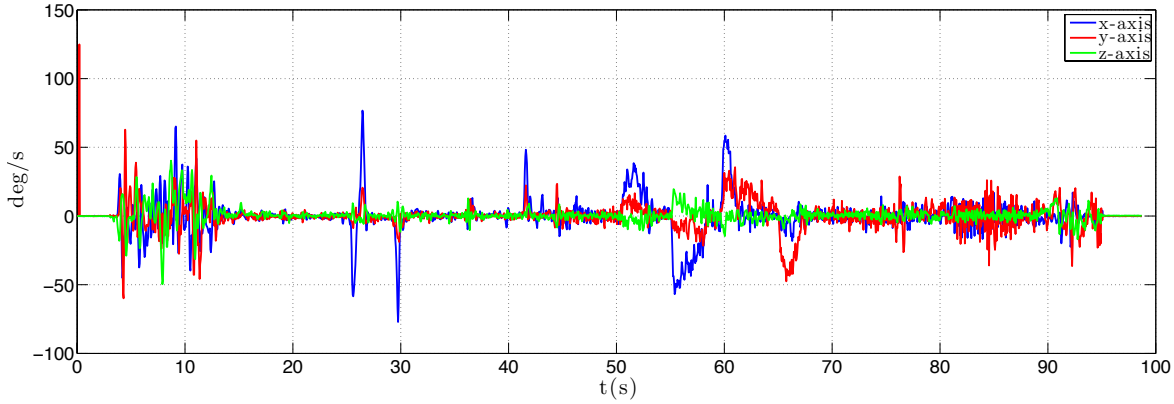

Figure 5.23: Gyroscope readings when exposed to motor vibrations.

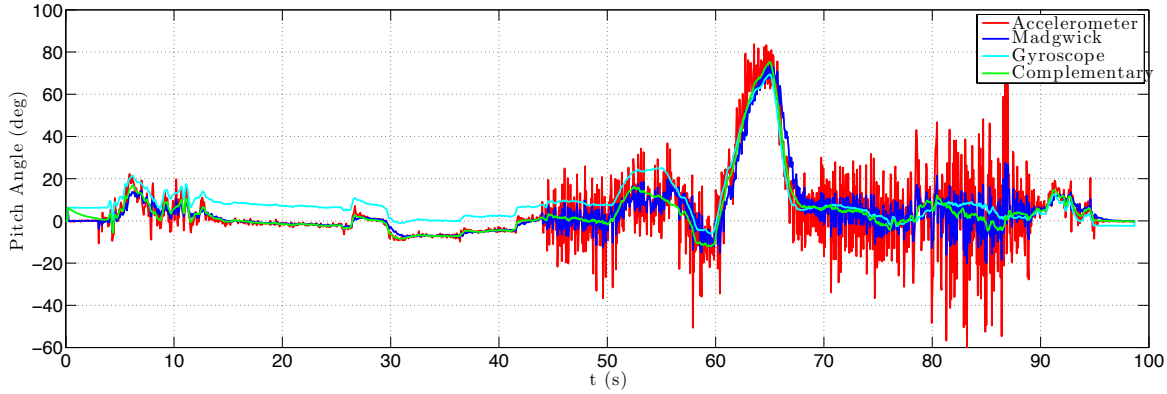

Figure 5.24: Pitch angle estimation using different fusion filters when exposed to motor vibrations.

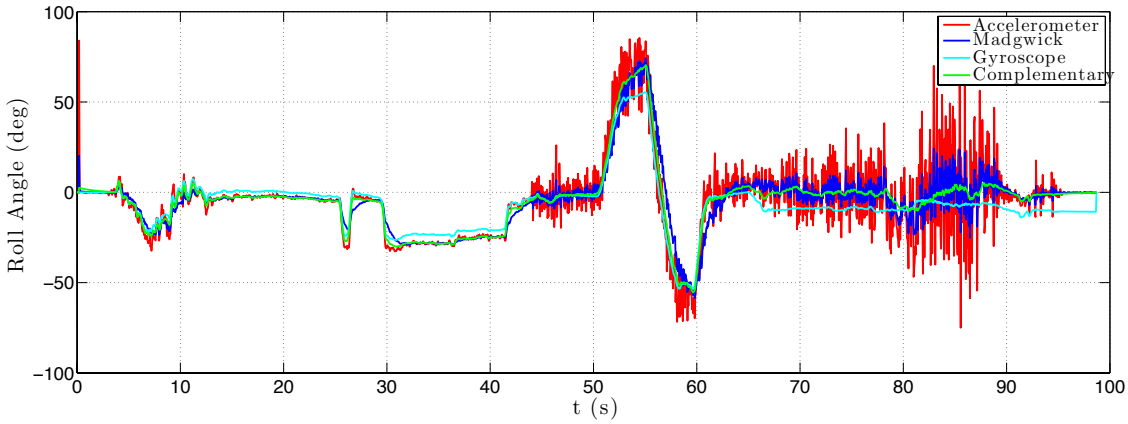

Figure 5.25: Roll angle estimation using different fusion filters when exposed to motor vibrations.

Sensor Fusion Summary and Results Discussion Regarding the single sensor estimations, the calculated results are in agreement with the expected values. The accelerometer presents a fast response but is very sensible to noise, while the gyroscope has a smooth response but shows drift problems over the time. Concerning to the sensor fusion filters used, the complementary filter presented better results in all the tests even though it requires much less computational power than the Madgwick filter.

The overall results are not very satisfactory, specially when the motors are working at high speed, making the angle estimation very difficult, with errors that are not acceptable for quadrotor implementation.

5.3 Barometer Test

In order to test the barometer, it was performed an altitude test. The test consisted in lifting the quadrotor from the ground to a height of 2m. The quadrotor motors were spinning and the barometer was enclosed in a protective chamber. The tests were made indoors, so it was also not expected much atmospheric noise. Figure 5.26 shows the altitude measured by the barometer during the test. Analysing figure 5.26, it is noticeable that the output is not smooth, exhibiting noise that in some cases almost reaches 1 meter of amplitude. However, the altitude changes as expected from zero meters (ground) to about 2.5m, back again to the ground, with 0.5 error and finalizing around 2m of altitude again.

As a conclusion, the barometer could be a good choice for this type of aircrafts depending on the use. It is not very good to perform automatic take-off and landing, since the error in some cases is bigger than 1m. However, it could be the perfect choice to estimate the current altitude of the vehicle, in high altitudes. It could be interesting, in some cases, to perform altitude control, like for example maintain the vehicle in an altitude range between 60m and 65m. To perform automatic take-off and landing, it would be a good idea to introduce a sonar sensor which in small distances (of about 2m) can provide good estimations of altitude.

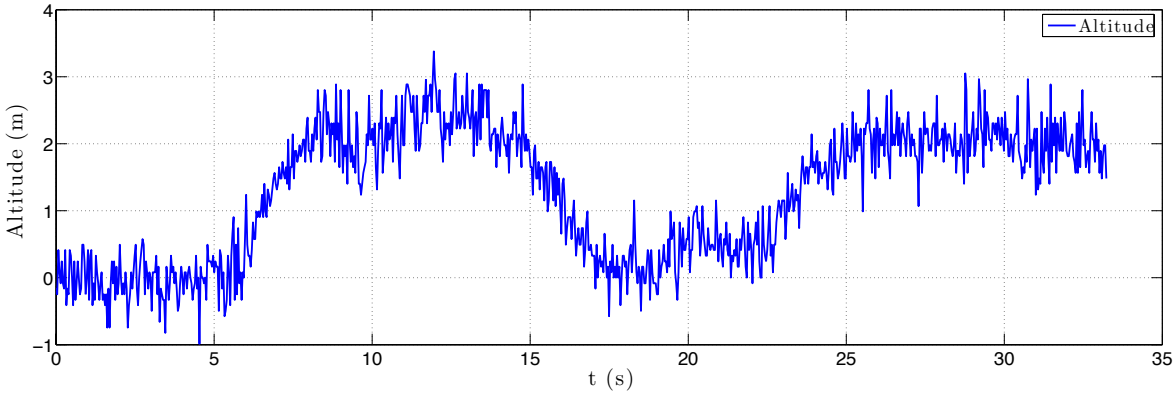

Figure 5.26: Barometer measuring altitude.

5.4 Control Test

After obtaining the current quadrotor attitude estimation, the PID algorithm tried to compensate angular displacements applying more power to some of the motors. After performing some tests, it was impossible to take off from the ground, since the angle estimation error is high. This causes the PID to try to compensate fake displacements leading the vehicle to instability. It was tried to tune the algorithm constants but sometimes angle estimation errors of almost 35°turn the stabilization impossible. Due to this errors, unfortunately it was not possible to perform much more tests about the control algorithm.

5.5 Autonomy Test

An autonomy test was performed to find how much time the system is able to fly without recharging the battery. The vehicle was controlled with human intervention by using the Hobbyking KK 2.0 control board and it was equipped with the 3 cell LiPo and the 10x45 propellers. In order to achieve the maximum results, the pilot tried to maintain the vehicle hoovering and avoid any acrobatic maneuver that cause a faster battery drain. The aircraft was able to fly during 12m03s discharching the battery from 12.6V to 11.2V. This value can be compared with an estimation using the values measured during the single motor test in section 5.1. Since the quadrotor weights 1115g, it means that each motor needs to lift 279g. Using tables D.1 and D.2 of the appendix, is possible to observe that to lift that weight, each motor needs to draw approximately 2.9A of current, which corresponds to a total of 11.6A. Since the battery is a 3300mAh LiPo the total flight time can be calculated as follows:

$$\frac{\text{Battery Capacity}}{\text{Current Drained}} \times 60 = \text{flight time (minutes)} \tag{5.2}$$

The battery did not discharged completely, in fact did not even reached the nominal voltage of 11.1V, so it was estimated that the battery discharged only to 20% of its capacity. Therefore, the estimated time flight is $\frac{3.3A/h*0.8}{11.6A} * 60 = 13m39s$ which is a little bit more than the measured time. However the estimation is based on a constant current draw which is very difficult to achieve piloting the quadrotor.

5.6 Payload Test

It was a requirement of the system to lift an additional payload of about 800g. The system was tested by adding extra payload to the vehicle until it was difficult or even impossible to take off the ground with that weight. The quadrotor was equipped with the 3 cell LiPo and the 10x45 propeller. The maximum value reached was 2437g, which corresponds to 1322g of extra payload considering the quadrotor own weight of 1115g. Although the throttle stick was not in the maximum position (only about 90%) it was becoming difficult to control the quadrotor, so it was chosen not to add more weight. However, the 800g required was well achieved and the vehicle still had a good controllability.

5.7 Summary

During this chapter, several results regarding the quadrotor operation were presented. In a first phase, the motors were characterized performing single tests finding a relation of the motor thrust with the power consumption. Then, a test to the quadrotor attitude angle estimation was performed, revealing that it is mandatory to apply a sensor fusion filter. It was verified that the complementary filter has better performance than the Madgwick filter. However, due to motors vibration, sometimes the angle estimation presented errors not acceptable for this application. Unfortunately, the yaw implementation was not tested because all the efforts were made to achieve better results for the roll/pitch estimations, leaving the yaw implementation for background.

Regarding to the aircraft characteristics, the quadrotor autonomy and extra payload were tested, achieving very satisfactory results and fulfilling the system requirements.

The objective of perform a stabilized flight was not achieved due to angle estimation errors.

Chapter 6

Conclusion and Future Work

This chapter presents the project conclusions as well as some suggestions for future work.

6.1 Conclusion

The propulsive pair proved to be well dimensioned being capable to lift the quadrotor own weight and extra payload, fulfilling the requirements. The achieved autonomy was acceptable, meeting the expectations for this kind of aircrafts. The structure proved to be very rigid and robust, by resisting to some falls. However, the lack of protection for the propellers was a problem putting the components and our own safety in risk.

The set of tests carried out with the motors resulted in an important characterization of their behaviour, not provided by the manufacturer.

Regarding to the attitude estimation, the fusion filters were not able to calculate accurate estimations in the presence of motors vibrations. As a consequence, it was not possible to perform the necessary tests to validate the control algorithm. When the vibrations were small, the complementary filter presented accurate estimations of the vehicle attitude. In all the tests the complementary filter presented better results, even though requires less computational power. Due to the magnetometer malfunction problem, it was not possible to test if it would work correctly in the presence of electromagnetic interference caused by the motors.

The communication protocol and the graphical user interface were working as expected providing visual feedback during the tests, allowing faster and efficient debugging.

6.2 Future Work

Concerning future work, there are plenty of ways to improve the system and add new features.

To solve the attitude angle estimation errors, two solutions are proposed: try to reduce the vibrations caused by the motors, introducing a material capable of absorbing vibrations between the board and the central plate of the structure. Another solution is to implement other types of sensor fusion filters, such as Kalman filter[25][26]. To improve the fusion filters accuracy, specially the yaw estimation, it is also important to replace the damaged magnetometer.

It is mandatory to build a protection for the propellers, or replace the structure for a new one with that feature built-in. This will avoid unwanted components damage and human

injuries.

Regarding to the control techniques, it is required to perform more tests to the current implemented algorithm, but it would be interesting to also implement other control algorithms. In addition to the current algorithms implementation, it is important to instantiate altitude control using the barometer for high altitudes, while the introduction of a sonar sensor to measure small altitudes could allow to perform automatic take-off and landing.

Other suggestion is to develop our own ESC, since most of the commercial ones have update rates of 50Hz that limit the closed loop control performance. In addition, the communication between ESC and the sensing and control board can be changed to digital communication protocols such as I^2C or SPI.

For autonomous behaviours, the introduction of sonar sensors and a GPS module would allow autonomous flying outdoors, avoiding obstacles and following pre-defined routes.

Finally, this project can open opportunities for other projects such as implementing a gimbal for camera stabilization attaching it to the quadrotor.

Bibliography

[1] BBC News. German railways to test anti-graffiti drones. http://aiweb.techfak.uni-bielefeld.de/content/bworld-robot-control-software/, May 2013.

[2] Science Network Leith Phillips. Quadcopter employed to eradicate weeds in albany. http://www.sciencewa.net.au/topics/agriculture/item/1594-quadcopter-employed-to-eradicate-weeds-in-albany.html, July 2012.

[3] Popular Mechanics David Hambling. Armed quadrotors are coming. http://www.popularmechanics.com/technology/military/planes-uavs/armed-quadrotors-are-coming-10720086, July 2012.

[4] Professor J.Gordon Leishman. The breguet-richet quad-rotor helicopter of 1907. 2002.

[5] J. Gordon Leishman. A history of helicopter flight, November 2011.

[6] Kenneth Munson. *Helicopters and other rotorcraft since 1907*. Blandford Press, 1973.

[7] G. Hoffmann, D.G. Rajnarayan, S.L. Waslander, D. Dostal, Jung Soon Jang, and C.J. Tomlin. The stanford testbed of autonomous rotorcraft for multi agent control (starmac). *Digital Avionics Systems Conference, 2004. DASC 04. The 23rd*, 2, 2004.

[8] Steven L. Waslander and Gabriel M. Hoffmann. Multi-agent quadrotor testbed control design: Integral sliding mode vs. reinforcement learning. *IEEE/RSJ International Conference on Intelligent Robots and Systems*, 2005.

[9] Gabriel M. Hoffmann, Steven W. Waslander, and Claire J. Tomlin. Quadrotor helicopters (slides). *IROS MAV Workshop*, November 2007.

[10] Samir Bouabdallah. *Design and Control of Quadrotors With Application to Autonomous Flying*. PhD thesis, École Polytechnique Fédérale De Lausanne, 2007.

[11] Samir Bouabdallah and Roland Siegwart. Backstepping and sliding-mode techniques applied to an indoor micro quadrotor. *IEEE/RSJ International Conference on Robotics and Automation*, 2005.

[12] M. Muller, S. Lupashin, and R. D'Andrea. Quadrocopter ball juggling. *Intelligent Robots and Systems (IROS), 2011 IEEE/RSJ International Conference*, pages 5113–5120, 2011.

[13] Raffaello D'Andrea. The astounding athletic power of quadcopters. http://www.ted.com/talks/raffaello_d_andrea_the_astounding_athletic_power_of_quadcopters.html, June 2013.

[14] Daniel Mellinger, Nathan Michael, and Vijay Kumar. Trajectory generation and control for precise aggressive maneuvers with quadrotors. *The International Journal of Robotics Research*, 31(5):664–674, 2012.

[15] Alex Kushleyev, Daniel Mellinger, and Vijay Kumar. Towards a swarm of agile micro quadrotors. In *Robotics: Science and Systems*, July 2012.

[16] Thomas Schneider. Fault-tolerant multirotor systems. Master's thesis, Swiss Federal Institute of Technology Zurich, 2011.

[17] Electropaedia. Battery and energy technologies. `http://www.mpoweruk.com/chemistries.htm`, November 2012.

[18] B. Michini, J. Redding, N. K. Ure, M. Cutler, and J. P. How. Design and flight testing of an autonomous variable-pitch quadrotor. In *IEEE International Conference on Robotics and Automation (ICRA)*. IEEE, May 2011.

[19] Department of Atmospheric Sciences (DAS) at the University of Illinois at Urbana-Champaign. Pressure with height. `http://ww2010.atmos.uiuc.edu/(Gh)/guides/mtr/prs/hght.rxml`, 2010.

[20] Bosch. *BMP085 Digital pressure sensor data sheet*, August 2011.

[21] Christopher J. Fisher. Using an accelerometer for inclination sensing. *Analog Devices AN-1057*, 2010.

[22] Michael J. Caruso. Applications of magnetic sensors for low cost compass systems. *Position Location and Navigation Symposium, IEEE 2000*, pages 177 – 184, March 2000.

[23] Shane Colton. The balance filter - a simple solution for integrating accelerometer and gyroscope measurements for a balancing platform (slides). June 2007.

[24] S.O.H. Madgwick, R. Vaidyanathan, and A.J.L. Harrison. An efficient orientation filter for inertial measurement units (imus) and magnetic angular rate and gravity (marg) sensor arrays. Technical report, Department of Mechanical Engineering, April 2010.

[25] Shaohua Wang and Ying Yang. Quadrotor aircraft attitude estimation and control based on kalman filter. *Control Conference (CCC), 2012 31st Chinese*, July 2012.

[26] F. Hoffmann, N. Goddemeier, and T. Bertram. Attitude estimation and control of a quadrocopter. *Intelligent Robots and Systems (IROS), 2010 IEEE/RSJ International Conference on*, October 2010.

[27] Padmaraja Yedamale. Brushless dc (bldc) motor fundamentals. *Microchip Technology Inc. AN885*, 2003.

[28] Ward Brown. Brushless dc motor control made easy. *Microchip Technology Inc. AN857*, 2011.

[29] Understanding d.c. motor characteristics, 1999.

[30] Brushless sine drives. *Galil Motion Control, Inc Application Note 1501*, 2011.

Appendix A

Architecture Design and Implementation

Material Overview

LiPo Batteries

LiPo battery cells can be organized in series or parallel. In the first case the total voltage voltage will be given by the sum of all cells voltage. If they are organized in parallel, the voltage will remain the same as 1 cell, but will increase the battery capacity given more flight time.

Each LiPo cell voltage varies from 2.7V to about 4.23V when fully charged. Although, if during operation, a LiPo cell voltage drops below 3V, it may become permanently damaged. Thus, it is required special attention and additional electronics to prevent a voltage drop below 3V. Some ESC have a low cut off feature to prevent this situation, however it is recommendable and usual to use additional alarm system (a buzzer for example).

When describing batteries is common to express discharge current as C-rate. A C-rate is a measure of the rate at which a battery is discharged relative to its maximum capacity. So a 1C battery will discharge the entire battery in 1 hour. Luckily LiPo batteries can achieve high discharge rates, providing the amount of current necessary to the motor in order to run properly.

Brushless Motors

BLDC are a type of synchronous motor and come in single-phase, 2-phase and 3-phase configurations. Due to different physical constructions, BLDC can be classified as Inrunners or Outrunners. On the first configuration the permanent magnets are part of the rotor, while the stator windings surround them. On the second approach the stator windings are at the center of the motor, surrounded by the permanent magnets that spin around the stator.[27]

In terms of power, the input power of an electric motor is the product of the voltage applied to the motor terminals and the current consumption.

$$P_{in} = V \cdot I_{in} \tag{A.1}$$

The Motor applies torque in a body that rotates with some angular velocity. Thus, the

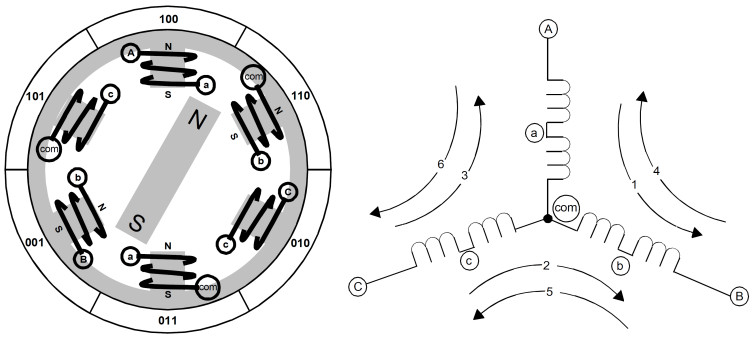

Figure A.1: Simplified BLDC motor diagram [28].

output power can be described as:

$$P_{out} = \tau \cdot \omega \tag{A.2}$$

Where τ is torque, and ω is angular velocity.

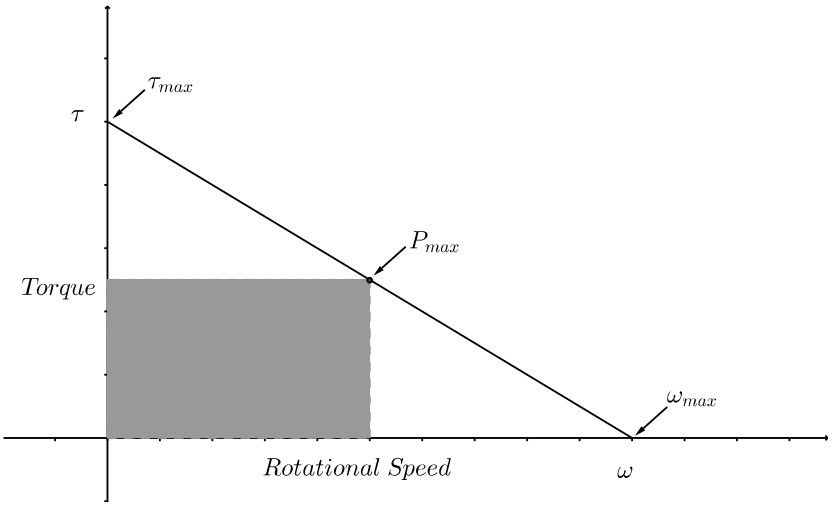

Figure A.2: Typical DC motor Torque vs Speed curve

Although every motor has is own torque/speed curve and power curve, the graph shown in figure A.3 illustrates a typical DC motor curve. Note that torque is inversely proportional to the speed, so the maximum point of torque will be when there is no rotation. From equation A.2 and figure A.3 is clear that the maximum point of power is when $\tau = \frac{1}{2}\tau_{max}$ and $\omega = \frac{1}{2}\omega_{max}$.[29][27]

Electronic Speed Controllers

There are two typical approaches to sense rotor position: through Hall effect or measuring EMF.

Sensored commutation (Hall effect)

Many manufacturers provide a 3-element Hall effect position. Each sensor outputs a high digital level for 180 degrees and a low digital level for the other 180 degrees. All sensors have a offset of 60 degrees from each other causing the alignment of one of the electromagnetic circuits with each sensor output.

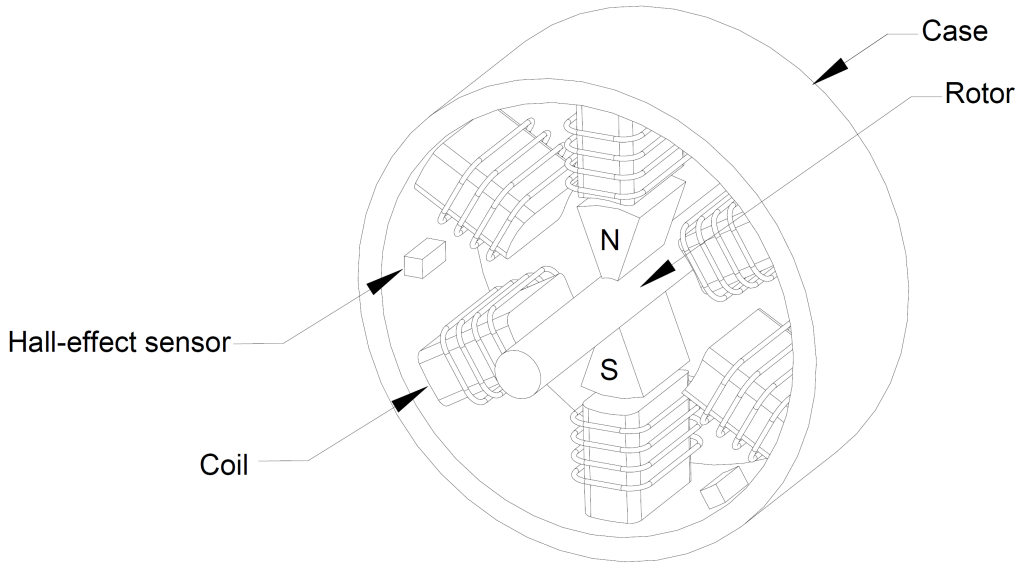

Figure A.3: Brushless motor diagram with 3-element Hall effect sensors[30].

Sensorless motor

In some cases, when the motor doesn't have Hall effect sensors, it is possible to control the motor measuring the back EMF voltage on an undriven terminal during one of the drive phases. There are several disadvantages with this approach:

- The rotor must be spinning at a minimum rate to generate sufficient EMF voltage to be sensed.
- If the speed goes further than ideal rate it will result in a discontinuous motor response.

In fact, the only advantage is that the motor is cheaper.

Motion Sensors

Accelerometer

Accelerometer is an electromechanical device that measures proper acceleration. Although, instead of measure the rate of change of velocity, it measures the force that is directed in opposite direction from the acceleration vector. This force is often called Inertial Force and they could be static, like the constance force of gravity, or dynamic caused by movement or vibration. In order to represent visually how accelerometers work, it is useful to think of it like a mass connected to a spring like in figure A.4.

When the accelerometer is under the influence of external accelerations, the mass will perform a displacement x. From the Newton's second law, it is known that $F = ma$, where F is the force, m the body mass and a the acceleration the body suffers. As the body is connected to a spring, it will generate a force opposite to the acceleration and proportional to x. From Hooke's Law, $F = kx$ where k is a constant related to the spring properties, so the acceleration can be calculated as $a = \frac{kx}{m}$.

If we take the accelerometer to a place with no gravitational fields (outer space), the mass will float in the middle of the accelerometer, like shown in figure A.4(a). On the other hand, if the accelerometer is placed on Earth while in rest(figure A.4(b)), the mass will perform a displacement, deflecting the spring and sensing a force of $-1g \approx -9.806m/s^2$.

Figure A.4(a) show us the model of an accelerometer when he is in free-fall or in outer space.

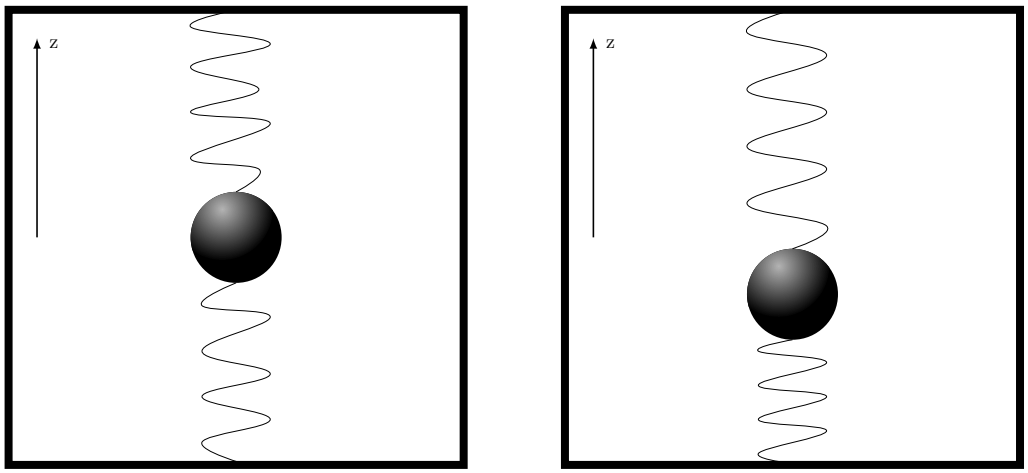

Figure A.4: a) Accelerometer in free fall. b) Accelerometer in rest.

Despite in figure A.4 is only represented z axis, most modern accelerometers perform measures in all 3 axis.

Recently, devices for this kind of application are based on MEMS (micro electro-mechanical systems) accelerometer. In figure A.5 we can see a simplified structure of a MEMS device, which is composed by fixed beams and a proof mass. Under the influence of external accelerations the proof mass deflects from its neutral position, changing the capacitance between plates. This change in the capacitance is related with the acceleration and it can be measured in a digital or analog manner.

Gyroscope

Gyroscopes are devices capable of measuring angular velocity. Similarly to accelerometers, most of recent gyroscopes are based in MEMS technology providing an analog or digital output. Gyroscopes can be understood as a spinning wheel in which the axle is free to assume any direction. Each type of MEMS gyroscope has some oscillating component where a direction change can be detected. This effect is caused because a vibrating object tends to continue vibrating in the same plane and any deviation can be used to derive a change in

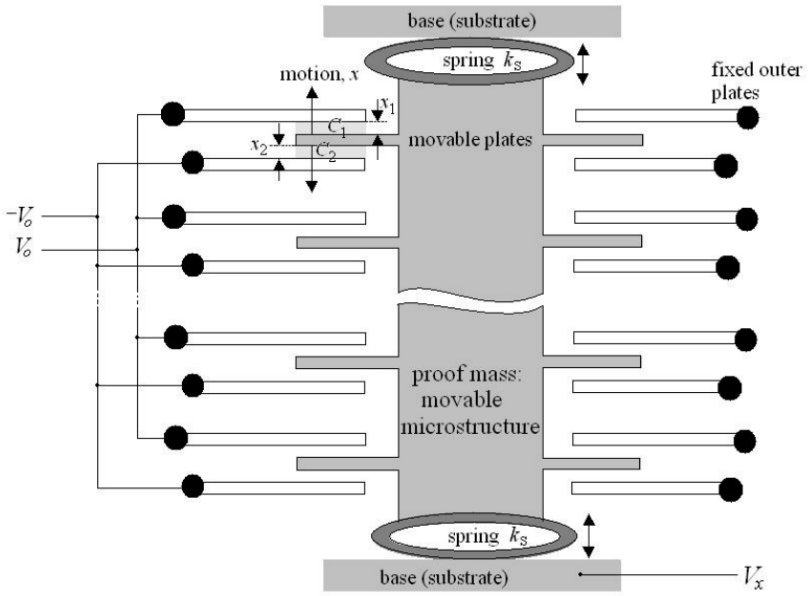

Figure A.5: MEMS accelerometer structure

direction. These deviations are possible because of Corolis force, which is orthogonal to the object that is vibrating.

For this kind of application we are interested in measure angles and no angular velocity, so this device needs to be integrated in order to be useful, but this topic will be explained in more detail in sensory fusion section.

Magnetometer

Magnetometer is a device capable of measuring strength and direction of magnetic fields. Although they can measure all types of magnetic fields we are interested in the Earth's magnetic field to measure the aircraft orientation.

Hall effect magnetometers consists basically of a thin p-type semiconductor material that as a continuous current passing through it. When the material approaches to a magnetic field, the magnetic flux exerts a force that deflects the electrons to either side of the semiconductor producing a potential difference between the two sides of the semiconductor. Measuring this voltage turns possible to find the existence of a magnetic field and it strength.

In order to sense the magnetic heading it is needed at least two axis magnetometer. By keeping the two-axis module level, maximum heading accuracy is achieved. Although, for this kind of applications, where the modules aren't level it is a request to have a third axis to perform tilt compensation. This compensation will be explained in detail in sensor fusion section.

[1] `http://wikid.eu/index.php/Hall_effect_Magnetometer`

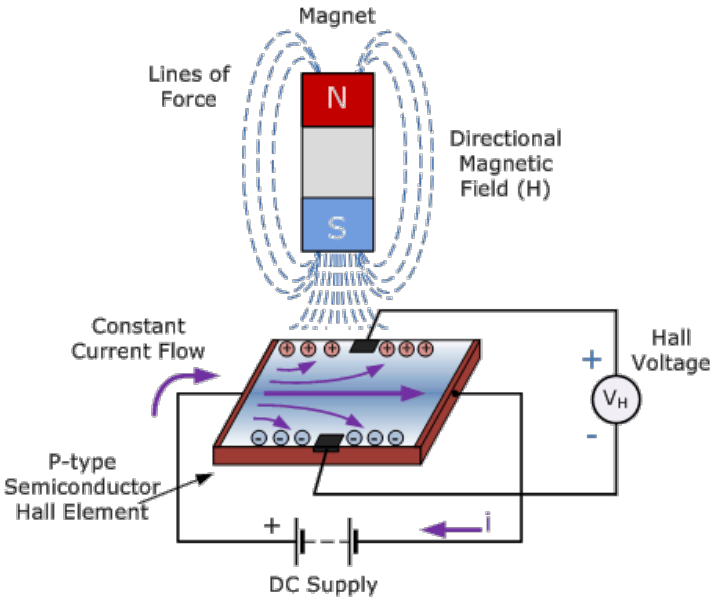

Figure A.6: Hall effect sensor.[1]

Appendix B

Control Board Schematics and Layouts

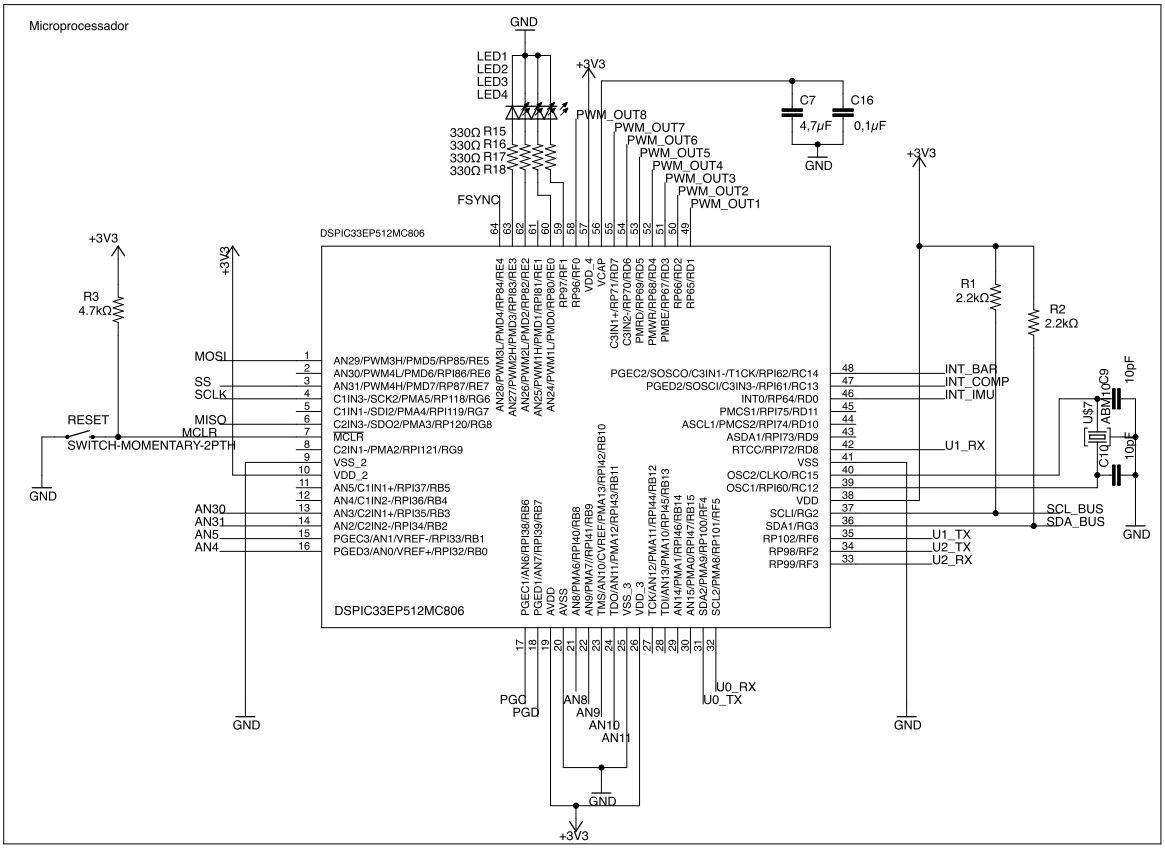

Figure B.1: Control Board schematic - Microprocessor Part

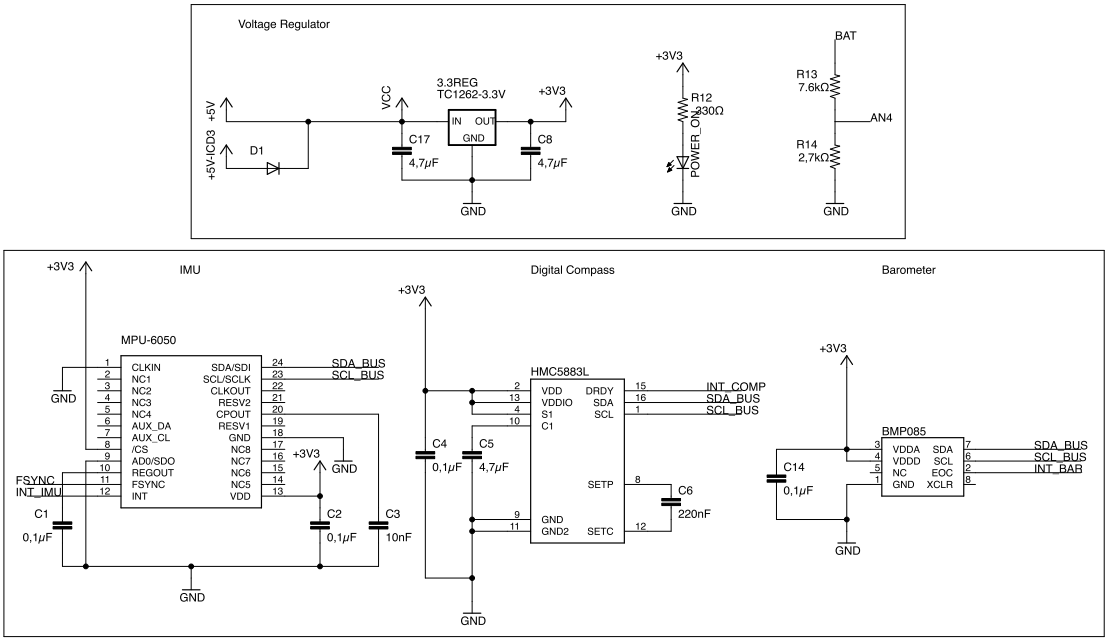

Figure B.2: Control Board schematic - Sensors Part

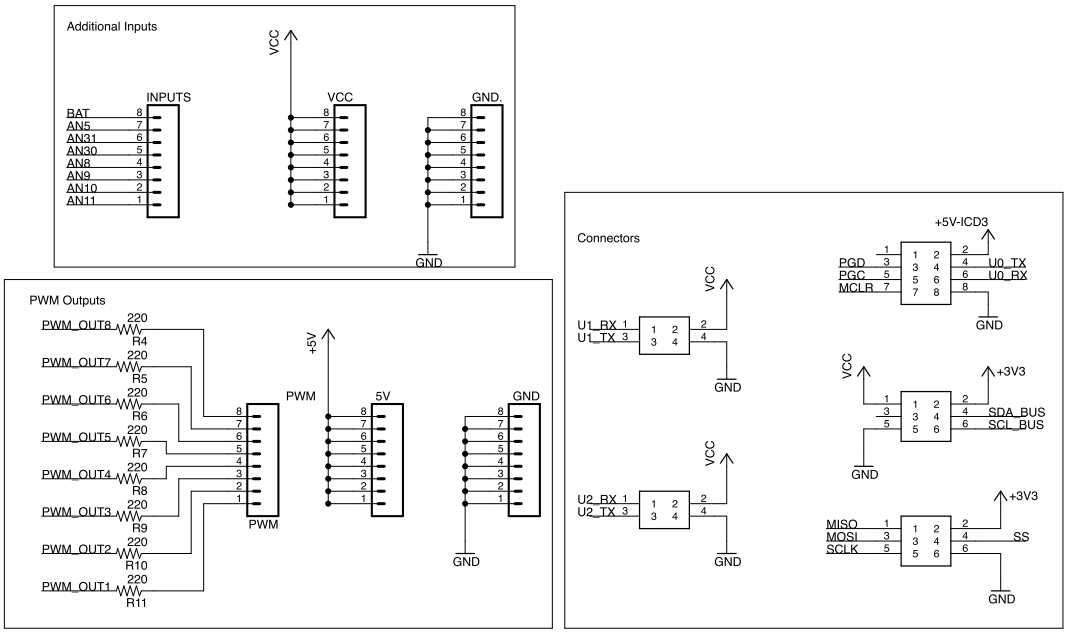

Figure B.3: Control Board schematic - Connectors Part

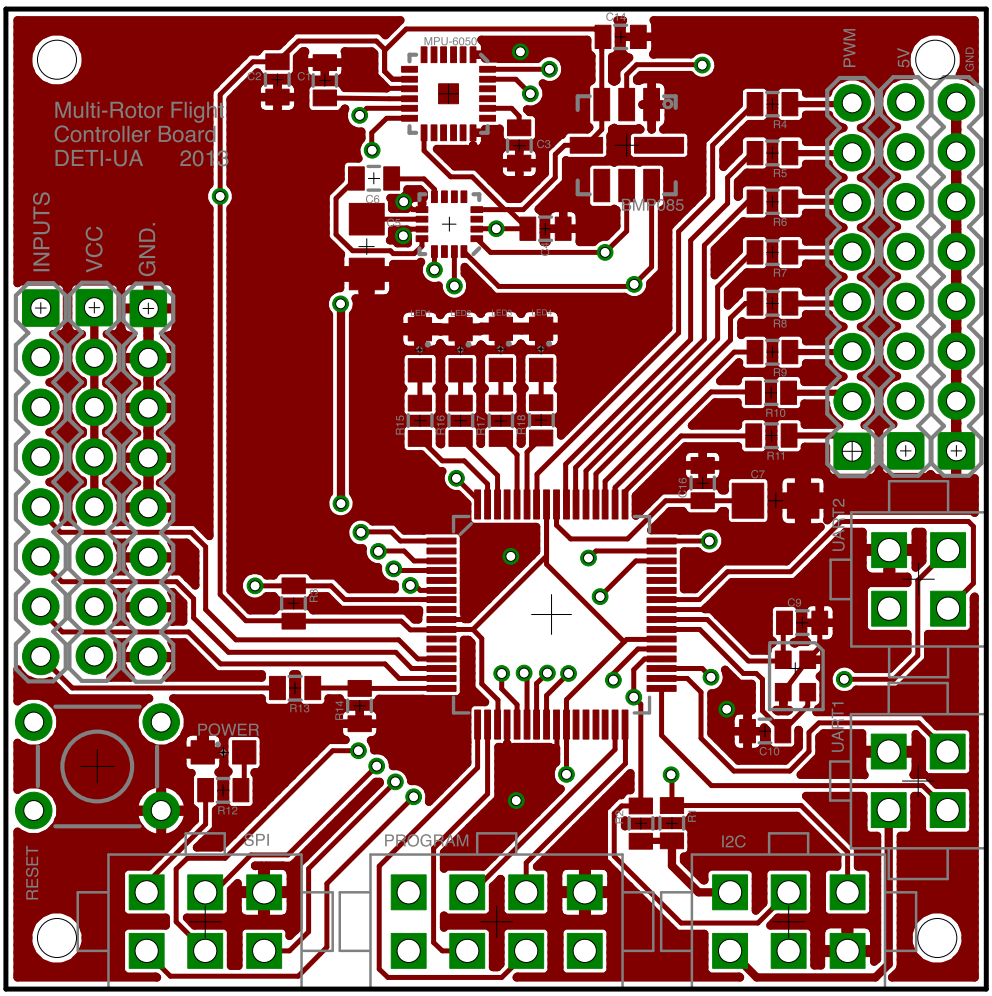

Figure B.4: Control Board top layer

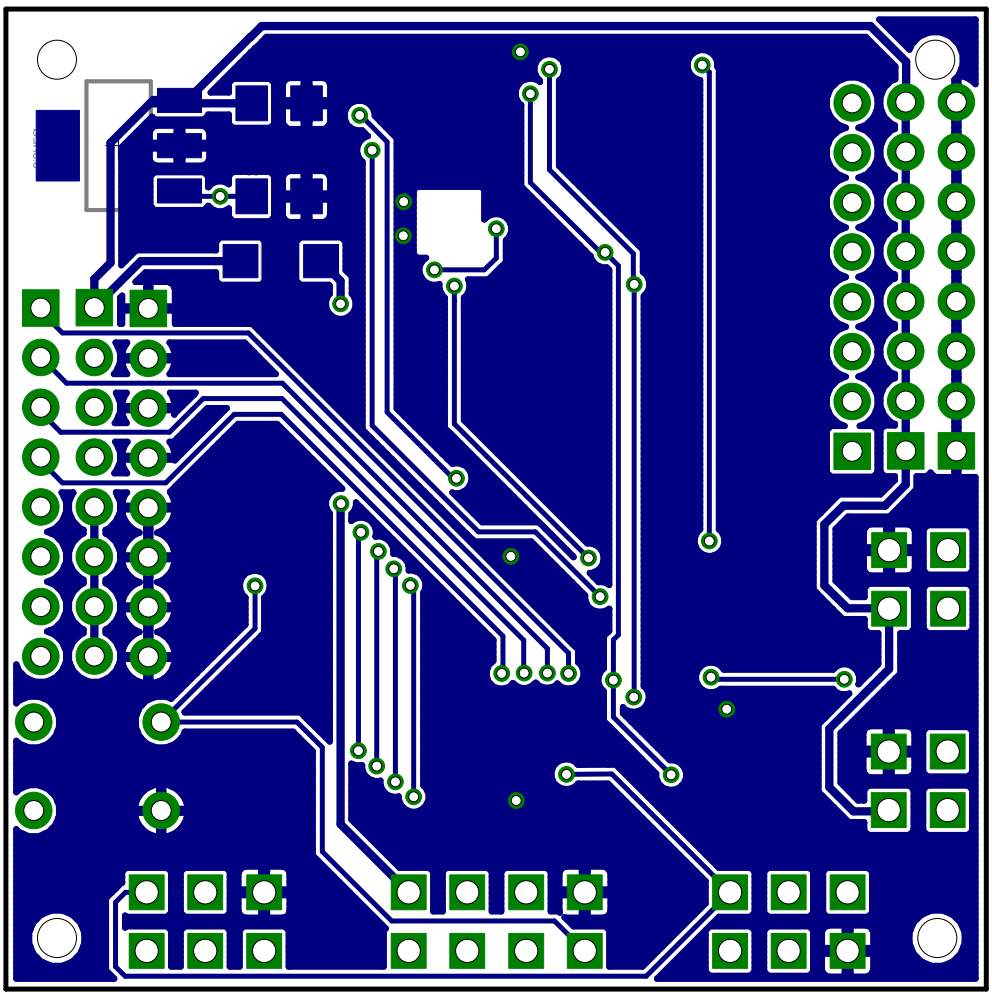

Figure B.5: Control Board bottom layer

Appendix C

Calibration Routines and Communication Protocol

BMP085 Calibration Routine

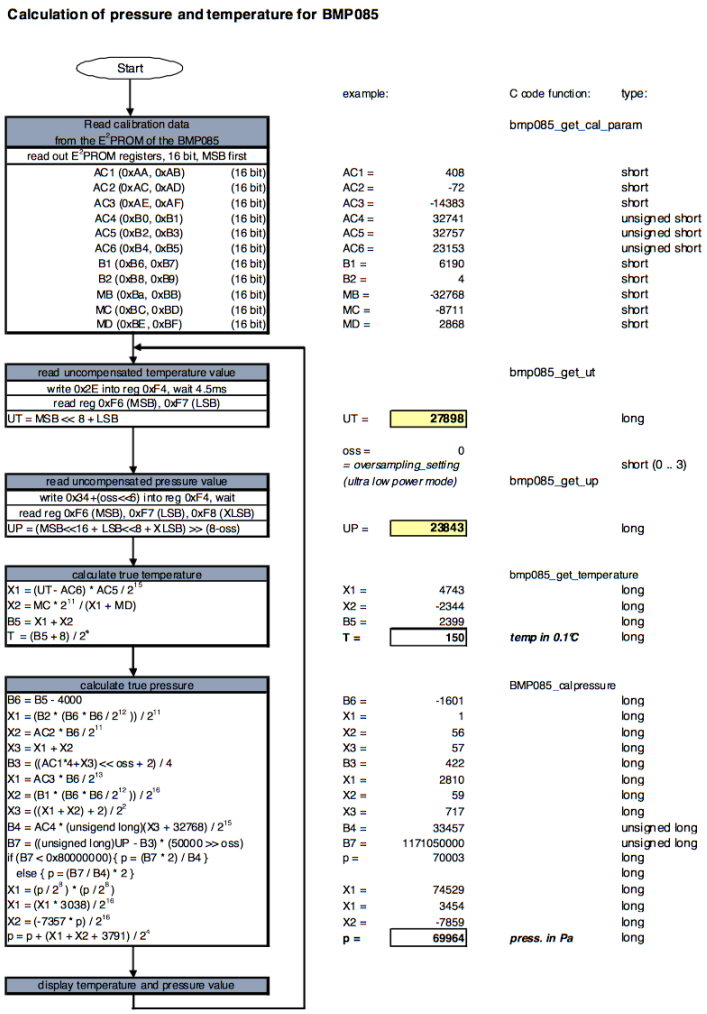

Figure C.1: BMP085 calibration routine

Communication Protocol

In this section it will be described the complete set of messages used to pass information from the control board to the PC and vice versa.

Figure C.2 describes the message frame that contains accelerometer information that will be used by the GUI to provide visual feedback to the user. The message uses the `0x10` for the ID, while it has six bytes of data containing information about the raw values of all the three axis of the accelerometer (A_x, A_y and A_z). The message frames to pass gyroscope and magnetometer information are very similiar to the accelerometer one. It also has 6 bytes of data containing the raw value for the 3 axis (G_x, G_y and G_z for the gyroscope, and H_x, H_y and H_z for the magnetometer). The ID it is described ate figures C.3 and C.4 for gyroscope and magnetomter respectivelly. All the raw values, are transmitted exactly has they were readen from the sensors, so the unit deppends on how the full scale range of the components is configured. For more information refer to section 3.3.2.

1 byte	2 byte	2 byte	4 byte	4 byte	4 byte	2 byte
SFD	01	NDB	A_x	A_y	A_z	CS

Figure C.2: Accelerometer message frame.

1 byte	2 byte	2 byte	4 byte	4 byte	4 byte	2 byte
SFD	02	NDB	G_x	G_y	G_z	CS

Figure C.3: Gyroscope message frame.

1 byte	2 byte	2 byte	4 byte	4 byte	4 byte	2 byte
SFD	03	NDB	H_x	H_y	H_z	CS

Figure C.4: Magnetometer message frame.

For the barometer frame it is only required one byte of data, since it is only passed the altitude information (which comes in meters). The frame structure is presented in figure C.5.

1 byte	2 byte	2 byte	4 byte	2 byte
SFD	04	NDB	Altitude	CS

Figure C.5: Barometer message frame.

The frames used for transmitting the current motors PWM, remote control state and info about the vehicle are very similar and are represented in figure C.7, C.8 and C.9 respectively. The first one contains information about the current PWM applied to the ESC which control the motors distributed in 8 bytes of data. Very similarly, the information about the current

1 byte	2 byte	2 byte	4 byte	4 byte	4 byte	2 byte
SFD	09	NDB	Roll	Pitch	Yaw	CS

Figure C.6: Estimated angles message frame.

stick values of the remote control is transfered containing the time (in μs) read by the microcontroller of all the four channels (Throttle, Rudder, Elevator and Aileron).

The last frame contains information about some system variables of the system, such as battery voltage (in volts), if it is armed or disarmed and if the control algorithm and remote controller are activated or de-activated (boolean variables, 1 meaning true and 0 meaning false).

1 byte	2 byte	2 byte	4 byte	4 byte	4 byte	4 byte	2 byte
SFD	30	NDB	Motor 1	Motor 2	Motor 3	Motor 4	CS

Figure C.7: PWM value applied to ESC message frame.

1 byte	2 byte	2 byte	4 byte	4 byte	4 byte	4 byte	2 byte
SFD	0x10	NDB	Throttle	Rudder	Elevator	Aileron	CS

Figure C.8: Remote Controller message frame.

1 byte	2 byte	2 byte	4 byte	2 byte	2 byte	2 byte	2 byte
SFD	20	NDB	Battery Voltage	Control ON/OFF	Remote ON/OFF	Armed/ Disarmed	CS

Figure C.9: Info message frame.

The messages that flow from the PC to the control board are generally to act on the system. There are four messages to act on the motors and one to arm/disarm the vehicle. The messages to act on the motors are represented in figures C.10 to C.13 and only contain two bytes of data which indicates the new PWM value to apply in the ESC. Of course this only applies if the control algorithms are switched off, otherwise they will change the PWM values in order to compensate the system. The other message, it is represented in figure C.14 and it is used to arm or disarm the vehicle for safety procedures. It only has one byte of data which is a 0 to disarm and 1 to arm.

1 byte	2 byte	2 byte	4 byte	2 byte
SFD	71	NDB	Motor 1 PWM	CS

Figure C.10: Motor 1 PWM message frame.

1 byte	2 byte	2 byte	4 byte	2 byte
SFD	72	NDB	Motor 2 PWM	CS

Figure C.11: Motor 2 PWM message frame.

1 byte	2 byte	2 byte	4 byte	2 byte
SFD	73	NDB	Motor 3 PWM	CS

Figure C.12: Motor 3 PWM message frame.

1 byte	2 byte	2 byte	4 byte	2 byte
SFD	74	NDB	Motor 4 PWM	CS

Figure C.13: Motor 4 PWM message frame.

1 byte	2 byte	2 byte	2 byte	2 byte
SFD	60	NDB	Arm/ Disarm	CS

Figure C.14: Arm/Disarm message frame.

Appendix D

Measured Values of Results

Single motor test measured values

Thrust (g)			
3S 9x47	**3S 10x45**	**4S 9x47**	**4S 10x45**
0	85	85	85
0	90	85	85
93	92	128	138
122	116	185	195
159	158	236	260
197	196	307	325
230	247	366	384
267	281	429	453
306	326	484	525
337	365	537	587
366	404	590	656
408	456	641	730
436	517	684	801
475	576	737	877
513	628	799	1020
570	692	866	N/A
623	741	922	N/A
669	789	N/A	N/A
725	838	N/A	N/A
779	892	N/A	N/A
829	935	N/A	N/A

Table D.1: Thrust values for different configurations.

Current (A)			
3S 9x47	**3S 10x45**	**4S 9x47**	**4S 10x45**
0.15	0.15	0.25	0.25
0.35	0.35	0.3	0.5
0.6	0.6	0.85	0.90
0.89	0.95	1.30	1.35
1.25	1.35	1.70	1.95
1.65	1.85	2.45	2.55
2.05	2.35	3.1	3.2
2.45	2.85	3.8	4
2.95	3.40	4.5	4.90
3.45	3.9	5.19	5.8
3.9	4.55	5.95	6.9
4.39	5.25	6.7	8.30
4.85	6.15	7.20	9.55
5.35	7.25	8.5	10.79
6	8.30	9.4	12.1
6.9	9.45	10.45	N/A
7.8	10.8	11.75	N/A
8.69	11.95	N/A	N/A
9.80	13.3	N/A	N/A
11.1	14.80	N/A	N/A
12.1	16.10	N/A	N/A

Table D.2: Current measured for different configurations.

Power (W)			
3S 9x47	**3S 10x45**	**4S 9x47**	**4S 10x45**
2	2	4	4
4	4	5	8
8	8	14	15
11	12	22	22
16	17	28	32
21	23	41	42
26	30	51	53
31	36	63	66
37	43	75	81
43	49	86	96
49	57	99	115
55	66	111	138
61	77	120	159
67	91	141	179
76	105	156	201
87	119	173	N/A
98	136	195	N/A
110	151	N/A	N/A
123	168	N/A	N/A
140	186	N/A	N/A
152	203	N/A	N/A

Table D.3: Power estimated for different configurations.

Appendix E

Instructions Manual

Graphical User Interface User Manual

The first step towards using the GUI is to connect the telemetry device, either the bluetooth module or the FTDI interface. After opening the Quadcopter Ground Station it is required to connect to the device using the connection box. The device should appear in the devices combo box, as this list is updated automatically everytime it senses new devices are connected. The user must also select the baudrate that the device is operating. It is possible then to connect to the aircraft using the **Connect** button, and if no error message appears, then the PC and aircraft are sucessfully connected.

As the device is connected, all the information regarding the quadcopter is automatically updated in the graphical user interface and refreshed every 100ms. The user then, can only visualize data about the quadcopter state, and not act on the vehicle. To act on the quadcopter the user must press the **arm** button, ensuring that the quadcopter is in the flat surface with no objects neither humans near it. It is possible then to act on the motors, using the sliders. On the left of the tab, it is possible to see how is the current position of the remote controller sticks, where the 50% of the progress bar represents that the sitck is at is rest position.

In the graphs tab it is possible to view in detail an output of all the quadcopter sensors. If one want to clean the graphs, it must use the menu button situated in the menu bar under *Graphs* > *Clear*.

Regarding to the console tab, it is also possible to clean the message history, using the clear button on the bottom of the interface. The textbox at the bottom can be used to send commands to the quadcopter, that must follow the protocol that was explained in detail in section C.

In order to use the program, the user must have the Java version 6 or later installed aswell the jssc[1] and jchart2d[2] libraries.

[1] `https://code.google.com/p/java-simple-serial-connector/`
[2] `htpp://jchart2d.sourceforge.net/`